Πανεπιστήμιο Κρήτης

Τμήμα Χημείας

Εργαστήριο Περιβαλλοντικών Χημικών

Διεργασιών Ε.ΠΕ.ΧΗ.ΔΙ.

Διδακτορική Διατριβή

Επίδραση οργανικών και ανόργανων αερολύματων στον σχηματισμό πρωτογενών κρυστάλλων πάγου στα νέφη μικτής φάσης

Μάριος Χατζηπαράσχος

Επιβλέπουσα καθηγήτρια: Μαρία Κανακίδου

Ηράκλειο, Μάϊος 2023

University of Crete

Department of Chemistry

Environmental Chemical Processes Laboratory, ECPL

Doctoral Thesis

Impact of organic and inorganic aerosol particles on the formation of primary ice crystals in mixed-phase clouds

Marios Chatziparaschos

Thesis supervisor: Maria Kanakidou

Heraklion, May 2023

Examination committee

1. Maria Kanakidou, Professor Department of Chemistry, University of Crete, Greece. **(Supervisor)**

2. Nikolaos Mihalopoulos, Professor Department of Chemistry, University of Crete, Greece.

3. Athanasios Nenes, Professor, École Polytechnique Fédérale de Lausanne (EPFL), Switzerland.

4. Spiros Pergantis, Professor Department of Chemistry, University of Crete, Greece.

5. Ilias Vardavas, Associate Professor (retired), Department of Physics, University of Crete, Greece.

6. Stelios Myriokefalitakis, Researcher, Institute for Environmental Research and Sustainable Development (IERSD), National Observatory of Athens (NOA), Greece.

7. Carlos Pérez García-Pando, Research Professor of Catalan Institute for Research and Advanced Studies (ICREA) and AXA Professor on Sand and Dust Storms, Barcelona Supercomputing Center (BSC), Barcelona, Spain.

ACKNOWLEDGEMENTS

The present work was carried out at the Environmental Chemical Processes Laboratory of the Department of Chemistry, University of Crete. It was funded by the project “PANhellenic infrastructure for Atmospheric Composition and climatE change” (PANACEA; MIS 5021516), which is implemented under the Action “Reinforcement of the Research and Innovation Infrastructure”, funded by the Operational Programme “Competitiveness, Entrepreneurship and Innovation” (NSRF 2014-2020) and co-financed by Greece and the European Union (European Regional Development Fund). I consider it necessary to thank the Chemistry Department for accepting me as a PhD candidate and the ECPL for providing the infrastructure needed for this work to be conducted.

First and foremost, I would like to express my special appreciation and thanks to my supervisor Professor Maria Kanakidou for her dedication and encouragement. Working with her has been an honor and a privilege. The opportunity she gave me to work with her, her continuous guidance and her trust made me the scientist –and person- I am today. She was always available, with insightful comments and input, and always willing to help, both on a professional and a personal level.

I would like to express my deep gratitude to Professor Athanasios Nenes for his invaluable scientific support and contributions to my research. His extensive experience in this research field has been critical in improving my understanding and taking my research to the next level. Prof. Nenes' expertise and knowledge have been instrumental in shaping the direction of my research. His insightful comments and suggestions have helped me

to refine my ideas and approach, and his feedback has been essential in improving the quality of my work.

I am sincerely grateful to Carlos Pérez García-Pando and his group for their invaluable guidance and expertise in the successful completion of my thesis. In particular I thank them for providing the dust mineralogy and guiding me in the IFS-TM5 model system. Without their support and assistance, I would not have been able to achieve what I have. Professor Perez's input and feedback were particularly instrumental in shaping my research, and his leadership helped me to navigate through challenges and obstacles. His willingness to share his knowledge and experience was truly appreciated and has enriched my work.

I would also like to express my thanks to Prof. Dr. Nikos Mihalopoulos and Prof. Dr. Spiros Pergantis who acted as advisors throughout this thesis. Also, the rest of the members of my examining committee, Dr. Stelios Myriokefalitakis and Prof. Dr. Ilias Vardavas for the honor of accepting to review my thesis.

I would also like to thank all the colleagues from the Computational Environmental Chemistry group of the Environmental Chemical Processes Laboratory for the really good environment and the excellent cooperation. In particular, I would like to specially thank Dr. Nikos Kalivitis, Nikos Gialesakis, Aggelos Gkouvousis, and Anna-Maria Neroladaki. Their support and friendship have been invaluable throughout my academic journey. I am grateful for the opportunity to work alongside such talented and dedicated individuals, who have not only been colleagues but also friends.

Finally, I would like to sincerely thank, my parents, my sister Komnini and my brother Andronikos for their unwavering support.

This thesis is dedicated to the memory of my father.

Curriculum vitae

MARIOS CHATZIPARASCHOS

Phone: +030 6982476162

Mailing Address: chemp873@edu.chemistry.uoc

Liabilities: Accomplished Military

Working address: Environmental Chemical Processes Laboratory (ECPL), Department of Chemistry University of Crete, 70013 Heraklion, Greece

Tel(lab): +302810545067

RESEARCH INTERESTS

Marios' research interests concern the study of chemistry and physics of the atmosphere, with focus on the impacts of aerosol chemical composition on cloud microphysical processes and climate, using modeling techniques.

Through his research activities he is trying to:

understand the impact of mineralogy on airborne dust particles acting as ice nuclei particles

assess the impact of natural emissions from terrestrial and marine primary organic aerosols on the formation of ice crystals over remote oceans

evaluate and optimize results comparing with field and laboratory measurements

EDUCATION

PhD University of Crete, Environmental and Chemical Processes Laboratory (ECPL), Chemistry Department Environmental Sciences	11.2018-04.2023
MS University of Crete, Environmental and Chemical Processes Laboratory (ECPL), Chemistry Department Environmental Sciences	11. 2016-2018
BS Aristotle University of Thessaloniki, Physics Department	11.2008- 2012

LANGUAGES

Greek: Native language

English: [Test of Interactive English (TIE) C1+, Irish ACELS]

COMPUTER SKILLS

Programming: Python*, Fortran* 77/90/95, IDL, BASH, C

* certified knowledge

HONORS AND AWARDS

2021

Award Early Career Scientist award, Poster Prize Winner International Global Atmospheric Chemistry (iCACGP-IGAC Joint Conference) Scientific Conference, Poster Title: “Dust minerals in the atmosphere as precursors of Ice Nuclei Particles” CCMI-52A

2022

Early Career Scientist Travel award (inscription fees, air plane ticket and hotel) για συμμετοχή στο Διεθνές Συνέδριο IGAC/iCACGP 2022 στο Μάντσεστερ, Αγγλία, Σεπτ. 2022.

PROJECTS

2022 -03.2023

European Union Horizon 2020 project FORCeS 821205 OPZ13613-30

“Global atmospheric simulations of the contribution of aerosols on ice nuclei and ice formation” Institute of Chemical Engineering Sciences (ICE-HT/FORTH)

(PhD)

2021

EUMETSAT Statement of Work for Climatological Characterization

of Ocean Greek Sites for OC-SVC in cooperation with Hellenic Centre 2021 for Marine Research (HCMR) (Researcher)

2019-2021

PANhellenic infrastructure for Atmospheric Composition and climatE change" (PANACEA), (MIS 5021516) "Global atmospheric simulations of the effect of aerosols on the composition, formation and optical properties of Clouds (Chemical Transport Model, TM-4) Environmental and Chemical Processes Laboratory (ECPL), Department of Chemistry, University of Crete(PhD)

Internship

05.2022 -09.2022

ERASMUS +, training at Barcelona Supercomputing Center (BSC), Atmospheric Composition group Project: Implementation of Marine Primary Organic Aerosols (MPOA) to EC-EARTH-3 model and investigation their impact on primary ice crystals formation.

TEACHING EXPERIENCE

Teaching, Atmospheric Chemistry (winter semester), 2021-2022

University of Crete, Department of Chemistry

Teaching, Atmospheric Chemistry (summer semester), 2021-2022

University of Crete, Department of Chemistry

Teaching Assistant, Physical Chemistry Laboratory II, 2018-2021

University of Crete, Department of Chemistry

Teaching Assistant, Physical Chemistry Laboratory I, 2018-2021

University of Crete, Department of Chemistry

Teaching Assistant, Laboratory of General Chemistry I, 2019

University of Crete, Department of Chemistry

OTHER EXPERIENCE

Scientific Personnel (technical assistant) on field measurements: 2020-2022

Finokalia (north coast of Crete, Greece) atmospheric monitoring station, part of the European Research Infrastructure for the observation of Aerosol, Clouds, and Trace gases – ACTRIS

https://finokalia.chemistry.uoc.gr/personnel/

PUBLICATIONS

Books

Publications

***Chatziparaschos M**., et al: Global simulations of primary ice crystals formed by immersion freezing of organic and mineral-dust aerosols, to be submitted, 2023*

Chatziparaschos, M., Daskalakis, N., Myriokefalitakis, S., Kalivitis, N., Nenes, A., Gonçalves Ageitos, M., Costa-Surós, M., Pérez García-Pando, C., Zanoli, M., Vrekoussis, M., and Kanakidou, M.: Role of K-feldspar and quartz in global ice nucleation by mineral dust in mixed-phase clouds, Atmos. Chem. Phys., 23, 1785–1801, 2023 https://doi.org/10.5194/acp-23-1785-2023

Chatziparaschos M., Daskalakis N., Myriokefalitakis S., Fanourgakis G., Kanakidou M. (2021) Global Simulations of Ice Nuclei Particles Derived from Organics and Inorganics Particles. In: Mensink C., Matthias V. (eds) Air Pollution Modeling and its Application XXVII. ITM 2019. Springer Proceedings in Complexity. Springer, Berlin, Heidelberg. https://doi.org/10.1007/978-3-662https://doi.org/10.1007/978-3-662-63760-9_363760-9_3

Chatziparaschos M., Daskalakis N., Myriokefalitakis S., Kalivitis N., Kanakidou M. Global simulations of Ice Nuclei and Cloud Condensation Nuclei Particles derived from insoluble mineral Dust, Proceeding of the 15th International Conference on Meteorology, Climatology and Atmospheric Physics, Bartzokas A., Nastos P. (eds), COMECAP 2021, P40-45, ISBN 978-960-233-267-2

Chatziparaschos M., Daskalakis N., Myriokefalitakis S., Fanourgakis G., Kanakidou M. (2018) Global atmospheric simulations of Ice Nuclei Particles from Marine Organic Aerosols and Dust. International Conference on Meteorology, Climatology and Atmospheric Physics, Alexandroupolis, Greece

CONFERENCE PARTICIPATION

2022

Montserrat Costa Surós, Maria Gonçalves, **Marios Chatziparaschos**, Paraskevi Georgakaki, Luka Ilić, Stelios Myriokefalitakis, Twan van Noije, Maria Kanakidou, Athanasios Nenes and Carlos Pérez García-Pando, : Dust-sensitive Heterogeneous Ice Nucleation in the EC-Earth3 Earth System Model: comparison with INP observations and radiative effects, AGU Fall Meeting, Chicago, December, 2022

Chatziparaschos M., Daskalakis N., Gonçalves Ageitos M., Kalivitis N., Surós M.-C., Nenes, A., Pérez García Pando, C., Myriokefalitakis, S., and Kanakidou M.:Sensitivity of simulated Ice Nuclei Particle concentrations to soil mineralogy, 17th International Global Atmospheric Chemistry (iCACGP-IGAC Joint Conference) Scientific Conference, Manchester, UK, 10-15 September, 2022; 2022

Chatziparaschos M., Daskalakis N., Myriokefalitakis S., Kalivitis N., Kanakidou M., Global relevance of Marine Organic Aerosols and Dust Minerals as principal contributors to Ice

Nucleating Particles formation, 11th International Aerosol Conference (IAC), Athens, Greece, 4-9 September, 2022

Kalivitis, N., **Chatziparaschos M**., Gialesakis N., Kouvarakis, G., Mihalopoulos N. and Kanakidou M., Climatology and trends of aerosol optical properties in southeastern Mediterranean derived from AERONET, MERRA-2, MODIS/Terra and surface measurements, 11th International Aerosol Conference (IAC), Athens, Greece, 4-9 September, 2022

N. Gialesakis, N. Kalivitis, **M. Chatziparaschos**, N. Daskalakis, G. Kouvarakis, M. Vrekousis, M. Kanakidou, "Seasonal and interannual variability of nitrogen dioxide and ozone in the South East Mediterranean.", COSPAR 2022, 16-24 July, 2022

M. Kanakidou, M. **Chatziparaschos**, N. Daskalakis and S. Myriokefalitakis "Organic aerosols and dust as contributors to ice nucleating particles formation in the marine atmosphere" https://doi.org/10.5194/egusphere-egu22-7951, 2022, AS2.9 – Air-sea Chemical Fluxes: Impacts on Biogeochemistry and Climate, EGU General Assembly 2022

2021

M. Chatziparaschos, N. Daskalakis, N. Kalivitis, S. Myriokefalitakis and M. Kanakidou "Dust minerals in the atmosphere as precursors of Ice Nuclei Particles" International Global Atmospheric Chemistry- IGAC 2021 (Early Career Scientist Poster Prize Winner)

M. Chatziparaschos, N. Daskalakis, N. Kalivitis, S. Myriokefalitakis and M. Kanakidou. "Global simulations of Ice Nuclei and Cloud Condensation Nuclei Particles derived from insoluble mineral Dust" 15th International Conference on Meteorology, Climatology and Atmospheric Physics - COMECAP 2021

Kalogeraki, E., Sfakianaki, M., Gialesakis, N., **Chatziparaschos**, M., Daskalakis, N.,Kanakidou, M. (2021) Influence of fires on atmospheric composition over Greece as seen by TROPOMI S5P in the Proceeding of the 17th International Conference on Environmental Science and Technology, 1-4 Sept, 2021

2020

M. Chatziparaschos, N. Daskalakis, N. Kalivitis, S. Myriokefalitakis and M. Kanakidou "The role of dust minerals in the atmosphere as precursors of Ice Nuclei Particles" PANhellenic infrastructure for Atmospheric Composition and climatE chAnge -PANACEA 2020

2019

M. Chatziparaschos, N. Daskalakis, N. Kalivitis, S. Myriokefalitakis and M. Kanakidou : "Global simulations of Ice Nuclei Particles derived from Organics and Inorganics Particles", in the proceedings of the ITM 2021 – 37th International Technical Meeting on Air Pollution Modelling and its Application, Katholische Akademie, Hamburg, Germany, 23-27 September, 2019

M. Chatziparaschos, N. Daskalakis, G. Fanourgakis, S. Myriokefalitakis and M. Kanakidou "Global simulations of Ice Nuclei Particles of Terrestrial and Marine Origin" European Geosciences Union EGU2019-16792, Poster Presentation, Session AS3.3; Atmospheric Ice

Particles, Vienna, Austria, 7–12 April, 2019.

M. Chatziparaschos, N. Daskalakis, G. Fanourgakis, S. Myriokefalitakis and M. Kanakidou "Global simulations of Ice Nuclei Particles of Terrestrial and Marine Origin" conference of Postgraduate students of Chemistry Department, University of Crete, Greece, 15 -17 May 2019

2018

M. Chatziparaschos, N. Daskalakis, G. Fanourgakis, S. Myriokefalitakis and M. Kanakidou Oral:Global atmospheric simulations of Ice Nuclei Particles from Marine Organic Aerosols and Dust, COMECAP 2018, 14thInternational Conference on Meteorology,Climatology and Atmospheric Physics, 2018 Alexandroupolis, Greece, October 15-17

Kanakidou M., Myriokefalitakis S., Fanourgakis G., **Chatziparaschos M.**, Tsigaridis, K., Nenes A., Organic aerosols and their impact on biogeochemical cycles and climate 14th iCACGP and 15th IGAC Quadrennial symposium, Takamatsu, Japan, 25-29 September, 2018

Abstract

Aerosol-cloud interactions consist one of the major sources of uncertainty in climate projections according to the recent IPCC report. Ice-nucleating particles (INP), which originate from terrestrial and marine environments, enable ice formation, profoundly affecting the microphysical and radiative properties, lifetimes, and precipitation rates of clouds. The simulated ice crystal concentrations in mixed-phase clouds are affected by uncertainties in the concentration of INP, leading to discrepancies in the climate sensitivity of the models.

The present work aims to investigate the global distribution of ice nucleating particles, identify their major source and aerosol types acting as INP, depending on location and season, and proposed laboratory-derived parameterizations for use in climate models after testing them against ground-based and aircraft observations. The study focuses on the impact of INP in mixed-phase clouds regime.

For this purpose, the 3-dimensional chemistry transport model TM4-ECPL has been used. The model has been further developed to account for INP concentrations from K-feldspar and quartz dust minerals, and organic-rich particles that are ejected into the atmosphere from oceans during bubble bursting or are emitted as terrestrial bioaerosols such as fungi and bacteria.

In this contribution, first we investigate the global and regional importance of quartz as a contributor to INP in the atmosphere relative to K-feldspar, applying state-of-the-art parameterizations based on ice-active surface-site approach for immersion freezing. Additionally, we investigate the impact of different soil mineralogy atlases on the simulated concentrations of INP, by comparing with observations.

The results show that, although K-feldspar remains the most important contributor to INP concentrations globally, affecting mid-level mixed-phase clouds, the contribution of quartz can also be significant. Quartz dominates the lowest and the highest altitudes of dust-derived INP, affecting mainly low-level and high-level mixed-phase clouds. These findings support the inclusion of quartz in addition to K-feldspar as an INP in climate models and highlight the need for further constraining their abundance in arid soil surfaces along with their abundance, size distribution, and mixing state in the emitted dust atmospheric particles.

The present study also evaluated the contribution of terrestrial and marine organic aerosols to the INP concentrations, identifying the dominant INP aerosol precursor per season and

region. Uncertainties in the calculations are determined and some of them are quantified by performing sensitivity calculations.

Additionally, it is found that at relatively warm temperatures (above −15 °C) the majority of INP have typically biological origin, while at lower temperatures and high altitudes INP from mineral dust prevails globally. Marine-derived INP are primarily found over oceans and coastal areas and dominate between 40°-70°S (Southern Ocean), with higher concentrations in regions of high sea spray and oceanic biota activity. Marine INP dominate primary ice nucleation over 600 hPa over the Northern Hemisphere, while dust INP are more abundant elsewhere. Mineral dust-derived INP are primarily found over and downwind desert regions, particularly the Sahara Desert, Gobi Desert and the Arabian Peninsula. INP from dust contribute more to total INP in the mid-latitudes in the Northern Hemisphere than in the Southern Hemisphere due to the location of dust sources and long-range atmospheric transport patterns. INP from terrestrial bioaerosols has the potential to form ice crystals in the NH subtropics at the outflow of continental air. Our simulated INP concentrations predict ∼ 64 % of the observations gathered from different campaigns within 1 order of magnitude and ∼ 79 % within 1.5 orders of magnitude.

Finally, in collaboration with Barcelona Supercomputing Center, the validated in TM4-ECPL dust and marine organic aerosol parameterizations of INP have been introduced in the atmospheric component of the EC-Earth3 Earth System Model and enabled us to provide the first preliminary evaluation of the impact of these INP on cloud cover, ice water path, surface temperature, long and short-wave radiation at the top of the atmosphere.

Overall, this thesis improves our understanding of INP global distribution and INP precursors as well as of the role of INP in the glaciation indirect effect and the broader impact of mixed-phase clouds on climate, with the ultimate goal of providing better parameterizations for use in climate models to improve climate simulations.

Keywords: global 3D chemistry-transport model, TM4, heterogeneous ice nucleation, Ice Nuclei Particles, Marine Organic Aerosol Particles, mineral Dust, Terrestrial Bioaerosols

Περίληψη

Οι αλληλεπιδράσεις μεταξύ των αερολυμάτων και των νεφών αποτελούν μία από τις κύριες πηγές αβεβαιότητας στις κλιματικές προσομοιώσεις σύμφωνα με την διεθνή έκθεση της διακυβερνητικής αναφοράς για το κλίμα (IPCC). Τα σωματίδια που σχηματίζουν πυρήνες συμπύκνωσης πάγου (INP), προέρχονται από χερσαία και θαλάσσια περιβάλλοντα, επηρεάζοντας σημαντικά τις μικρο-φυσικές ιδιότητες, τη διάρκεια ζωής και τους ρυθμούς βροχόπτωσης των νεφών. Οι προσομοιωμένες συγκεντρώσεις κρυστάλλων πάγου σε νέφη μικτής φάσης επηρεάζονται από αβεβαιότητες στη συγκέντρωση των INP, οδηγώντας σε σοβαρές αποκλίσεις στις προγνώσεις του κλίματος από τα διάφορα κλιματικά μοντέλα.

Η παρούσα εργασία στοχεύει στη διερεύνηση της παγκόσμιας κατανομής των σωματιδίων συμπύκνωσης πάγου. Επικεντρώνεται στον εντοπισμό των κύριων πηγών τους και τα είδη των αερολυμάτων που δρουν ως INP, ανάλογα με την τοποθεσία και την εποχή χρησιμοποιώντας πειραματικές παραμετροποιήσεις, και προτείνοντας την χρήση τους σε κλιματικά μοντέλα μετά τη σύγκρισή τους με εναέριες και επίγειες μετρήσεις πεδίου. Η μελέτη αυτή επικεντρώνεται στον προσδιορισμό της επίπτωσης των INP σε νέφη μικτής φάσης.

Για το σκοπό αυτό έχει χρησιμοποιηθεί το τρισδιάστατο μοντέλο μεταφοράς και χημείας TM4-ECPL. Το μοντέλο αναπτύχθηκε περαιτέρω για να λαμβάνει υπόψη τις συγκεντρώσεις INP από ορυκτά σκόνης όπως άστριος και χαλαζίας, καθώς και σωματίδια πλούσια σε οργανικά που εκπέμπονται στην ατμόσφαιρα είτε από τους ωκεανούς είτε από τις ηπείρους ως χερσαία βιο-αερολύματα όπως μύκητες και βακτήρια.

Στην μελέτη αυτή πρώτα διερευνήσαμε την επίδραση της ορυκτής σκόνης στην παγκόσμια κατανομή των πυρήνων συμπύκνωσής πάγου, εξετάζοντας την συνεισφορά του χαλαζία σε σχέση με τον εμπλουτισμένο με κάλιο άστριο. Ορυκτά τα οποία αποτελούν κύρια συστατικά της αιωρούμενης σκόνης. Για τον σκοπό αυτό, εφαρμόσαμε παραμετροποιήσεις αιχμής με βάση την προσέγγιση της ενεργού επιφανείας των σωματιδίων κατά την δημιουργία πάγου με εμβάπτιση. Επιπρόσθετα, διερευνήσαμε την επίδραση διαφορετικών ορυκτολογικών δεδομένων εδάφους, που χρησιμοποιεί το μοντέλο, για τις προσομοιωμένες συγκεντρώσεις των INP, συγκρίνοντας τες με παρατηρήσεις.

Τα αποτελέσματα δείχνουν ότι, αν και ο άστριος παραμένει ο πιο σημαντικός παράγοντας που συμβάλλει στις συγκεντρώσεις INP παγκοσμίως, επηρεάζοντας τα νέφη μικτής φάσης

μεσαίου ύψους, η συμβολή του χαλαζία μπορεί επίσης να είναι σημαντική. Ο χαλαζίας κυριαρχεί σε χαμηλά και υψηλά υψόμετρα, επηρεάζοντας κυρίως τα ψυχρά νέφη και τα νέφη μικτής φάσης.

Η παρούσα μελέτη αξιολόγησε επιπλέον τη συμβολή των χερσαίων και θαλάσσιων οργανικών αερολυμάτων στις συγκεντρώσεις INP, προσδιορίζοντας τα κυρίαρχα πρόδρομα αερολύματα που δρουν ως INP ανά περίοδο και περιοχή. Οι αβεβαιότητες στους υπολογισμούς προσδιορίστηκαν και ορισμένες από αυτές ποσοτικοποιήθηκαν από υπολογισμούς ευαισθησίας.

Τα ευρήματα της έρευνας υποστηρίζουν την αναγκαιότητα συμπερίληψης του χαλαζία στα κλιματικά μοντέλα για τον υπολογισμό της αριθμητικής συγκέντρωσης των INPs στην ατμόσφαιρα, υπογραμμίζοντας την ανάγκη για περαιτέρω προσδιορισμό της αφθονίας τους σε ερημικές περιοχές, την κατανομή μεγέθους τους και την κατάσταση ανάμειξης τους στα εκπεμπόμενα σωματίδια σκόνης της ατμόσφαιρας.

Από τα ευρήματα της παρούσας έρευνας, διαπιστώθηκε ότι σε σχετικά υψηλές θερμοκρασίες (πάνω από -15 °C) η πλειονότητα των INP είναι βιολογικής προέλευσης, ενώ σε χαμηλότερες θερμοκρασίες και μεγάλα υψόμετρα επικρατούν παγκοσμίως INP από ορυκτή σκόνη. Τα INP που προέρχονται από θαλάσσια οργανικά βρίσκονται κυρίως πάνω από απομακρυσμένους ωκεανούς και σε παράκτιες περιοχές, και κυριαρχούν μεταξύ 40°-70°N (Νότιους Ωκεανούς). Υψηλές συγκεντρώσεις των INPs από θαλάσσια οργανικά παρατηρούνται σε περιοχές με υψηλές συγκεντρώσεις θαλάσσιων αερολυμάτων και έντονη βιολογική δραστηριότητα. Τα θαλάσσια INP κυριαρχούν στον πρωτογενή σχηματισμό πάγου πάνω από τα 600 hPa στο βόρειο ημισφαίριο.

Τα INP που προέρχονται από ορυκτή σκόνη παρατηρούνται κυρίως πάνω και κατάντη από ερημικές περιοχές, ιδιαίτερα στην έρημο Σαχάρα, στην έρημο Γκόμπι και στην Αραβική Χερσόνησο. Τα INP από τη σκόνη συμβάλλουν περισσότερο στα συνολικά INP στα μεσαία γεωγραφικά πλάτη στο βόρειο ημισφαίριο παρά στο νότιο λόγω της θέσης των πηγών σκόνης και των μοτίβων ατμοσφαιρικών μεταφορών μεγάλης εμβέλειας. Το INP από τα χερσαία βιο-αερολύματα μπορούν να σχηματίσουν κρυστάλλους πάγου στις υποτροπικές περιοχές νοτίου ημισφαίριου κατά τις εκροές του ηπειρωτικού αέρα. Οι προσομοιωμένες συγκεντρώσεις INP προβλέπουν ~ 64 % των παρατηρήσεων που συγκεντρώθηκαν από διαφορετικές εκστρατείες εντός 1 τάξης μεγέθους και ~ 79 % εντός 1.5 τάξης μεγέθους.

Τέλος, σε συνεργασία με το Barcelona Supercomputing Center, οι επικυρωμένες στο TM4-ECPL παραμετροποιήσεις της σκόνης και του θαλάσσιου οργανικού αερολύματος των INP εισήχθησαν στην ατμοσφαιρική συνιστώσα του Μοντέλου Γήινου Συστήματος EC-Earth3 και μας επέτρεψαν να παράσχουμε την πρώτη προκαταρκτική αξιολόγηση του αντίκτυπου αυτών των INP στη νεφοκάλυψη, τη διαδρομή του νερού του πάγου, την επιφανειακή θερμοκρασία, την ακτινοβολία μεγάλου και μικρού μήκους κύματος στην κορυφή της ατμόσφαιρας.

Συνοψίζοντας, η παρούσα διατριβή αποσκοπεί στη βελτίωση της κατανόησης του ρόλου των INP στην ατμόσφαιρα, στην πιο ρεαλιστική αναπαράσταση της έμμεσης επίδρασής τους στον σχηματισμό παγοκρυστάλλων, καθώς και στην επίδρασή τους στα νέφη μικτής φάσης και στο κλίμα γενικότερα, με απώτερο στόχο τη χρήση καλά τεκμηριωμένων παραμετροποιήσεων σε κλιματικά μοντέλα για την βελτίωση των προσομοιώσεων κλίματος.

Λέξεις κλειδιά: Πυρήνες συμπύκνωσης πάγου, Παγκόσμιες προσομοιώσεις, ατμοσφαιρικό μοντέλο, τρισδιάστατο μοντέλο χημείας και μεταφοράς παγκόσμιας κλίμακας, TM4-ECPL, θαλάσσια αερολύματα, ερημική σκόνη, ετερογενής πυρηνοποίηση πάγου, βιο-αερολύματα

Contents

1. Introduction - Aerosol Particles, Health and Climate

Atmospheric aerosols are an essential part of Earth's atmosphere. Aerosols consist of solid, liquid, and gaseous material. They are of varying chemical complexity and size. Atmospheric scientists define aerosols as solid or liquid particles suspended in the atmosphere, excluding all forms of hydrometeors, such as cloud droplets, ice crystals, raindrops, snowflakes, and graupel. In this thesis, the terms particle and aerosol will be both used together to describe all suspended solid matter.

In this section, we examine the characteristics of aerosol particles in the atmosphere. The main focus is on the microphysical and chemical properties of these particles, and how they can vary depending on their sources, photochemical processes, and transport through the atmosphere.

1.1 Aerosol Sources

The variability in the amount and properties of aerosols make them difficult to be quantified as individuals, which is why the focus is on characterizing a population of aerosols. To do this, it's important to characterize the size distribution, chemical composition, and shape of the particles within the population. Aerosols are often categorized into different groups based on their properties.

To differentiate aerosol particles based on their origin, aerosols are classified base on the pathway through which they are found in the atmosphere which can be either primary emissions (formed directly at the source) or secondary source (formed through chemical reactions in the atmosphere followed by gas-to-particle conversion):

1. **Primary aerosols** are directly emitted into the atmosphere as particles and originate from wind friction on oceanic or land surfaces and incomplete combustion, forming particles ranging from a few hundred nanometers (accumulation mode) to several micrometers in size (coarse mode). Coarse particles can also be generated by wind and vehicles acting on the ground or roads. They are also formed within tenths of a second or a few seconds after combustion from sources such as motorized vehicles,

chimneys, wood burning, etc., resulting in particles around 10 nm in diameter (nucleation mode) or 40-100 nm in diameter (Aitken mode).

2. **Secondary aerosols**, on the other hand, are not emitted as particles but formed through the nucleation of gases during gas-to-particle conversion, creating particles with diameters below 10 nm (nucleation mode). The chemical composition of the aerosols usually indicates whether they are primary or secondary. The condensation of gases onto pre-existing (larger) particles can also be considered within this definition.

Aerosols can vary in their properties depending on the location and environment, and can be classified as urban, semi-urban, continental, desertic, marine, volcanic or stratospheric. Although this categorization is not perfect, as aerosols can be transported far from their emission sources, it can still be useful when local effects are dominant.

Additionally, aerosols can be classified based on their source of origin into natural or anthropogenic. Natural sources include emissions from oceans, soils, vegetation, fires, and volcanoes. Anthropogenic sources are mainly from burning fossil fuels, biofuels, other fuels, and human-caused fires. Industrial activities, transportation, heating, and cooking in developing countries also contribute to anthropogenic aerosol emissions, as well as primary aerosols from industrial dust and arable dust in agriculture.

All above classifications can be used together for a more comprehensive description, with primary and secondary particles having the potential to be of natural/biogenic or anthropogenic origin.

On a global level, natural emissions make up 70-90% of the mass emitted particle fluxes (Delmas et al., 2005). Some significant natural sources of particles include soil and rock fragments, volcanic eruption, sea spray, biomass burning, and chemical reactions with natural gas emissions. Table 1 provides a range of emission estimates of particles from natural and anthropogenic sources worldwide. Human activities primarily contribute to particulate matter emissions from four sources: fuel combustion, industrial processes, non-industrial fugitive sources (such as roadway dust from paved and unpaved roads, wind erosion of croplands, construction, etc.), and transportation sources (like cars, etc.).

Table 1: Approximative emission fluxes from different types of primary aerosols and gaseous precursors of secondary aerosols. ((Boucher, 2015 except if noted differently)

Source	Estimated flux (per year)	
Natural		
Primary		
Mineral dust	130- 5000 Tg	(Kok et al., 2023, 2021)
Seasalt	3140-3860 Tg	(Weng et al., 2020)
Biomass burning aerosols	20-35 Tg	(Boucher, 2015)
Biogenic aerosols	62- 123 Tg	(Hoose et al., 2010; Myriokefalitakis et al., 2017)
Including bacteria	0.75-28 Tg	(Hoose et al., 2010; Jacobson and Streets, 2009)
Including spores	0.04-3.7 Tg	(Janssen et al., 2021)
Including pollen	47-84 Tg	(Hoose et al., 2010; Burrows et al., 2009b)
Secondary		
Dimethylsulphide (DMS)	17.6–34.4 Tg S	(Hulswar et al., 2022; Lana et al., 2011)
Volcanic SO_2	6-20 Tg S	
Terpenes	40-400 Tg	
Anthropogenic		
Primary		
Industrial dust	40-130 Tg	
Biomass Burning	50-90 Tg	
Black carbon (from fossil fuel)	6-10 Tg	
Organic carbon (from fossil fuel)	10-30 Tg	(Andreae and Merlet, 2001; Boucher, 2015)
Secondary		
SO_2	70-90 Tg S	
Volatile Organic compounds (VOCs)	100 - 563 Tg C	(Weng et al., 2020; Boucher, 2015)
NO_X	20-50 Tg N	
NH_3	30-40 Tg N	

C carbon, S sulfur, N nitrogen

The following text will discuss the major sources of aerosols, both natural and anthropogenic, focusing on both the primary emissions and their precursor emissions.

There are two main natural sources of atmospheric dust - mineral and volcanic.

- **Mineral dust** originates from the wind affecting soil particles. The largest sources are located in arid and semi-arid regions, covering approximately one-third of the world's land surface. The biggest source is in the Sahara-Sahel region of northern Africa, while central Asia (Gobi Desert) is the second largest source globally. However, there is a large uncertainty range in the estimates of global dust emissions, which can range from 130 to 5000 Tg per year (Kok et al., 2021b, 2023), due to the complexity of the processes that lead to dust emissions into the atmosphere. The emission rate is influenced by factors

such as wind speed, the type of surface, and the particle size. Dust particles typically stay in the atmosphere for around 2 weeks and can travel long distances. For example, Saharan dust often reaches the Caribbean and Europe, while dust from Asia can be detected on the west coast of North America. Additionally, with urbanization worldwide in recent decades **anthropogenic dust** emissions due to heavy urban construction, off-road vehicle and transportation have been increasing. These activities can create large amounts of dust, which can have significant impacts on both human health and the environment. Anthropogenic dust can contain a variety of harmful substances which can cause respiratory issues. Significant direct anthropogenic dust contributions to pollutants have been demonstrated, particularly over India and northern China. The total area of potential anthropogenic dust sources was found slightly higher than that of natural dust sources.

- **Volcanic** sources have temporally variable emissions that depend on the frequency of eruptions that release volcanic ash into the atmosphere. The primary aerosols are usually larger than one micron and have a short lifetime, unless they are expelled at high speeds and reach the free troposphere or higher. At the same time, these eruptions also release gases that are rich in sulfur compounds, such as SO_2 and H_2S, with annual emissions ranging from 6 to 20 Tg of sulfur per year. The oxidation of these precursor gases in the atmosphere leads to the formation of sulfate aerosols, which can have a lifetime of a few weeks to several months or even years, depending on the altitude at which they are emitted.
- **Marine** sources are the main contributors of aerosols, releasing between 1000 to 6000 Tg of sea spray each year. These aerosols are formed from wind speed on the surface of oceans and the size of the sea spray can range from 20 nanometers to 10 micrometers. The majority of the marine salts in these sprays are in the supermicron fraction, meaning particles larger than 1 micrometer.
- **Biogenic** sources emit particles released from natural sources, including pollens, spores, bacteria, and viruses. The size of these particles can range from a few nanometers to several microns. The organic material suspended by marine life and forested areas can also result in emissions of precursor gases, such as volatile organic compounds and nitrogen oxides. One example is dimethyl sulfide (DMS) which is primarily emitted by phytoplankton and bacteria in the ocean, but microbial uptake and photochemical degradation often control the removal of this compound (Simó and Pedrós-Alió, 1999). Oxidation of DMS in the atmosphere by hydroxyl, nitrate and halogen radicals produces

many degradation products including CO_2, COS, dimethyl sulfoxide, dimethyl sulfone, organic oxyacids of sulfur, and sulfate (Bentley and Chasteen, 2004).

- **Natural Biomass Burning** refers to the burning of vegetation over land which releases combustion products into the atmosphere. This is a major source of emissions, including volatile organic compounds, nitrogen oxides, sulfur dioxide, and ammonia. The quantity and type of emissions from a biomass fire vary depending on factors such as the type of vegetation, temperature, humidity, and wind speed. Emissions from biomass burning include methane, carbon monoxide, organic and black carbon aerosols, as well as nitrogen oxides contributing 7.1 Tg yr^{-1} globally compared to 33 Tg yr^{-1} from fossil fuel burning.
- **Anthropogenic Biomass Burning** sources such as wood-burning, represent emissions of 50 to 90 Tg yr^{-1} on a global scale (Table 1). In terms of primary aerosol emissions, the anthropogenic BB source appears to be superior to the natural source. In addition, these primary aerosols have predominantly submicron diameters (Rau, 1989) and a supermicron fraction (Park et al., 2003).

1.2 Chemical composition

The chemical composition of an aerosol is a significant factor that affects its hygroscopicity (the ability to absorb water and grow in size as humidity increases), its susceptibility to being scavenged by precipitation, its potential to function as a cloud or ice nucleus, and its optical properties. Previously referred the various aerosol types, including mineral aerosols (inorganic), sea spray (primarily inorganic with some organic components), biogenic aerosols (organic-dominant), industrial aerosols (a combination of inorganic and organic materials, with volatile and nonvolatile components), and biomass burning aerosols (organic-dominant, with both volatile and nonvolatile components and black carbon). This section will introduce the concept of mixing before deepening into the chemical composition of atmospheric aerosols.

1.3 Aerosol Mixture

It is common to differentiate between two types of aerosol mixtures : **external** and **internal** (Boucher, 2015). Conceptual Figure 1 displays three different aerosol mixtures, represented by circles that correspond to the size distribution of the particles (x-axis). The color of the circles indicates the variable degrees of mixture. In an external mixture (Figure 1a), particles are chemically pure, but the mixture can have different chemical compositions. As a result, it is possible to differentiate particles according to their distinct chemical composition, such as black carbon, ammonium sulfate, sodium chloride, and organics. For external mixtures, a different size distribution can be assigned to each aerosol type. On the other hand, in internal mixtures, different chemical species are mixed within each particle. In the case of a perfect internal mixture, all particles have the same chemical composition and can be described by a single size distribution.

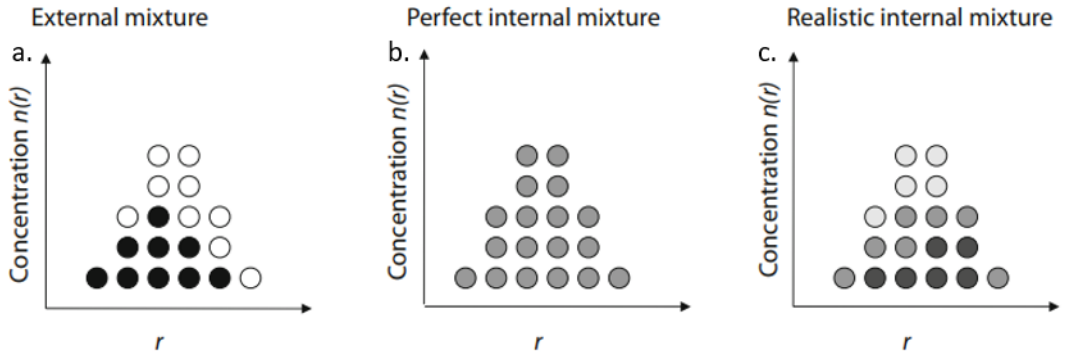

Figure 1: Schematic representation of three different aerosol mixtures.

However, it's important to note that external and internal mixtures are just conceptual models and the reality is somewhere in between these two extremes. The more realistic internal mixture is comprised of internally-mixed particles but with varying degrees of mixing for a given aerosol size and across the size distribution. Typically, the chemical composition of aerosols varies with both size and within a size class. Mixing in aerosols can occur through coagulation of particles with different chemical compositions, both outside and inside clouds, and through the condensation of semi-volatile or low-volatility compounds on pre-existing particles. For instance, non-soluble primary aerosols like black carbon and mineral aerosols can be coated with soluble species, changing their properties such as hygroscopicity(Stevens and Dastoor, 2019) or optical properties (absorption/scattering).

1.3.1 Inorganic Aerosols

The presence of inorganic substances in aerosols is very common, for instance sea spray which primarily contains sodium chloride or sulphate aerosols which have variable chemical composition depending on the level of neutralization of sulphuric acid. The chemical composition of sulphate can range from pure sulphuric acid (H_2SO_4) to ammonium bisulphate (NH_4HSO_4) and ammonium sulphate $(NH_4)_2SO_4$. In addition to sulphate (SO_4^{2-}) and ammonium ions, nitrate ions (NO_3^-) can be found in aerosols, creating a mixture of SO_4^{2-}–NH_4^+ –NO_3^-. The physical, chemical, and optical properties of inorganic aerosols, such as density, water uptake, and refractive index, are well understood through measurements and modeling of inorganic mixtures (Wexler, 2002). This is challenging for mineral dust that is a mixture of several minerals, not all of them taken into consideration in numerical models. Inorganic aerosols are highly hygroscopic, with the exception of pure dust, and scatter solar radiation. Soil dust aerosols play a vital role in the climate system by interacting with both short and long-wave radiation (Granados-Muñoz et al., 2019), acting as cloud condensation nuclei or ice nuclei (Kumar et al., 2009; Chatziparaschos et al., 2023), impacting atmospheric chemistry (Tang et al., 2017), and participating in biogeochemical cycles by supplying nutrients like iron and phosphorus (Myriokefalitakis et al., 2022; Usher et al., 2003). The impact of dust on these processes is determined by its physical and chemical characteristics, which are not uniform but rather shaped by the diverse mineral composition found in different regions. The proportion of minerals present in dust varies significantly depending on the source area, displaying considerable geographical diversity (Gonçalves Ageitos et al., 2023).

1.3.2 Black Carbon Aerosols

Black carbon (BC) is a special type of aerosol that is formed when carbon-rich fuels are burned in low oxygen environments, such as incomplete combustions of biomass, biofuels, and fossil fuels. The combustion process produces small spheres made of graphite layers and high C:H ratio compounds, which then aggregate to form black carbon chains (Bond et al., 2013). The exact density of black carbon is not known and it is estimated to range from 1.7 to 1.9 g cm^{-3} (Bond and Bergstrom, 2006). The size of black carbon particles varies depending on the source, but it is typically around 100 nm. BC particles are identified as a strong light-absorbing

atmospheric component and result in positive radiative forcing at the top of atmosphere, driving global warming (Schwarz et al., 2008).

During atmospheric transport, black carbon becomes coated by organic carbon and sulphate, which change its physical and optical properties. The coatings on BC can lead to its absorption enhancement, and its complicated mixing state, particularly its internally mixing with Brown Carbon (BrC), has been one of the biggest uncertainties in an estimate of radiative forcing of aerosols (Curci et al., 2019). Nonabsorbing coatings on BC particles can enhance BC absorption via the well-known lensing effect (Zhang et al., 2021). Additionally, the large specific surface area of BC particles creates a potential for heterogeneous reactions with trace gases (such as volatile halocarbons) in the atmosphere (Qiu et al., 2012) thus heavily impacting atmospheric chemistry and air quality.

The coatings on BC particles can modify its hygroscopicity, by altering the physical, chemical, and optical properties. These changes can include adjustments to particle size and morphology development, which can ultimately affect aerosol radiation, cloud and ice nuclei formation. The contribution of organic components to the overall hygroscopicity in BC particles is considered very important (Wang et al., 2020).

1.3.3 Organic Aerosols

Organic matter has been known to exist in aerosols since a long time, but it took many years of research to accurately measure its concentration and composition. Advances in mass spectrometry, both on bulk and individual aerosol particles, enable substantial progress in understanding and characterizing organic aerosols. The composition of organic aerosols is complex and since they contain a wide range of chemical compounds, making it difficult to fully monitor and represent their complexity. To simplify the characterization of these compounds, it is important to distinguish primary and secondary organic aerosols (see above). Secondary organic aerosols are created from volatile organic compounds that are oxidized in the atmosphere, some of which can evaporate from primary organic aerosols. The chemical composition of organic aerosols that come from burning fossil fuels differs from that of organic aerosols from biomass burning. Organic aerosols from fossil fuels are largely composed of polycyclic aromatic hydrocarbons (PAHs) and nitrated PAHs, which are produced through incomplete combustion of fossil fuels (Tsiodra et al., 2021). On the other hand, among

all organic biomass burning markers, levoglucosan (1, 6 – anhydro-β-D-glucopyranose) is the most suitable and well recognized due to its high abundance and longer stability in different environmental conditions(Bhattarai et al., 2019). Levoglucosan and its isomers (mannosan and galactosan) are also associated with biomass burning (open and domestic fires) in general and in particular with thermal pyrolysis of cellulose and hemicellulose (Fabbri et al., 2009).

Organic aerosols containing oxygen-rich compounds are referred to as oxygenated organic aerosols and the O:C ratio in organic aerosols is a useful indicator of their chemical composition. As organic aerosols age in the atmosphere, they become more oxygenated, less volatile, and more hygroscopic, and there is a clear positive relationship between the O:C atomic ratio and the hygroscopicity of the aerosol (Jimenez et al., 2009). There is also an inverse relationship between the volatility of the organic aerosol and the O:C atomic ratio.

Different types of volatile organic compounds (VOCs) are categorized by the two ways on the bases of boiling points of chemicals and of sources. On the base of boiling points, very volatile organic compounds (VVOCs) are very volatile and have boiling point 0 to 50-100 °C. Examples are methyl chloride, propane etc. VOCs include carbon have boiling point less than 250 °C at the 101.3 kPa pressure. Examples are acetone, ethanol, toluene etc. Semi volatile organic compounds (SVOCs) have higher boiling point than water (250- 390 °C). Examples are polyaromatic hydrocarbons, phenol etc. Classification of VOCs with respect to their characteristics and some examples are depicted in the Table 2.

Table 2: Classification of volatile organic compounds(Menezes et al., 2013)

Characteristic	**Class**	**Examples**
Volatility	Very volatile (boiling point < 100°C)	Alkanes, alkenes, alkynes from C_2 to C_8
	Volatile (75 ± 25°C < boiling point < 250 ± 10°C)	Hydrocarbons, saturated and unsaturated aldehydes, ketones, esters, alkyl halides, and alcohols
	Semivolatile (250 ± 10°C < boiling point <390 ± 10°C)	Phthalic-acid esters, polyaromatic hydrocarbons, polychlorinated biphenyls
	Nonvolatile (> 390 ± 10°C)	Particulate organic matter
Impact on ecosystems	High potential for generating photochemical oxidants	Alkanes, alkenes, alkynes from C_2 to C_8, xylenes, arenes, and terpenes
	Highly capable of destroying the stratospheric ozone layer	Chlorofluorocarbons, halocarbons, chlorinated hydrocarbons
	High positive or negative global warming potential	Methane

1.4 Geographic Distribution of Aerosol Chemical Composition

It is difficult to determine the chemical composition of aerosols from space, so the information about it is obtained mainly from in-situ measurements made by a vast network of ground-based stations. The measurement of organic aerosols is challenging because of their chemical complexity, volatility, and the requirement for immediate analysis. In contrast, the measurement of inorganic aerosols is relatively straightforward as they are typically more stable. Figure 2 shows the mass concentrations (μg m^{-3}) of seven major chemical species of the atmospheric aerosol in different regions of the world (Boucher, 2015) summarizing the mass concentration of the major aerosol components for particles with diameter smaller than 10 μm (PM_{10}). Figure 3 depicts the global population-weighted $PM_{2.5}$ (Particulate matter with an aerodynamic diameter less than 2.5 microns) composition as derived by combining aerosol optical depth retrieved from the MODIS (Moderate Resolution Imaging Spectrometer) and MISR (Multi-angle Imaging Spectro-Radiometer) satellite instruments, with coincident profile and composition information from the GEOS-Chem global chemical transport model (Philip et al., 2014).

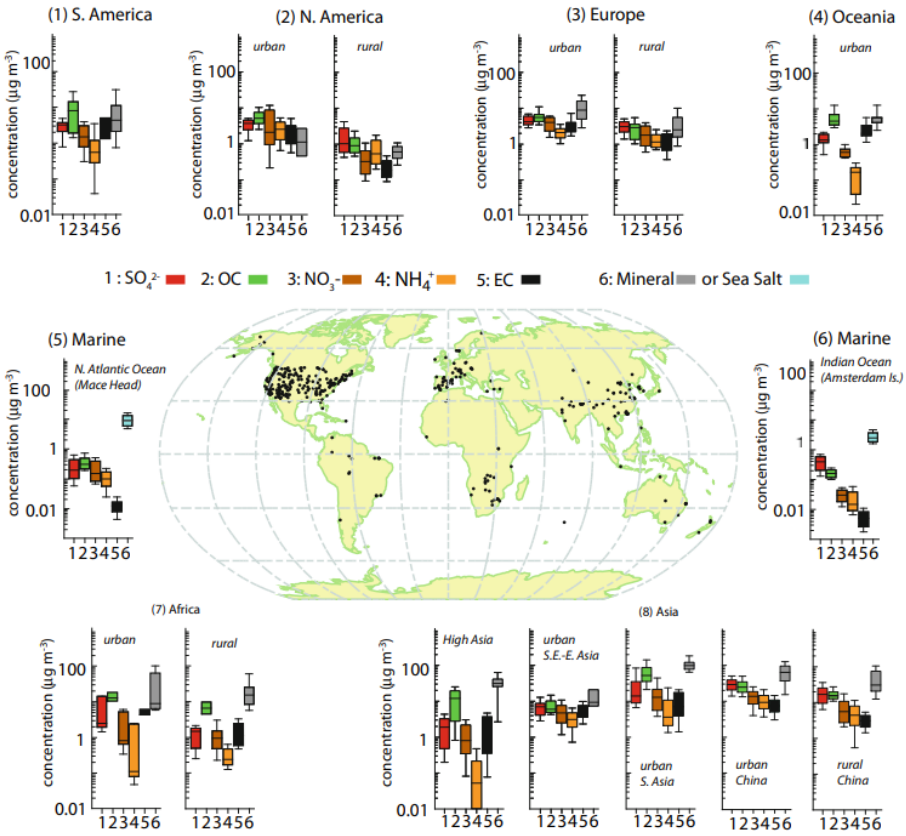

Figure 2: Bar chart plots summarizing the climatology mass concentration (µg m^{-3}) of seven major aerosol components for particles with diameter smaller than 10 µm, from various rural and urban sites. The locations of the stations are shown on the central map. For each area, the panels represent the median, the 25th to 75th percentiles (box), and the 10th to 90th percentiles (whiskers) for each aerosol component. (Reproduced from Boucher et al. (2014)*, © IPCC)*

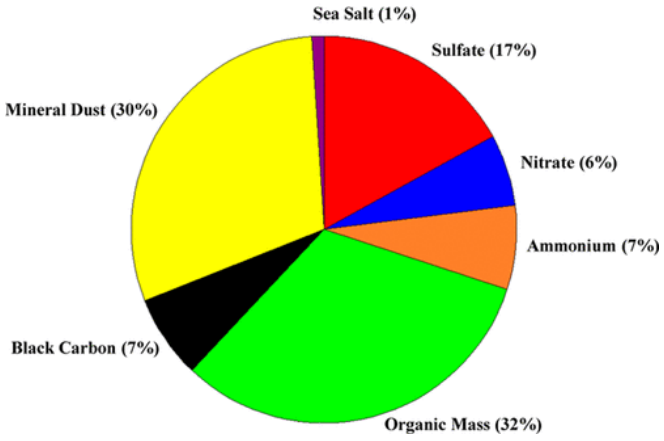

Figure 3: Global population-weighted $PM_{2.5}$ composition (Philip et al., 2014)

It appears very clearly that both inorganic and organic fractions of the aerosol are important and one or the other can dominate the mass concentration. Sulphate is an important component of the inorganic fraction of the aerosol, and is systematically accompanied by ammonium. Nitrate can be present in very variable quantities but concentrations decrease rapidly increasing the distance from the source. Mineral dust dominates over and downwind the emitting desertic regions. Sea-salt, largely composed of sodium chloride, dominates in marine environment.

1.5 Microphysical properties

The wide range of sources and processes involved in aerosol formation leads to significant variability in the size, distribution, and shape of aerosol particles. These particles can range in size from just a few nanometers to tens of microns, and can be expressed in terms of number, mass concentration, or surface/volume. Accurately measuring and characterizing the size distribution of aerosols is crucial for understanding their sources and the effects of different atmospheric processes on them. It is possible to distinguish several aerosol classes according to their size (e.g., Whitby (1978)).

More specifically, one can observe up to about five size modes, here defined from the smallest to the largest: the nucleation mode, the Aitken mode (named after the Scottish meteorologist and physicist John Aitken), the accumulation mode (so named because mass accumulates in this size range by coagulation and condensation), the coarse mode, and the super-coarse mode (that is not depicted in Figure 4).

The representation of the most widespread particle size distribution (PSD) is described by the log-normal statistical distribution. The variation of the number of particles as a function of the logarithm of the diameter is given according to Seinfeld and Pandis (2006) as:

$$\frac{dN}{dlogD} = \sum_i \frac{Ni}{log\sigma\sqrt{2\pi}} \exp\left(\frac{(log\ Di\ -\ log\ \overline{D})^2}{2\,.log\ \sigma}\right) \qquad \textit{Eq. 1}$$

Where σ = standard deviation Di = midpoint particle diameter of the i^{th} bin, Ni = number of particles in group i having a midpoint size Di, $\overline{D}$ =mean diameter

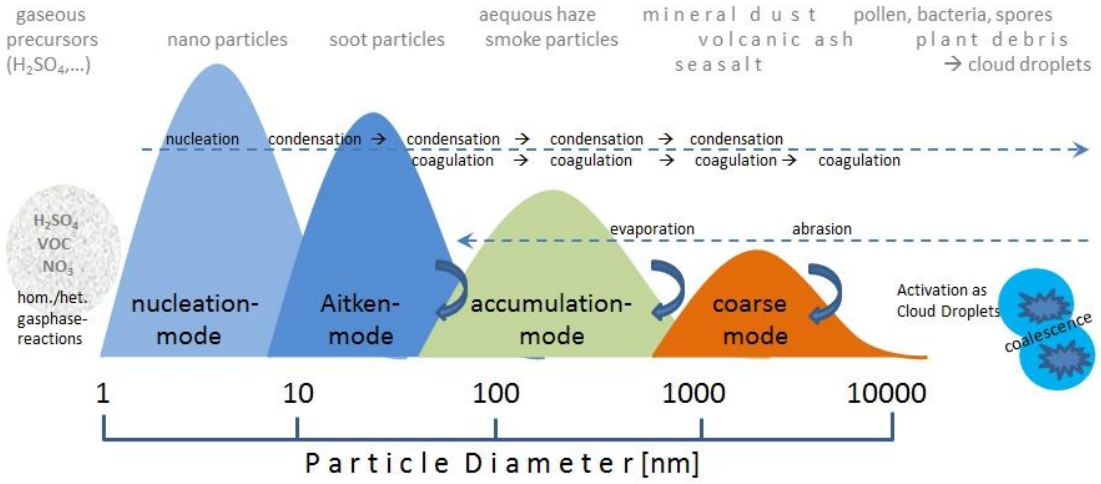

Figure 4: Schematic multi-modal particle size distribution (based on number concentration) with typical transformations and example particle types within each mode[1].

Additionally, the combination of nucleation and Atken modes usually called as ultrafine particles (UFPs, particles with an aerodynamic diameter of 0.1 µm (100 nm)). Each of these modes corresponds, at least in principle, to a relative maximum of the number aerosol size distribution (Figure 4). The number of modes that can be detected in the observations can however vary, but it is usual to be able to distinguish three or more modes. The nucleation and Aitken modes appear clearly in the aerosol number distribution, with particle radius in the range from a few nanometres to 0.05 µm.

The accumulation mode appears generally in the aerosol surface distribution, but is sometimes also visible in the aerosol number distribution. It is comprised of particles with radii ranging between 0.05 and 0.5 µm. The upper limit of the accumulation mode is generally considered to be 1 µm (Seinfeld and Pandis, 2006) although other studies reported the value of 2 µm (Jacobson, 2005). The coarse mode generally dominates the aerosol volume and mass size distribution. It includes particles beyond 1µm diameter or 2.5µm. Aerosols with larger diameters up to 10µm belong to the coarse mode, mainly consisting of primary particles of natural origin such as mineral dust pollen or sea salts. A potentially important super-coarse mode (10-100µm) can be found close to the sources but is generally absent from a more aged aerosol population, i.e., aerosol particles physico-chemically modified during transport in the

[1] Figure adapted from https://www.dwd.de/EN/research/observing_atmosphere/composition_atmosphere/aerosol/cont_nav/particle_size_distribution_node.html

atmosphere. Sometimes, the Aitken and accumulation modes are referred together as the fine mode but the terms are used somewhat loosely and interchangeably.

During atmospheric transport, aerosol particles can undergo changes and move from one mode to another due to physical and chemical processes affected by weather conditions. For example, the particles can absorb gases from their surroundings and grow in size through condensation, or they can merge together and get bigger through coagulation. On the other hand, processes such as abrasion or evaporation can cause the particle size to decrease (transition from liquid to gaseous state, e.g. NH_4NO_3).

1.6 Aerosols and Health

The presence of atmospheric aerosol particles has been linked to a number of negative health effects. Studies have shown that exposure to high levels of airborne particulate matter, including both fine and coarse aerosols, is associated with increased risk of respiratory and cardiovascular disease (Pope, 2000; Brook et al., 2004).

In general, short-term and long-term epidemiological studies have shown that an average increase in mortality of about 1% is expected at an elevation of PM_{10} levels of about 10 μgm^{-3} (for PM_{10} concentrations normally found in ambient environments, Pope, 2000). Besides mortality, increases in hospitalization and disease are dependent on PM levels. The main diseases associated with aerosol particles are cancer, asthma, and cardiovascular and pulmonary diseases. Many epidemiological studies rely on PM_{10} or $PM_{2.5}$ (total particle mass below 2.5 µm diameter) as an indicator of particle pollution. However, these indicators can have several sources at the same time, at one measurement location, e.g., exhaust emissions from traffic, long-distance-transported pollutants, and dust generated by vehicles. Therefore, health effects resulting from different sources should be differentiated and the relation between health effects and type of aerosol may be stronger when other more source-specific indicators are considered.

More specifically, the size and shape of aerosol particles also impact their ability to penetrate deep into the lungs and cause damage to respiratory and cardiovascular systems (Nazaroff, 2004). These particles are deposited into the airways in the head region when inhaled. "Fine particles," are 2.5 micrometers ($PM_{2.5}$) in diameter or smaller and when inhaled they are deposited into lung airways or the tracheobronchial region (Figure 5).

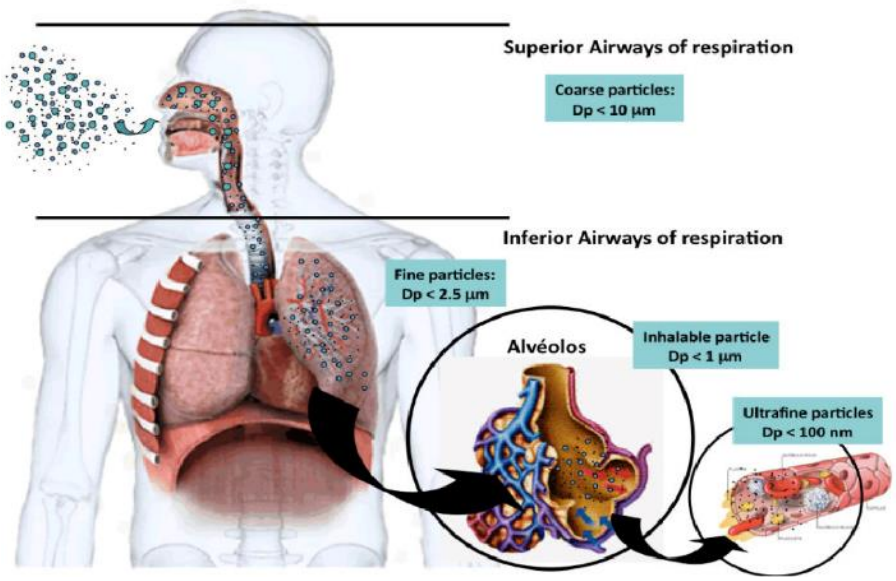

Figure 5: Represents the areas where particulate material from incomplete combustion processes is deposited in the body.(Nani Guarieiro, 2013)

In addition, research has also suggested that the chemical composition of aerosol particles plays a significant role in determining their health effects. For example, particles that contain heavy metals, polycyclic aromatic hydrocarbons (PAHs) (Tsiodra et al., 2021), or other toxic substances are believed to pose a greater risk to human health compared to particles without these components (Xu et al., 2020).

To mitigate the potential health risks associated with atmospheric aerosol particles, it is important to understand the sources and characteristics of these particles, as well as the mechanisms by which they impact human health. This knowledge can then be used to develop and implement effective air quality control strategies, such as source control and regulation of emissions from industrial and transportation sources (Kim et al., 2015). In addition, monitoring and assessment of airborne particulate matter can be used to track changes in particle composition and size, and to identify areas where further research is needed to better understand the health impacts of atmospheric aerosols (Wang et al., 2020b).

1.7 Aerosol–Cloud–Radiation Interactions

The interactions between aerosols, clouds, and electromagnetic radiation are illustrated in Figures 6 and 7. Aerosols interact with electromagnetic radiation that propagates in the atmosphere in several ways. Solar (shortwave) radiation that interacts with aerosols is

anisotropically deflected in all directions, which is referred to as scattering (Figire 6a-b). This leads to localized cooling since less solar radiation reaches the surface. The aforementioned aerosol interactions that are referred as *aerosol direct effect* (Figure 6), note that the new terminology used is *aerosol-radiation interactions* (Boucher, 2015).

Some aerosols also absorb solar radiation, converting it into heat. This heats the aerosol layer but the surface which receives less solar radiation, can cool locally (Figure 6c). However, at larger scale net warming of the surface and atmosphere occurs due to atmospheric circulation and mixing processes that redistribute thermal energy (Figure 6d). The absorption of solar radiation by aerosols modifies the vertical temperature profile (Figure 6c). This impacts the relative humidity, atmospheric stability, and therefore cloud formation. Aerosols can also scatter and absorb terrestrial (longwave) radiation emitted by the Earth's surface and atmosphere and can emit this type of radiation. These effects have traditionally been called the aerosol semi-direct effect, but it can also be seen as a rapid adjustment of the atmospheric state that follows *aerosol–radiation interactions (ari)*.

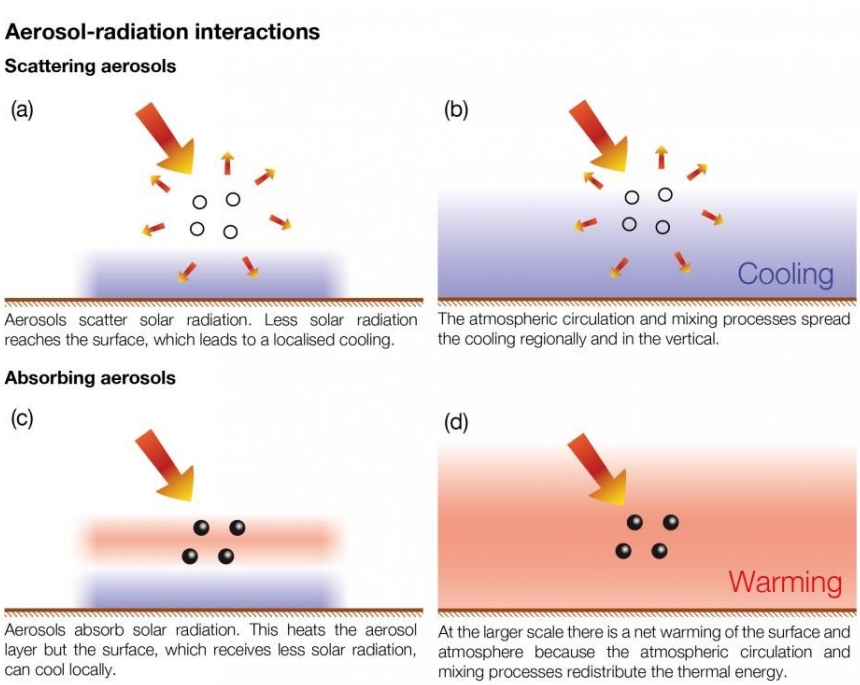

Figure 6: Illustration of aerosol-radiation interactions as illustrated by the IPCC (2013)

Absorbing aerosols that deposit onto snow and ice surfaces, thus making these surfaces less reflective (more absorbing). This contributes to warm the surface and thus the climate system.

This effect is known as the aerosol on snow effect but can be categorized as part of aerosol–radiation interactions or *aerosol–surface interactions* (Boucher, 2015).

Aerosols can also affect the microphysical properties of liquid clouds, specifically by serving as cloud condensation nuclei (CCN) for water vapor to condense on, which partially controls the concentration and size of cloud droplets. The chemical composition of the aerosols can also determine the acidity of the cloud droplets and the rate at which chemical reactions occur within the droplets (Pye et al., 2020). Aerosols can also impact the microphysical properties of ice clouds by serving as ice nucleating particles (INP), and therefore influence mixed-phase clouds (i.e., clouds that contain both liquid droplets and ice crystals).

Clouds scatter solar radiation much more than they absorb it, causing reflection of a significant portion of solar radiation back into space, thus cooling the climate system (Fig 7a). More aerosols for the same amount of atmospheric water vapor available, result in a larger concentration of smaller droplets, leading to a brighter cloud (Fig 7b) back scattering more incoming solar radiation and cooling the climate system. However, many other possible aerosol-cloud-precipitation interactions may amplify or dampen this effect (Murray et al., 2021). When the concentration of aerosols increases, the number of CCN also increases, which in turn leads to an increase in the number of cloud droplets. This dependence is however not linear. CCN is controlled by both aerosol particle number and composition, while number of cloud droplets are sensitive to CCN at low and moderate CCN concentrations and to the updraft velocity when CCN levels are high (Fanourgakis et al., 2019). This effect was previously known as the aerosol first indirect effect, but in this study, it is referred to as the *aerosol-cloud interactions*, which encompasses this and related effects. The change in the microphysical properties of clouds is expected to affect the way clouds develop, specifically with regard to the formation of droplets big enough to cause precipitation. This effect is commonly referred to as the second indirect effect of aerosols and is rooted in aerosols serving as nuclei for cloud condensation. The impact of INP on mixed-phased and ice clouds has been referred to glaciation effect and it is also part of *aerosol–cloud interactions (aci)*.

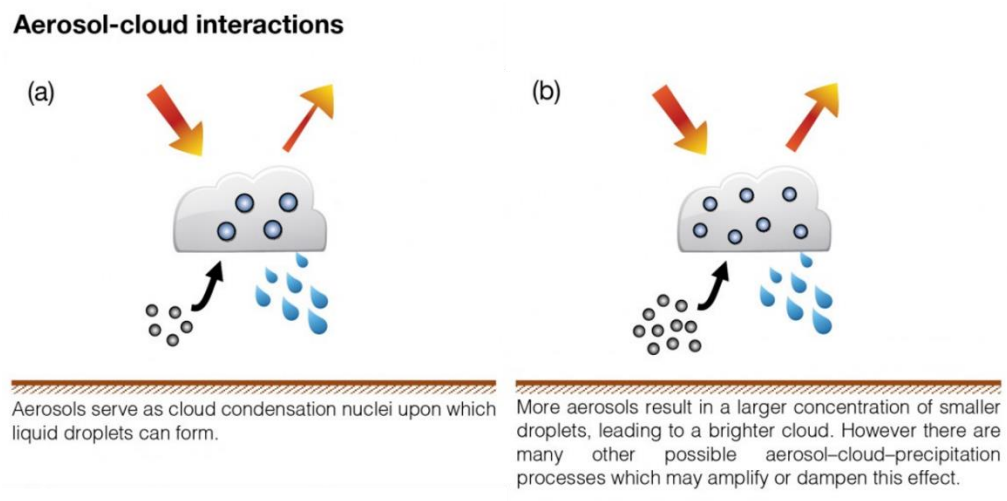

Figure 7: Aerosol-cloud interactions as illustrated in the IPCC (2013).

Clouds can also have an impact on aerosol populations. Precipitating clouds help to remove aerosols from the atmosphere through a process known as wet deposition. There are two types of wet deposition: *in-cloud scavenging*, where aerosols are captured by water droplets within the clouds before precipitation, and *below-cloud scavenging*, where they are captured by falling raindrops. The same holds for ice clouds although scavenging by ice crystals and falling snowflakes is much less efficient (Boucher, 2015). Non-precipitating clouds will ultimately evaporate and release the residual of cloud droplets into the atmosphere, resulting in aerosols which can subsequently serve as CCN, forming again clouds. The CCN are initially composed of mixtures of $(NH_4)_2SO_4$, H_2SO_4 and H_2O and are in equilibrium with gaseous SO_2 and NH_3 concentrations (Rood and Currie, 1989). Sulfur dioxide is readily oxidized in cloud droplets. In addition, other interstitial aerosol material can be incorporated into cloud droplets by dissolution, and the coalescence of cloud droplets forms larger droplets. These processes are changing the chemical and physical properties of the aerosol population that has gone through a cycle of condensation and evaporation. The aerosols size distribution is shifted to larger sizes and the aerosols become more chemically mixed with more soluble material in the larger size range. This cloud processing effect is particularly important in convective clouds, where ascending updraft velocity is dominant, enabling the activation of

small particles producing larger aerosols that can serve as CCN or INP in clouds (Bougiatioti et al., 2017).

Clouds also absorb and emit terrestrial infrared radiation, leading to a greenhouse effect and warming of the climate system. The difference between radiative fluxes at the top of the atmosphere with and without clouds is referred to as the cloud radiative effect, which can be split into a shortwave component that has a cooling effect and a longwave component that has a warming effect. The net effect depends on the thickness and height of the clouds, as well as the cloud microphysical and optical properties. Radiation also plays a significant role in the evolution of a cloud. Heating through radiation absorption and cooling through emission of terrestrial radiation modify the vertical temperature profile in the cloud and its stability. In conclusion, the interactions between aerosols, clouds, and radiation are complex and it is important to understand these processes to comprehend the role of aerosols in the climate system.

As shown in Figure 8, these multiple effects can be grouped into two main types of interactions: *aerosol–radiation interactions (ari)* that include the direct effect and the semidirect effect (RFari - Radiative forcing associated with *ari*, ERFari - Effective radiative forcing associated with *ari*). *Aerosol–cloud interactions* that include the first and second aerosol effect and the glaciation effect (RFaci - Radiative forcing associated with aci, ERFaci - effective radiative forcing associated with aci)

Absorbing aerosols may deposit onto snow and ice surfaces, thus making these surfaces less reflective, warming the surface and thus the climate system. This effect is known as the aerosol on snow effect but can be categorized as part of aerosol–radiation interactions or aerosol–surface interactions. Additionally, it is important to note that aerosols interact with vegetation through changes in incoming solar radiation, fraction of diffuse radiation and as a source of nutrients. These are other contributions to *aerosol–surface* interactions.

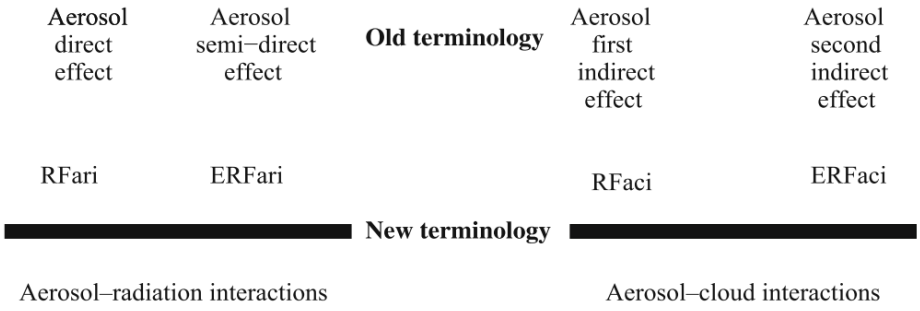

Figure 8: Aerosol–radiation interactions and aerosol–cloud–radiation interactions and how they relate to the original terminology (Boucher, 2015)

Aerosols can affect clouds and precipitation in various ways, either as CCN or INP, or by redistributing thermal energy within cloud layers. These processes are summarized in Table 3. Aerosols can alter the physicochemical properties of clouds, leading to changes in net radiative fluxes at the top of the atmosphere, resulting in either net cooling (negative effect) or net warming (positive effect). However, the understanding of aerosol-cloud interactions is currently low, and cloud feedbacks remain a significant source of uncertainty in climate sensitivity estimates (Fan et al., 2016). Mixed-phase clouds, which are particularly uncertain in climate models, are affected by aerosols in various ways. These clouds contain water vapor, ice, and supercooled liquid droplets, and their properties make them favorable for ice formation, depending on the presence of aerosols acting as ice nuclei.

Table 3: *Overview of the different aerosol indirect effects and their sign of the net radiative flux change at the top of the atmosphere (TOA), (IPCC, 2007).*

Effect	Cloud Types Affected	Process	Sign of Change in TOA Radiation	Potential Magnitude	Scientific Understanding
Cloud albedo effect	All clouds	For the same cloud water or ice content more but smaller cloud particles reflect more solar radiation	Negative	Medium	Low
Cloud lifetime effect	All clouds	Smaller cloud particles decrease the precipitation efficiency thereby presumably prolonging cloud lifetime	Negative	Medium	Very low
Semi-direct effect	All clouds	Absorption of solar radiation by absorbing aerosols affects static stability and the surface energy budget, and may lead to an evaporation of cloud particles	Positive or negative	Small	Very low
Glaciation indirect effect	Mixed-phase clouds	An increase in IN increases the precipitation efficiency	Positive	Medium	Very low
Thermodynamic effect	Mixed-phase clouds	Smaller cloud droplets delay freezing causing super-cooled clouds to extend to colder temperatures	Positive or negative	Medium	Very low

In the following Chapter is presented the current state of knowledge from both observational and modeling perspectives for INP. We discuss the state of knowledge on various INP particle types, their formation mechanisms, their impact on climate and briefly discuss the challenges faced in understanding the cloud impacts of INP with present-day models focusing on mixed-phase clouds regime.

2. Ice Nucleating particles

Atmospheric ice-nucleating particles (INP) are required to initiate ice formation in clouds with temperatures between −38 and 0°C, and can influence the formation of ice crystals in clouds below −38°C. The impact of INP on the process of ice freezing and deposition affects the rate at which the *primary ice* forms in the clouds (Burrows et al., 2022).

Primary ice formation, triggers cloud microphysical and dynamic processes, including the production of *secondary ice* (Georgakaki et al., 2022), and ultimately determines the cloud structure, extent, radiative properties, weather and climate. However, INP are scarce in the atmosphere and their concentrations can vary greatly in space and time, from fewer than 0.01 to more than 100 L^{-1} for INP that are active at −30°C (DeMott et al., 2010). Additionally, their high sensitivity to aerosol chemical and physical properties make their measurement and characterization challenging.

Recent decades have seen a resurgence in research on atmospheric INP (DeMott et al., 2010; Kanji et al., 2017) which has advanced our understanding of their measurement methods and expanded the range of their observations. While, substantial uncertainties remain, these advances in laboratory and field experiments, theory and numerical modeling have built confidence that the abundance of INP can affect mixed-phase cloud properties, and their interactions with planetary radiation and precipitation (DeMott et al., 2010). Studies have shown that introducing INP into supercooled clouds can change the timing and location of precipitation, and climate models have demonstrated the significant impacts of INP on clouds (Seinfeld et al., 2016). Evidence from satellites and lidars also suggests that INP are an important factor in determining cloud phase (Marinou et al., 2019; Choi et al., 2010). Despite these advances, many challenges remain in achieving the ability to accurately represent INP and their effects on clouds and precipitation in numerical models used for weather and climate research(Burrows et al., 2022). A critical obstacle that requires attention is the gap between current measurement-based insights into the sources of INP and their representation in large-scale models. In order to make progress in this field of research, the observational community should receive guidance on which types of measurements will offer the most valuable types of measurements that can be used to provide inputs and constraints for models. Similarly, the modeling community requires clarification on the physical understanding of INP parameterizations and the appropriate ways to apply them within large-

scale atmospheric models. Collaborative studies are essential for enhancing scientific understanding of aerosol-cloud interactions.

The inaccuracy in the simulation of ice crystal concentrations in mixed-phase clouds leads to discrepancies in the modelled top-of-atmosphere radiative flux, and thereby to the climate sensitivity of the models. Murray et al. (2021) suggested that in a warmer future climate, ice in mixed-phase clouds will be replaced by liquid water, potentially leading to strong negative climate feedback (net cooling). However, it remains uncertain whether clouds dampen (negative feedback) or amplify (positive feedback) climate warming, and a key factor of this uncertainty is how models estimate the concentration of INP. Many thermodynamic and microphysical feedbacks determine the glaciation state and properties of mixed-phase clouds, all of which can be affected by perturbations in CCN and INP concentrations (Solomon et al., 2018).

The purpose of this chapter is to provide in detail the appropriate information we need to know about INP in the atmosphere in order to achieve a more realistic simulation of INP globally with a chemistry-transport model (CTM). Then, topics such as IN definitions, main mechanics and their sources will be covered.

2.1 Definitions

In this thesis, we use the terminology proposed by Vali et al. (2015), which we briefly summarize here.

Ice nucleation (IN) is defined as the first appearance of a thermodynamically stable ice phase (Vali et al., 2015).

Ice Nucleating Particle (INP) can be considered as insoluble entity, material, substance, object, item, unit larger than 0.5-µm diameter (DeMott et al., 2010) that is assumed to be the agent responsible for observed heterogeneous ice nucleation (Vali et al., 2015). The term "insoluble" refers to the limited solubility of these particles in water, which allows them to act as ice nucleation sites.

Homogeneous freezing is freezing of a supercooled liquid droplet without the presence of a solid particle. It is frequently an important process in the upper troposphere, including in the well-studied case of orographic clouds and occurs at temperature range T<-37^{o}C.

Heterogeneous freezing is the occurrence of ice nucleation catalyzed by an INP that enables freezing at a lower supersaturation or supercooling than is needed for homogeneous freezing and occurs at temperature range 0^{o}C <T<-37^{o}C.

Site density is the number of sites (Preferred location for ice nucleation on an INP) causing nucleation per unit surface area of the INP , or equivalent as functions of temperature or supersaturation; the quantitative measure of the abundance of sites of different ice nucleating effectiveness (Vali et al., 2015).

Ice-active surface site density, $n_s(T)$ is the surface density of sites (number per unit surface area of INP) active above specific temperature (Niemand et al., 2012; DeMott et al., 2010).

Ice-active mass site density, $n_m(T)$ is defined as cumulative number of nucleation sites per unit mass (Wilson et al., 2015; Murray et al., 2012).

Parameterizations of ice nucleation can be distinguished into two categories: *"deterministic" parameterizations*, where freezing behavior is modeled as a function of temperature, humidity, and aerosol properties (e.g., size, surface area, and chemical composition), *"stochastic" parameterizations*, which additionally include a functional dependence on time (Vali et al., 2015).

Deterministic parameterizations typically identify the effects of particle surface physicochemical properties on freezing and are usually represented by the "*ice active surface site density*" parameter (*ns(T)*), which is a function of temperature, T. *Time-dependent parameterizations* typically are variations of the classical nucleation theory (CNT; (Hoose and Möhler, 2012; Murray et al., 2012)) and represent particle surface effects through a nucleation rate coefficient $J_{het}(T, q)$, depending on temperature and humidity (*q*).

2.2 Mechanisms of heterogeneous ice nucleation

There are several ways in which a suspended particle in the atmosphere will trigger the formation of ice crystals heterogeneously in Mixed Phase Clouds (MPCs). In the following, the possible modalities will be considered separately as summarized in Figure 9 by Kanji et al, (2017)

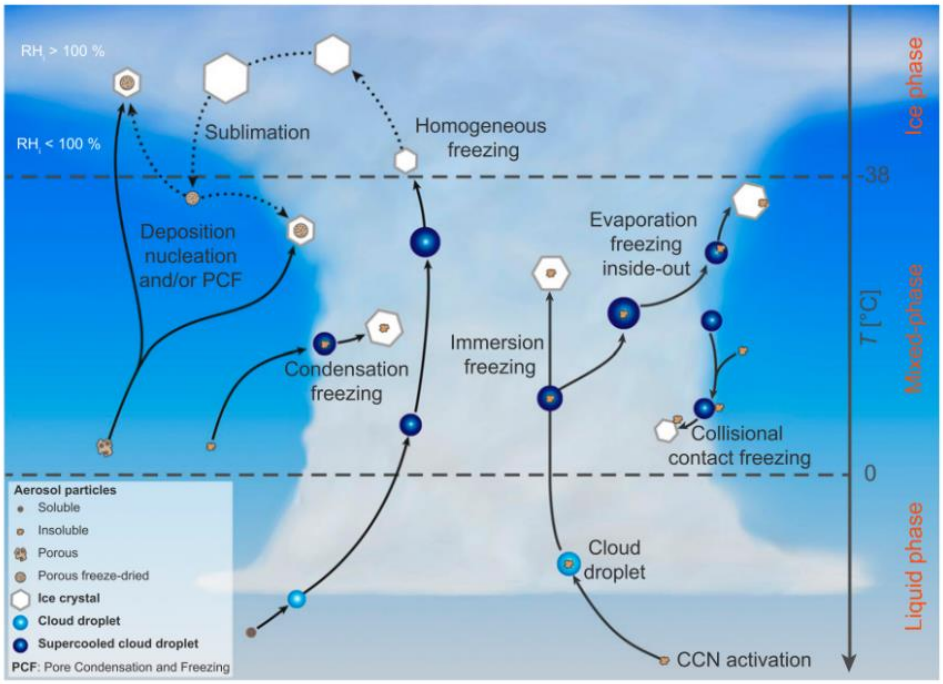

Figure 9: Schematic depicting known primary ice nucleation pathways possible in the atmosphere (Kanji et al., 2017).

2.2.1 Immersion freezing

Immersion freezing is initiated by an INP that becomes immersed in an aqueous solution or water droplet via activation of CCN during liquid cloud formation (Vali et al., 2015). In other words, when an aerosol particle is immersed in a supercooled liquid cloud droplet and then triggers the ice formation (Kanji et al., 2017; Vogel et al., 2022; Hoose and Möhler, 2012), immersion freezing occurs. Some CCN can also be effective INP. This process is thought to be the predominant mode of primary, ice formation in MPCs, which occur at temperatures too warm for homogeneous freezing (Ansmann et al., 2008; Westbrook and Illingworth, 2013; De Boer et al., 2011). A typical example is the laboratory study by Murray et al. (2012) where the nucleation ability of different IN species was studied, assuming that particles triggered the formation of crystals only during nucleation by immersion, based on the hypothesis that this

mechanism is the predominant in atmospheric ice nucleation processes. Recently, Hande and Hoose (2017) found that immersion mode freezing was the dominant mode of primary ice formation in all cases.

The study of immersion mechanism through experimental processes was first carried out by Bigg in 1953 (Bigg et al., 1953). In later studies the investigation of the mechanism was carried out in cloud simulation chambers (Aerosol Interaction and Dynamics in the Atmosphere (AIDA; Möhler et al. 2003), Leipzig Aerosol Cloud Interaction Simulator (LACIS; Hartmann et al. 2011), Immersion Mode Cooling Chamber IMCA (Kohn et al., 2016) in which the contribution of certain aerosol systems to atmospheric cloud droplet and ice formation was studied. Regardless of chamber's size, the basic working principle of cloud expansion chambers is based on adiabatic cooling induced by a controlled pressure reduction inside the cloud chamber. The decreasing temperature causes the ice and water saturation ratio (S_{ice} and S_{water}, respectively) to increase and to reach values larger than 1, where the air is supersaturated and liquid cloud droplets and ice crystals can form (Vogel et al., 2022). Ice crystallization by immersion is clearly observed when all particles are subjected to sufficiently high (Garimella et al., 2017) saturation (supersaturation) or to $RH_w \geq 105\%$ relative humidity conditions (DeMott et al., 2015)

2.2.2 Deposition ice nucleation

Deposition nucleation is the only heterogeneous IN mechanism where liquid water is presumed to be absent (Figure 9). It occurs when supersaturated vapor with respect to ice (RH_i>100%) comes into direct contact with an INP (Kanji et al., 2017). Recent study by Marcolli (2014) proposed that condensation in pores and freezing (PCF) in cavities on the surface of INP could be interpreted as deposition ice nucleation. The "*inverse Kelvin*" effect at RH_i <100% causes water to condense in cavities, leading to homogeneous freezing at low temperatures (T < -38°C). The effect was estimated to take place in pores of sizes of 5–8 nm. Specifically, in the pores of particles, ice formed homogeneously at sufficiently low temperature but decreasing RH_i<100%, ice was retained (up to -13°C). Once RH_i was increased again slightly above saturation, it triggered ice growth. This also was observed by Wagner et al. (2016) and was called pre-activation. Sullivan et al. (2010) studied dust particles that were exposed to nitric acid (HNO_3) and observed a sharp increase in their ice nucleating ability just below water saturation at RH_w<97%. They interpreted this as a shift from the deposition nucleation to the

condensation/immersion freezing mechanism. Generally, It remains unclear to what extent data reported in the past as deposition ice nucleation actually occurred directly via the vapor phase. However, this mechanism is not expected to play a significant role in the formation of ice in mixed-phase clouds (Ansmann et al., 2008), but it may still be important in pure ice clouds, the so-called cirrus clouds (Cziczo et al., 2013; Vogel et al., 2022; Marcolli, 2020).

2.2.3 Contact freezing

Freezing through contact occurs when an INP comes into contact with either the surface of a droplet or the air-water interface (Figure 9). This can occur from the outside of a droplet (such as through a collision) or from the inside of the droplet. Recent advancements in technology have allowed for the examination of contact freezing (Niehaus et al., 2014), and studies (Nagare et al., 2016) have shown that the likelihood of contact freezing is proportional to the surface area of the INP . However, the same studies also suggest that the involvement of the entire particle in contact freezing may not be necessary. Niehaus and Cantrell (2015) found that contact freezing can also occur when deliquesced particles consisting of different soluble substances come into contact with a supercooled droplet, even if they are not solid. Nevertheless, the size of the droplets used in their study (diameters of 25-150mm) limits the atmospheric relevance to larger wet particles colliding, rather than collisions between cloud droplets and INP, which would be much smaller. The overall contribution of contact freezing to MPCs remains uncertain, but it could still play a role (Seifert et al., 2011).

2.2.4 Condensation freezing

Condensation freezing (Figure 9) is a separate mechanism for heterogeneous freezing, but historically has been grouped together with immersion freezing and deposition nucleation. Condensation freezing is defined when freezing occurs simultaneously with the initial formation of liquid on CCN at supercooled temperatures (Vali et al., 2015; Kanji et al., 2017). However, Vali et al. (2015) mention that it is not fully confirmed whether condensation freezing is truly different from deposition nucleation or immersion freezing and advise caution in using it as a standalone mechanism.

2.2.5 Summary

Concluding, there are four main modes of heterogeneous ice nucleation that can rule the formation of ice crystals and impact on cloud microphysics. According to the lidar observations the presence of a high number of INP does not automatically result in the obvious generation of ice, but the observations indicate that cloud top temperatures must typically reach values as low as -20°C before significant ice production starts. Liquid clouds are obviously required before ice crystals form via heterogeneous freezing mechanisms (Ansmann et al., 2008). Additionally, using large eddy simulations of several idealized and realistic MPCs cases, it is proved that immersion freezing was the dominant mode of primary ice formation in all cases (Hande and Hoose, 2017). These observations are in agreement with the concept that INP are activated efficiently as CCN, due to their large size, and because they are typically internally mixed with soluble components. Consequently, these particles are likely to be present inside cloud droplets, being available for immersion freezing, but unavailable for contact freezing, which requires the participation of an interstitial particle. As a consequence, these findings reveal immersion freezing to be the most vital pathway of ice formation in mixed-phase clouds (De Boer et al., 2011).

Contrary, Cirrus cloud regime is dominated by the interplay of three ice nucleation mechanisms: homogeneous freezing, deposition nucleation, and immersion freezing. Understanding the relative significance of these mechanisms and their competition has been the subject of ongoing research for many years (Kärcher and Voigt, 2006). However, there has been some doubt on the concept of deposition nucleation as a heterogeneous freezing mechanism in cirrus clouds. Ice nucleation activity of particles in the cirrus regime is determined by the porosity and wettability of pores (David et al., 2019). Evidence from experiments suggests that ice formation at RH_w below 100% may occur through the condensation of liquid in phase pores, followed by freezing (David et al., 2019).

2.3 Composition of INP residuals

Primary aerosol particles are emitted into the atmosphere by a large variety of sources at different rates. It is known that only a small fraction of atmospheric aerosols are efficient ice nuclei, the critical ingredients that make those aerosols so effective have not been established (Cziczo et al., 2013). The most relevant natural sources are deserts, volcanic eruptions, oceans,

and vegetation debris, whereas important anthropogenic sources of atmospheric aerosol are particles from agricultural practices, deforestation, biomass burning, transportation, and industrial processes. Particle types that can act as INP are a small subset of those aerosol populations. INP have different characteristics depending on their composition and origin. Previous studies have shown that mineral dust, primary bioaerosols (e.g., fungal spores, bacteria, and pollen), and volcanic ash can be effective INP (Kanji et al., 2019; Möhler et al., 2007; Hoose and Möhler, 2012; Murray et al., 2012). However, large uncertainties exist with regard to the ice-nucleating properties of black carbon (Vergara-Temprado et al., 2018) and organic carbon from biomass burning (Jahl et al., 2021; Schill et al., 2020). Cziczo et al. (2013) found that mineral dust and metallic particles are the main sources of residual particles in cirrus crystals after the ice was sublimated, while sulfate and organic particles are underrepresented, and elemental carbon and biological materials are essentially absent (Figure 10a). Furthermore, Pratt et al. (2009) classified INP by types (dust, sea salt, biological, etc.), (Figure 10b). They identified that 50% and 33% of the ice crystal residual particles sampled in cloud as mineral dust and biogenic aerosol respectively. A majority of INP are of terrestrial origin. Although mineral dust is abundant in the atmosphere, bioaerosols (like fungal spores, bacteria, pollen etc.) have higher ice activity stimulating ice formation at relatively high temperatures (Murray et al., 2012). However, only a small proportion of biological materials could trigger ice nucleation (Huang et al., 2021). In the following subsections, we describe main INP types with a focus on results from the last decade and current gaps in knowledge.

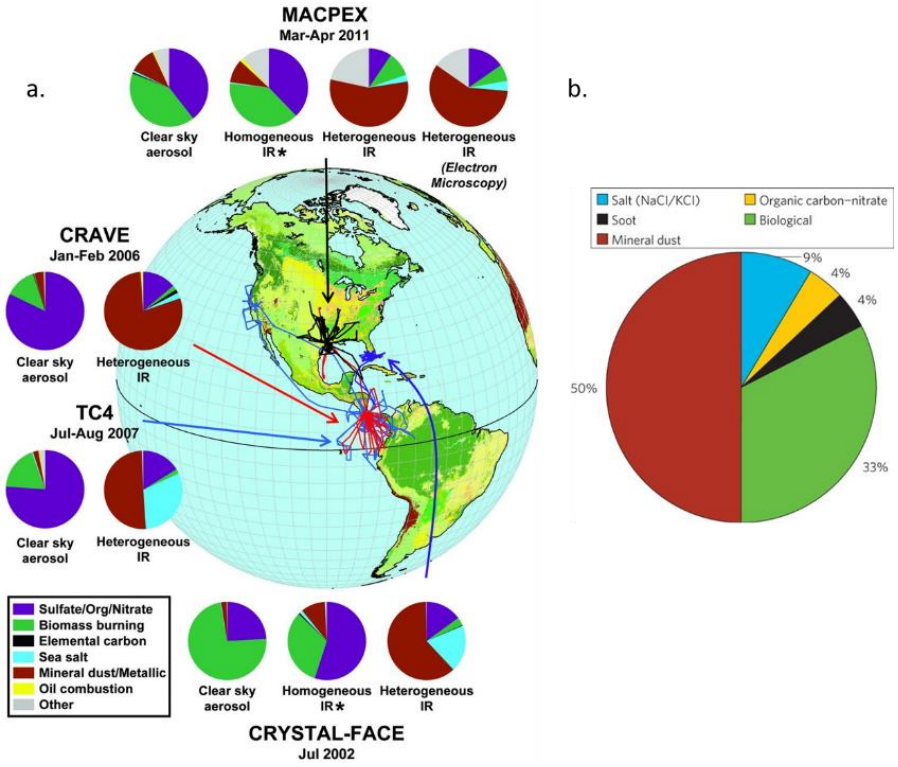

Figure 10: (a) Flight tracks of ice cloud–residual measurements for four aircraft campaigns spanning a range of geographic regions and seasons (Cziczo et al., 2013). (b) Relative contributions of different particle types in ice-crystals residual particles sampled (average of 46 samples) in a wave cloud at ~8 km above Wyoming as determined by aerosol time of flight mass spectrometry . (Pratt et al., 2009)

2.4 Surface interactions leading to ice formation

It has long been suggested that solid or insoluble inorganic particles (e.g., mineral dust) may be capable of inducing ice nucleation at specific locations on their surface, such as cavities, cracks, or hydrophilic sites (Pruppacher et al., 1998). Studies have reported that the probability of these sites to occur are proportional to the surface area of the particle (Abbatt et al., 2006) and this concept has been approved quantitatively by Hartmann et al. (2016). This assumption forms the basis for many parameterizations of ice-nucleating particles (e.g., Niemand et al., 2012; Murray et al., 2012; Atkinson et al., 2013). Since these ice-nucleating sites occur with a finite probability, small particles with a diameter of less than 500 nm are less likely to act as INP. Studies have shown that the number concentrations of atmospheric IN active under MPCs conditions are related to temperature and the number concentrations of aerosol particles with diameters larger than 0.5 µm (DeMott et al., 2010). However, it was

suggested that particles with a diameter of around 200 nm make up the majority of all INP, based on the mode size in ice residual number distributions (Mertes et al., 2007).

Several studies tried to explain the dependence of these particles ice activity on their surface and chemical composition. More specifically, functional groups, such as hydroxyl (-OH) groups on the surface of an INP, can play a role in promoting IN by hydrogen bonding with water molecules. In this regard, Kanji et al. (2008) observed that the ice nucleating activity of silica particles in deposition freezing is completely suppressed by functionalizing the -OH groups with a chain of $-(CH_2)_7CH_3$. Additionally, Freedman (2015) have also suggested that the -OH groups on edge sites of aluminosilicate clay minerals could be important for ice nucleation in deposition mode, as that study inferred that ice nucleation proceeds via condensation/immersion mode, forming soluble alunogen $[Al_2(SO_4)_3 17H_2O]$ on these clay particles.

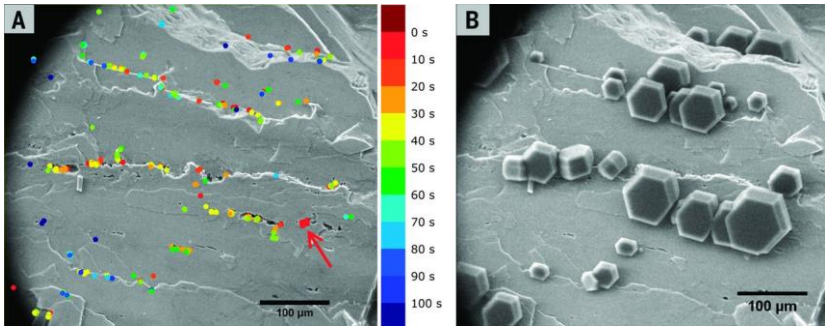

Figure 11: Nucleation sites of individual ice crystals in eight subsequent nucleation-evaporation cycles, plotted over the image of the bare feldspar face. The color code gives the time of nucleation (in seconds) with respect to the first detected crystal (the color scale bar is on the right). Preferential nucleation on steps and cavities is apparent. The red arrow shows the site of the first nucleation event that repeatedly occurs in all cycles. (B) Snapshot of the ice crystals nucleated at 233 K in the first nucleation-evaporation cycle (Kiselev et al., 2017).

Molecular dynamics calculations of graphitic soot (Lupi et al., 2014) and empirical studies of ice nucleation with silver iodide (Vonnegut, 1947), dust, and volcanic ash particles (Maters et al., 2019) proposed that a lattice match between ordered hexagonal bilayer patches of the active surface can have a positive influence on ice nucleation. Kiselev et al. (2017) identified microscopic patches of the crystalline plane with orientation exposed at surface defects such as steps, cracks, and cavities as the preferential ice nucleating sites on K-feldspars (Figure 11). When fully functionalized with hydroxyl groups, this high-energy plane exhibits a strong affinity to the prismatic plane of ice, thus inducing a preferential orientation of ice crystals

formation on the surface of the feldspar. However, it remains to be determined to what extent the properties of INP, such as their lattice structure, size, surface defects, and nature of chemical functional groups, are responsible for the initiation of IN and their molecular identity.

On the other hand, protein complexes embedded in a cell membrane of biological fragments and macromolecules are known to be responsible for ice nucleation (Pummer et al., 2015). Recently studies in tropospheric cloud, has demonstrated that biological ice nucleating active macromolecules (INMs) with sizes about 10nm can dissociate from their carriers, such as, pollen (Diehl et al., 2001), fungal spores (Tobo et al., 2013), and marine organic aerosol (Wilson et al., 2015) and from organic material in soil dusts (O'Sullivan et al., 2015). These studies reveal that INP (for ice cloud formation) need to be insoluble, or be above a certain size threshold (Pruppacher et al., 1998b). The insolubility requirement for an INP remains a challenge since it has been shown that effloresced ammonium sulfate ($(NH_4)_2SO_4$) particles (Abbatt et al., 2006) and a variety of solid soluble salts already deliquesced at the surface can form ice heterogeneously (Niehaus and Cantrell, 2015).

Other studies show that a single INM alone can trigger ice nucleation and depending on their size, they can nucleate ice at different temperatures, where the size of INMs scales with the size of the critical (Augustin et al. 2013; Hartmann et al. 2013) ice embryo at the respective temperature (Pummer et al., 2015). However, there are also proteins that inhibit freezing of larger ice crystals, known as antifreeze proteins (Davies, 2014), sharing structural similarities with ice nucleating proteins but are smaller in size (e.g., 8–9kDa) compared to ice nucleating proteins (typically >100kDa to several hundreds of kDa). Ice nucleating ability of INMs could be attributed to water molecules arranging around the ice active macromolecules functional groups via hydrogen bonds with -OH and amino ($-NH_2$) groups. Such INMs can be bound to host particles (e.g., mineral or soil dust particles (O'Sullivan et al., 2015) providing the active site or chemical bond requirement necessary to stabilize ice nucleation. The adsorption of INMs on host particles could be scaled depending on the size/surface area of the particle carrier but the IN activity arising from such INMs should not scale with the host particle size for cases where the host particle is probed after the removal of such INMs (in the same temperature range). Indeed, biologically-rich samples reduced dramatically their IN efficiency after heating (Figure 12) or digestion treatments (McCluskey et al., 2018; Suski et al., 2018).

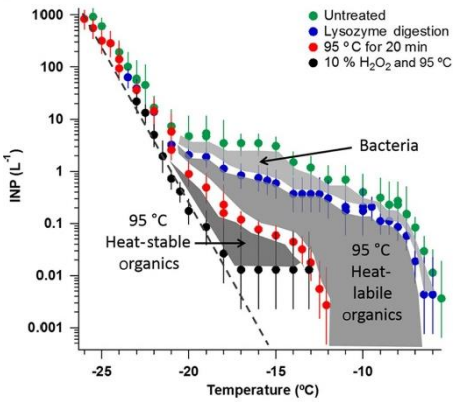

Figure 12: Differences in INP number concentrations after heating and lysozyme and H_2O_2 digestion of the samples (Huang et al., 2021)

2.5 Main sources of INP

2.5.1 Mineral Dust

While several aerosol types, like bioaerosol, black carbon, and dust, have been identified to act as INP , the most important INP in the global atmosphere is thought to be mineral dust emitted into the atmosphere from deserts and other arid and semi-arid regions (Murray et al., 2012; Seinfeld et al., 2016). Mineral dust is a dominant source of both immersion and deposition nuclei in the upper troposphere, and is an important contributor to mixed-phase and cirrus cloud freezing (Cziczo et al., 2013; Chatziparaschos et al., 2023).

Since the 1980s, global climate models have incorporated dust emission parameterizations, which typically consider soil properties, soil moisture, and surface wind speed to represent dust emissions (Albani et al., 2014). In recent years, there has been an evolution in soil data sets and dust representations in large-scale models to include dust mineralogy (Journet et al., 2014; Claquin et al., 1999; Nickovic et al., 2012), which has been found to affect the ice-nucleating particle efficiencies of mineral dust (Atkinson et al., 2013; Boose et al., 2016)

Initially, most ice nucleation studies focused on clay minerals (Hoose and Möhler, 2012). Clays tend to be hydrophilic and, therefore, can act as a CCN, which is a prerequisite for acting as an immersion mode INP (Kumar et al., 2011). Clays are transported over long distances from the source regions due to their higher abundance in the smallest dust sizes and hence their long lifetime (Kok et al., 2017). More recently, it was shown that, among dust minerals, alkali feldspar, in particular the potassium feldspar (K-feldspar), nucleate ice more efficiently than plagioclase (Ca-feldspar) (Harrison et al., 2016). Also, Na-rich feldspar is very ice active but loses its ice activity with time compared to K-feldspar (Harrison et al., 2016); thus, K-feldspar is the most efficient INP. Thus, their abundance is partly compensating for their lower ice nucleating activity with respect to K-feldspar. They found that quartz INP dominate at lower altitudes over locations with abundant dust emissions and that quartz and K-feldspar INP concentrations could be comparable at temperatures at about −30°C. Similarly, Boose et al. (2016) investigated the representativeness of surface-collected dust for the airborne dust particles and showed a correlation between the INP activity of nine desert dust types and the combined concentration of quartz and K-feldspar. They also emphasized the importance for INP modelling of taking into account the presence of both quartz and K-feldspar in the atmosphere.

Although we have a good understanding of mineral dust aerosols and their potential as INP, there are still gaps in our knowledge and modeling capabilities. Boose et al. (2016) found that there were significant differences in the laboratory-derived INP activity of dust samples and ambient samples of naturally occurring dust aerosols, with a difference of up to one order of magnitude. IN activity of transported particles is affected by atmospheric aging of the particles through coating by acids or water-soluble organics (Iwata and Matsuki, 2018; Jahl et al., 2021; O'Sullivan et al., 2016). Additionally, there is a significant difference among global models in their ability to accurately simulate dust concentrations, particularly in regions that are far away from dust sources. Recent research has suggested that current global models may overestimate dust removal and underestimate concentrations of super-micron dust particles (Adebiyi and Kok, 2020; Kok, 2011). Therefore, continuous efforts are required to improve our understanding of dust aerosol physics, including size distribution, loss mechanisms, and optical properties, and to implement dust INP parameterizations for aged and transported dust aerosols in large-scale models, as recommended by Albani et al. (2014).

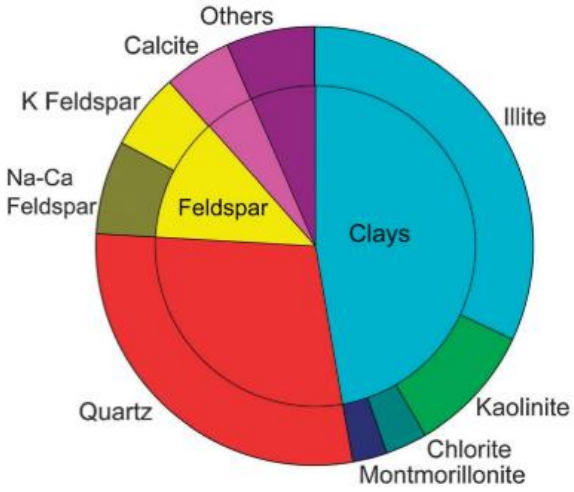

Figure 13: Average of atmospheric dust compositions. Averaging is done without any weighting. Where mineralogy of different particle size bins are provided in a particular study only the smaller size is included. (Murray et al., 2012)

2.5.2 Bioaerosols

2.5.2.1 Marine Organic Aerosols

The sources of aerosol species that initiate ice nucleation in remote oceanic regions, where terrestrial INP are rare as well as the mechanisms involved in the process remain largely unknown. Historically, sea spray was considered unimportant as a source of atmospheric INP. However, recent observational and modeling studies have revealed that marine primary organic aerosol (MPOA) is potentially an important or even the only source of INP of marine origin (Wilson et al., 2015; Vergara-Temprado et al., 2018; McCluskey et al., 2018).

Laboratory experiments showed two distinct marine INP populations: dissolved organic carbon INP (i.e., ice nucleating molecules) and particulate organic carbon INP (i.e., intact cells and microbial fragments) (McCluskey et al., 2018b). In particular, the planktonic diatom species Thalassiosira pseudonana (either intact or fragmented diatoms) and its exudates can initiate ice formation, which may explain the observed high IN of sea surface layer samples (Wilson et al., 2015). The majority of ice-nucleating entities in bulk and surface seawater samples are between 0.02 and 0.2 µm diameter (Irish et al., 2017; Wilson et al., 2015). An intriguing recent study finds that supermicron sea spray particles have higher ice activity than submicron sea spray particles (Mitts et al., 2021).

Marine organic aerosols can be produced through primary and secondary processes resulting in the formation of either water-soluble or insoluble organic aerosols. It has been suggested that water-insoluble marine organic matter is primarily generated together with the emissions of sea spray aerosols (SS) through bubbles bursting driven by surface wind at the air-sea surface (Wilson et al., 2015). Seasonal co-variations in SS and particulate organic matter in remote marine environments have been observed, indicating that particulate organic matter is linked to ocean biological activity (O'Dowd et al., 2008; Rinaldi et al., 2013).

Laboratory experiments have also shown that phytoplankton blooms can significantly affect the number and size distribution of emitted SS and the SS organic content. Various parameterizations for the primary emission of marine organic aerosols have been developed for use in models (Vignati et al., 2010). These parameterizations generally relate marine organic aerosol emission fluxes to chlorophyll a concentration [Chl a], which is globally available from satellite-based measurements. Although, [Chl a] accounts for only a small fraction of the organic matter in the ocean, it has been used as a proxy for the biomass of

phytoplankton in ocean surface waters. Many studies have found that the amount of organic matter in submicron SS is strongly correlated with [Chl a], rather than other ocean chemistry variables (e.g., particulate organic carbon, dissolved organic carbon, and colored dissolved and detrital organic matter (Rinaldi et al., 2013)). Therefore, empirical relationships between satellite-observed Chla and the observed contribution of marine organic aerosols to submicron SS have been derived and used in numerical models. O'Dowd et al. (2008) proposed a parameterization for the emission of marine organic aerosols, which has been modified by Vignati et al. (2010) for the use in the global TM5 chemical transport model. In this parameterization, the fraction of emitted organic matter in SS is linearly related to ocean [Chl a] and is independent of surface wind speed. Another, MPOA emission parameterization was further developed by Gantt et al (2011) that accounts for the organic matter fraction as a function of ocean [Chl a], 10m wind speed, and aerosol size. This parameterization and the one by Vignati et al. (2010) were both able to estimate the MPOA fluxes from surface sea water to the atmosphere. Alternatively, Burrows et al. (2014) introduced a physically-based approach, to model the MPOA emissions instead of using the empirical [Chl a].

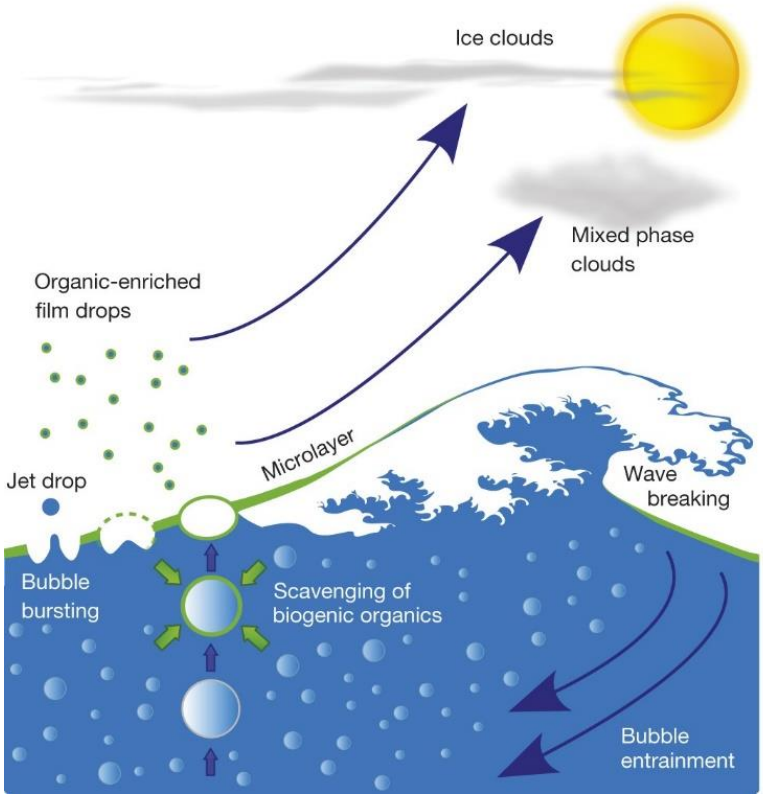

Figure 14: Sea-spray aerosol particles enriched in organic material are generated when bubbles burst at the air–sea interface. Surface active organic material of biological origin is scavenged at the interfaces of bubbles as they rise through the water column. (Wilson et al., 2015)

Although, observations indicate that MPOA are important as INP in cloud, there have been limited modeling studies to quantify their effects. Yun and Penner (2013) conducted the first global study on MPOA's effects on ice formation and radiative forcing using the CAM3 model. Their findings suggested that MPOA INP are the dominant INP for MPCs over the Southern Hemisphere (SH), and the model produced a reasonable ice water path (IWP) after including MPOA INP, compared to the International Satellite Cloud Climatology Project (ISCCP) data. However, their study may have overestimated the frozen fraction of MPOA, with values that are higher than recent measurements of ice nucleation efficiency of MPOA (Wilson et al., 2015) and SS (McCluskey et al., 2018). Furthermore, while Huang et al. (2018) found that MPOA had only a small effect on cloud ice number concentration and effective radius, and did not significantly affect the global radiative balance, Vergara-Temprado et al. (2018) and McCluskey et al. (2019) came to different conclusions. These studies using different models, GLOMAP and CAM5, respectively and different parameterizations, both found that MPOA was dominant INP over the Southern Ocean (Vergara-Temprado et al., 2018; McCluskey et al., 2019)

Over the last decade, research efforts have led to a better understanding of the role of sea spray aerosols as an important source of INP in marine boundary layer air, particularly in regions without continental aerosol sources like the Southern Ocean. However, there are still gaps in knowledge of the seasonal variations in sea spray aerosol INP levels, the impact of ocean biological activity on its ice-nucleating efficiency, and its relevance at cloud altitudes, where long-range dust transport may also contribute to the INP population (Vergara-Temprado et al., 2018; McCluskey et al., 2019; DeMott et al., 2015; McCluskey et al., 2018).

2.5.2.2 Terrestrial Bioaerosols

Primary biological aerosol Particles (PBAPs) consist of cellular material that is aerosolized in the atmosphere, such as pollen, bacteria, fungal spores, and plant debris including whole cells or fragments (Burrows et al., 2009b; Després et al., 2012).They can be passively or actively emitted and are present in low concentrations in the atmosphere (through wind-driven emissions or being ejected by certain fungi). Due to their high freezing efficiency, the role of some biological particles as INP at warmer temperatures has attracted significant research interest. The contribution of biological INP is often indirectly inferred by quantifying the loss of INP activity in samples that are exposed to heat, enzymes or other treatments that break down bacterial cell walls and can denature complex biological macromolecules. Field experiments have revealed correlations between biological particles and INP, and observed high concentrations in PBAP and INP have been linked to rainfall events (Tobo et al., 2013; Mason et al., 2015). Tobo et al. (2013) found that the variation pattern of INP concentration was similar to that of fluorescent biological aerosol particles in a mid-latitude Ponderosa pine forest in summertime, suggesting that PBAPs were critical contributors to INP. Additionally, observations show that the seasonal cycle of INP concentrations, with higher concentrations during summer, was attributed to PBAPs in the Finnish boreal forest (Schneider et al., 2021). Generally regions with abundant biological particles, such as the Amazon (Prenni et al., 2009), may be significant sources of INP (Huffman et al., 2012).

Parameterizations for the IN ability have been provided for different types of biological particles by several studies, including deterministic (Tobo et al., 2013) and Classic Nucleation Theory (CNT)-based (Hoose et al., 2010)(Figure 15). Ice nucleation ability for PBAPs has been described experimentally for different nucleation mechanisms (section 2.2) such as contact freezing (Niehaus et al., 2014), deposition nucleation and immersion freezing (Hoose and

Möhler, 2012). Spracklen and Heald (2014) proposed that PBAPs have little impact on global immersion freezing rates, also they found that PBAPs may be important at altitudes between 400 and 600 hPa, inhibiting the formation of ice from soot and dust (Figure 15). However, immersion freezing of PBAPs is assumed to be the most atmospherically relevant ice formation process, due to their particularly strong freezing efficiency at the warmer temperatures characteristics of MPCs (Hoose et al., 2010). Cloud-resolving models have suggested that mid-latitude, mixed-phase clouds may be sensitive to biological INP when they are present in concentrations significantly exceeding their typical background concentrations (Phillips et al., 2009).

All these suggested parameterizations that describe ice nucleation efficiency of PBAPs come from laboratory and field campaigns mainly referred to the ice nucleation ability of a specific type or species of PBAPs or a specific location such as, forests and mountains. Therefore, despite the usefulness of parameterizations especially in modelling simulations for INP derived from PBAPs, it should be regarded as having significant caveats due to the large variation of nucleation ability both between and within taxa, and in response to environmental conditions (Burrows et al., 2009b; Després et al., 2012).

Additionally, several developments of global emission parameterizations for bacteria-bearing particles, fungal spores, and pollen have been done. For regional-scale emissions, parameterizations for pollen have been provided that are focused on applications to human allergen forecasting (Sofiev et al., 2015). However, there are limited quantitative measurements of airborne biological particles worldwide (Burrows et al., 2009b), and therefore it should temper expectations for the accuracy and precision of simulations of biological particle concentrations. Models have the ability to simulate the mean number and mass concentrations of PBAPs within the order of magnitude (Burrows et al., 2009b; Janssen et al., 2021), but they tend to lack skills in reproducing day-to-day variability (Twohy et al., 2016). Therefore, the currently available parameterizations may be more informative for gaining an order of magnitude understanding of the potential relative contribution of PBAPs to total atmospheric INP and cloud impacts in a climatological sense, rather than for short-term weather forecasting.

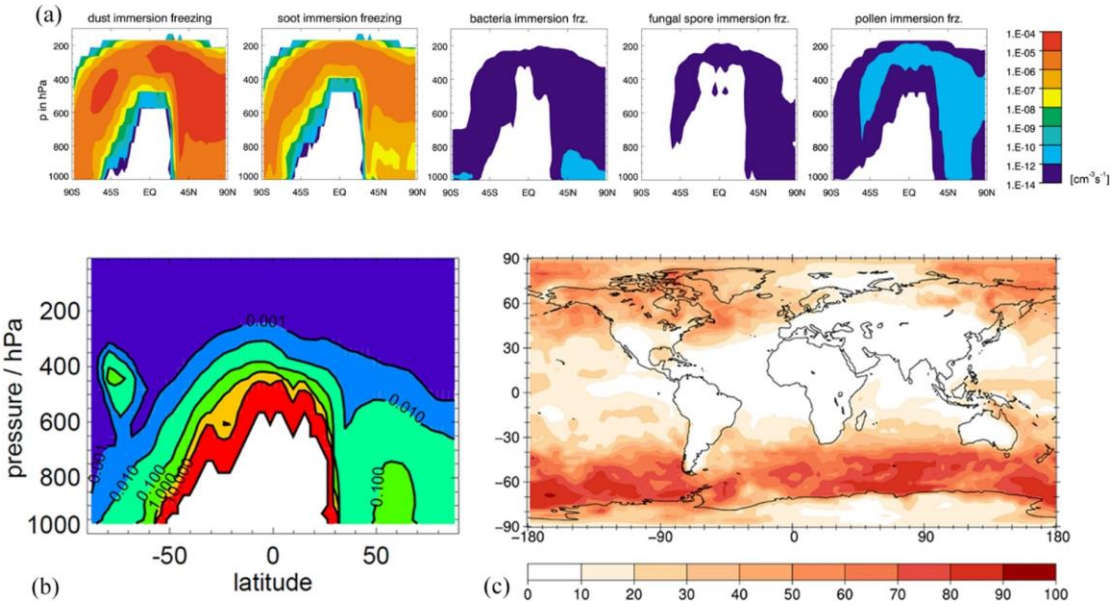

Figure 15: Model simulation results of biological INP. (a) Simulated zonal annual mean immersion freezing rates for the various INP types (Hoose et al., 2010) (b) Percentage contribution of PBAPs (bacteria and fungal spores) to zonal annual mean immersion freezing rates (Spracklen and Heald, 2014). The number of the contour lines indicate the upper and lower percentage for each color. (c) The simulated relative contribution of marine biological INP to marine boundary layer INP concentrations at –15 ◦C, as a percent of the sum of the annual mean dust INP and marine biogenic INP (Burrows et al., 2013). This figure is adapted from (Huang et al., 2021).

2.5.3 Biomass burning

The ice-nucleating activity of biomass-burning aerosol varies greatly and is often much lower than that of mineral dust (Schill et al., 2020; Burrows et al., 2022). However, it is still of interest due to the high concentrations of aerosol in biomass-burning plumes. Schill et al. (2020) found that biomass burning black carbon (BC) particles only contributed minimally (about 5%) to INP populations on a global average. Vergara-Temprado et al. (2018), using a combination of field measurements and laboratory experiments to investigate the INP activity of BC, concluded that BC is a relatively weak INP, with an ice nucleation efficiency that is several orders of magnitude lower than that of other common INP types such as mineral dust. They found that heterogenous ice nucleation by BC can be important only at very low temperatures, close to homogenous freezing and they suggested that BC is unlikely to play a significant role in the formation of MPCs or in modulating their properties. Ullrich et al. (2017), investigating IN efficiency of soot of different nucleation mechanisms, found that the deposition nucleation was the most important for soot particles, especially for low temperatures. This is because

soot particles are not very efficient at nucleating ice through immersion freezing, which involves the incorporation of particles into the liquid droplets of cloud water. They suggested that accounting for the deposition nucleation mechanism is important for accurately modeling the ice nucleation activity of soot particles in mixed-phase clouds. Generally, the impact of biomass burning INP is expected to be limited, and only relevant at local and episodic levels, with limited global relevance.

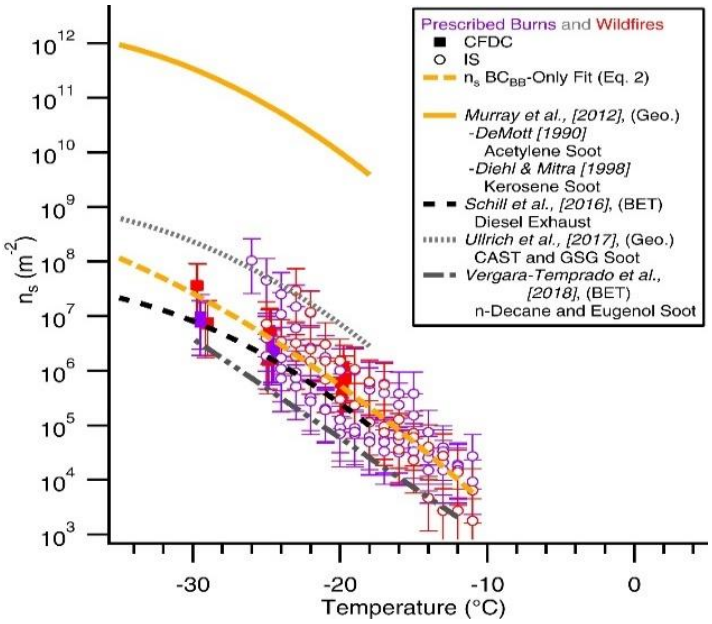

Figure 16: Ice nucleation active surface site densities (ns) for BC as a function of temperature. Lines are limit-of-detection parameterizations from previous works (Schill et al., 2020)

Numerous field studies have characterized biomass-burning INP (Barry et al., 2021; Schill et al., 2020; Vergara-temprado et al., 2018; Jahl et al., 2021). However, identifying the specific aerosol types responsible for INP activity in ambient biomass-burning particles is challenging because various types of particles (e.g., soot, organic particles, dust) are typically present in these plumes (McCluskey et al., 2014). Furthermore, complex chemical transformations occur during the transport of biomass-burning plumes, which may modify ice-nucleating activity and cannot be fully captured by models. Recent studies have suggested that organic components may serve as a useful indicator of INP that are active at temperatures above -25°C in biomass-burning plumes and that these may be associated with in-situ production of tarballs (Schill et al., 2020). Interestingly, Jahl et al. (2021) reported that the ice-nucleation ability of biomass-burning aerosol may be enhanced during atmospheric transport and aging, which was an unexpected finding.

2.6 Impact of INP on climate- state of knowledge

The different broadly defined categories of INP discussed above, are summarized in Figure 17. This figure reviews the observed INP concentrations that are taken from studies in the field conducted globally, as a function of temperature. It reveals that different types of INP with different chemical composition and sampled locations can trigger ice at different temperature range (Murray et al., 2012; Kanji et al., 2017). Temperature as well as humidity are of paramount importance to calculate the activity spectra of these particles acting as INP at different altitudes (Ullrich et al., 2017). Thus, a temperature change would alter the behavior of this spectra affecting cloud-phase microphysics (Murray et al., 2021). In the following section we will discuss the impact of INP on cloud-phase and potential future climate feedback.

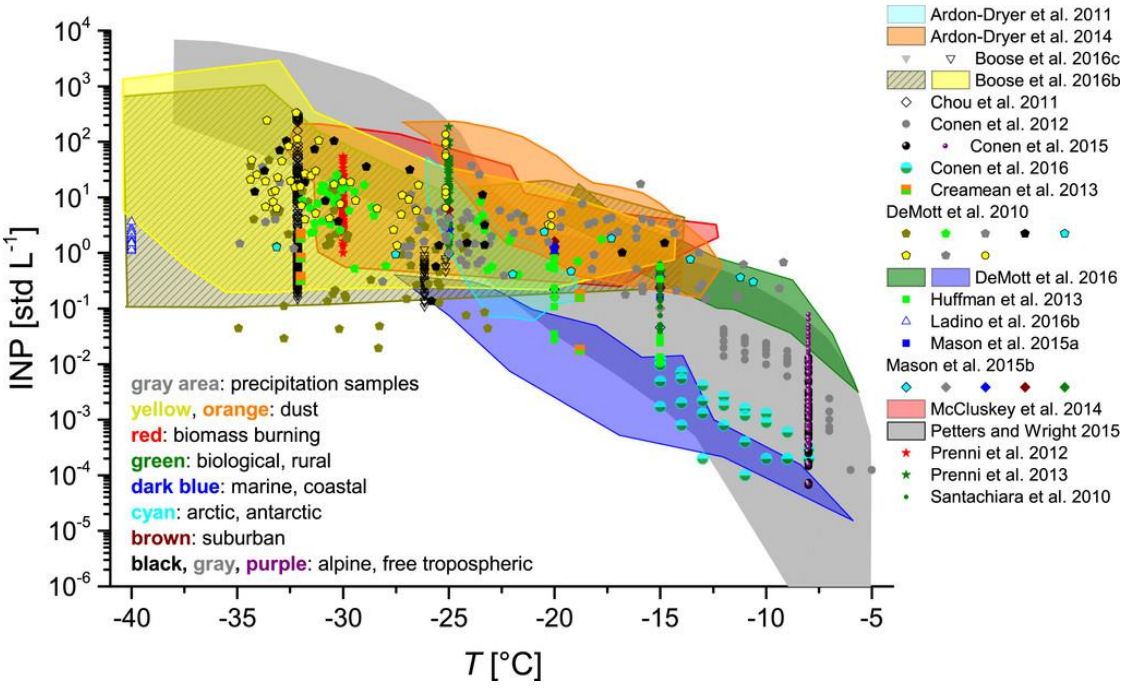

Figure 17: Summary of INP concentrations taken from studies of field measurements conducted globally. Symbol colors correspond to the font color that give information on airmass type or sampling location. Dual-colored symbols indicate INP concentrations influenced by two classes of particles or air masses. Symbol sizes in this plot are only different to avoid masking of data. Shaded areas are enclosures of data from the indicated studies and have been presented to avoid masking of individual data points (Kanji et al., 2017).

The impact of greenhouse gas emissions on climate is certain, but the degree of warming in the future is highly uncertain due to the significant divergence among climate models. Clouds'

response to the forcing caused by CO_2 is one of the primary causes of uncertainty in climate projections. This uncertainty is related to the feedback that clouds can produce, either amplifying (positive feedback) or dampening (negative feedback) climate warming, which varies among models and affects their predicted equilibrium climate sensitivity[2] (ECS) values (Murray et al., 2021). Recent models show a shift towards higher ECS values, and the extent of warming will depend on the feedback mechanism of clouds in response to greenhouse gas emissions that is not yet fully understood.

Clouds are influenced by many factors, including the availability of INP, which play a crucial role in the formation of ice crystals in clouds. The presence of INP can affect the cloud phase, lifetime, and radiative properties, which can in turn affect the overall cloud feedback on climate (DeMott et al., 2010). There are significant differences between model projections. One of the key differences between the older CMIP5 (Coupled Model Intercomparison Project Phase 5) models and the new CMIP6 models, used for climate projections, is the treatment of clouds in the middle to high latitudes where clouds can persist in a mixed-phase state (Murray et al., 2021).

"Mixed-phase" clouds, which have both liquid and ice, have smaller amount of supercooled liquid water due to ice crystal formation and precipitation, resulting in reduced cloud reflectivity than liquid (warm) clouds. INP present in the atmosphere can significantly reduce the supercooled liquid water content and albedo of these clouds through ice-related microphysical processes. A warmer climate in the future can result in water replacing ice, leading to a increase in cloud albedo (Figure 18b).

More specifically, the amount of liquid water in a cloud greatly affects its shortwave cloud radiative effect because cloud liquid water consist of numerous small droplets that scatter shortwave radiation (Murray et al., 2021; DeMott et al., 2010). Conversely, the glaciation of a supercooled cloud results in fewer larger particles that promote precipitation and reduce clouds' lifetime and reflection of sunlight. Therefore, the microphysical processes responsible for the depletion of liquid water content and the formation of ice are critical for determining cloud feedbacks (Vergara-Temprado et al., 2018).

[2] A useful single-number proxy for how sensitive the planet is to forcing by CO_2 is given by the equilibrium climate sensitivity (ECS, °C). ECS is defined as the temperature rise associated with a doubling of CO_2 once the planet has come to equilibrium (which takes more than 1000 years).

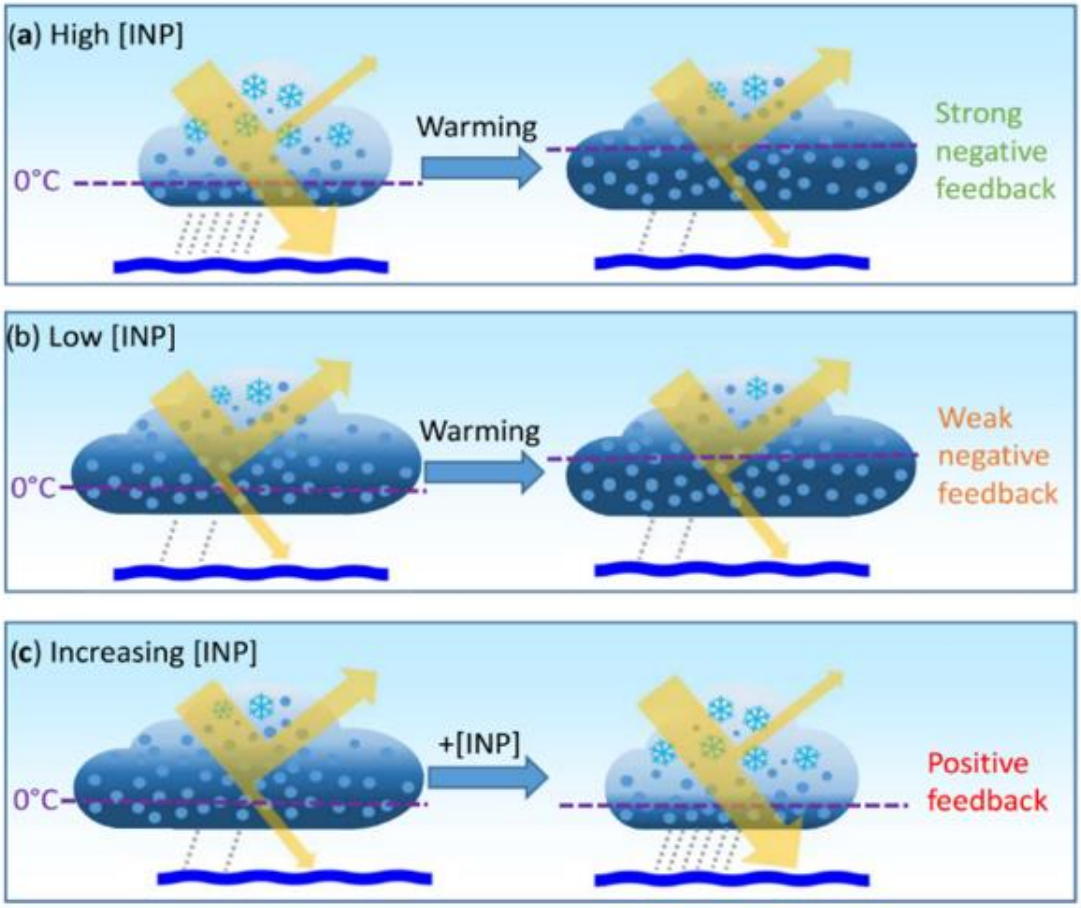

Figure 18 : illustration of the response of MCPs in a changing INP control. (a) With a relatively high INP concentration ([INP]), there is a large potential for liquid to replace ice as climate warms and isotherms shift upwards, resulting in strong negative shortwave feedback. (b) With a relatively low INP concentration, clouds contain relatively little ice in the present climate, so there is less ice to be replaced by liquid water and relatively small negative feedback. (c) Setting the temperature changes aside, there may be either increases or decreases in INP concentration in the future that clouds will respond to (Murray et al., 2021).

The reason for the shift towards fewer but larger hydrometeors during glaciating of supercooled clouds is due to the abundance of available aerosols for cloud droplet and ice crystal nucleation, as well as subsequent ice-related microphysical processes. CCN which form cloud droplets, are relatively common with tens to hundreds per cubic centimeter over remote oceans, while INP are much less abundant (only a few per cubic centimeter) (DeMott et al., 2010). Therefore, a small number of cloud droplets may contain INP, triggering freeze. These frozen droplets then find themselves in an environment that is strongly supersaturated with respect to ice, hence they grow rapidly to hundreds of micrometers in diameter by diffusional growth and accretion of droplets, depleting the liquid water content (Wegener–Bergeron–Findeisen process, WBF) as they grow and precipitate. In some cases, the impact of

INP may be enhanced through secondary ice production (SIP), which involves mechanisms resulting in the production of additional ice crystals (Sotiropoulou et al., 2020; Field et al., 2016). It is important to note that these processes, subsequent to ice nucleation, such as SIP, WBF, and riming, are not well understood and require attention (Komurcu et al., 2014).

Several studies prove that INP concentrations are higher in the Northern Hemisphere (NH) as compared to the Southern Hemisphere (SH), potentially due to the presence of terrestrial sources like mineral dust. However, a significant input of INP to clouds in the Southern Ocean in a warmer climate would imply strong negative cloud feedback and that these clouds have a strong buffering effect on warming by anthropogenic CO_2 (Figure 18a). On the other hand, contemporary measurements by McCluskey et al. (2018) and Welti et al. (2020) suggest weak INP sources in the Southern Hemisphere, which would result in a less negative cloud-phase feedback (Figure 18b). However, the sources of INP may become more prominent in the Southern Hemisphere in response to future warming, leading to positive cloud feedback.

Figure 18 illustrates the response of mixed-phase clouds to a changing climate, hypothesizing three different variations of INP concentration. a) With a relatively high INP, concentration [INP], there is a large potential for liquid to replace ice as climate warms and isotherms shift upwards, resulting in strong negative shortwave feedback. (b) With a relatively low INP concentration, clouds contain relatively little ice in the present climate, so there is less ice to be replaced by liquid water and relatively small negative feedback is expected. (c) Setting the temperature changes aside, there may be either increases or decreases in INP concentration in the future that clouds will respond to. Although increases in [INP] above 0.1 L^{-1} could potentially deplete most liquid water, strongly affecting cloud radiative properties (Vergara-Temprado et al., 2018). Additionally, the various types of INP have different temperature dependences and for those with steeper temperature dependences there is a greater potential to replace ice by liquid in a warmer climate (Murray et al., 2021).

The representation of supercooled water in climate models varies greatly, with some models removing liquid water at temperature as warm as -10°C while others retain unrealistically high amounts of liquid water at temperatures down to -35°C (Komurcu et al., 2014). The differences between models are complex and likely related to the specifics of the ice nucleation scheme as well as other ice-related microphysical processes (including secondary ice production, ice vapor growth and the processes of conversions between cloud ice and ice-phase precipitation) (Komurcu et al., 2014). However, many relevant processes occur on scales finer than the grid resolution of climate models, indicating sub-grid variability.

Additionally, the parametrizations of these processes can affect the distribution and amounts of ice and liquid (Kay et al., 2016). Recent studies have shown that linking primary ice production to aerosol concentrations can improve the representation of cold oceanic clouds, but the existing models do not account for many important ice-nucleating particle sources, especially at high latitudes (Vergara-Temprado et al., 2018). To address this issue, climate models need to incorporate a comprehensive model of INP that includes sources and removal processes specific to cloud systems. This would enable the simulation of primary ice particle concentration, which is necessary for a realistic representation of precipitation and cloud reflectivity and the response of clouds to global warming (DeMott et al., 2010).

2.7 Aim of the study

The present study aims to improve our understanding of the role of ice nucleating particles in the glaciation indirect effect and the broader impact of mixed-phase clouds on climate, with the ultimate goal of improving parameterizations in climate models.

Therefore, we focus on particles that are involved in the glaciation indirect effect and generally in mixed-phase clouds climate impact. This thesis

i) investigates the global distribution of INP,
ii) identifies their major sources and the specific aerosol types that can act as INPs, depending on the location and season,
iii) proposes parameterizations for use in climate models by using them in the TM4-ECPL off line chemistry-transport global model and evaluating them against global observations,
iv) highlights the significance of utilizing different soil mineralogy data to determine INP concentration from dust aerosol,
v) explores the impact of INP on climate by using an on-line model that takes into account meteorological variables and is part of the Earth System Model EC-Earth3,
vi) investigates the variation between aerosol dependent and aerosol independent parameterizations on ice formation and provides preliminary results that demonstrate changes in cloud coverage, liquid water content, ice water path,

short and long wave radiation forces, as well as temperatures changes, induced by aerosol dependent ice formation.

This is the first global modeling study that accounts simultaneously for quartz and K-feldspar, dust aerosol as well as marine and terrestrial bioaerosols as precursors of ice nucleating particles. For this, the global chemistry transport model TM4-ECPL is here developed further to account for the major types of INPs, using experimentally derived parametrizations that link INP activity to aerosols type and surface concentration.

Chapter 3 presents the methodological approach of the thesis: the model, the developments made, the observational data used for model evaluation and the statistical variables calculated when comparing model results with observations. Chapter 4 presented the results of the statistical analysis to validate the geographic distribution of the primary sources of ice nucleating particles, which include terrestrial bioaerosols and mineral dust. This was achieved by quantifying the variability of dust concentration through comparison of observed intra-annual dust surface concentrations and deposition. The comparison was carried out using data collected from stations located in the outflow of the Saharan Desert as well as globally, providing us with valuable insights for the accuracy of the model's results.

In Chapter 5, the performance of the model is tested as to its ability to reproduce the observed INP concentrations when considering airborne mineral dust with a comparison of the model results with observations from various regions of the globe. Uncertainties in the calculations are identified and some of them are quantified by performing sensitivity calculations to the dust mineralogy used in the model and are thoroughly discussed in this Chapter.

In Chapter 6, the simulated concentrations of the various INP characterized by different aerosol precursor species including marine and terrestrial bioaerosols, are discussed, along with the identification of the dominant INP aerosol precursor, per season and region. Additionally, the model performance in reproducing INP observations is discussed based on different assumptions of aerosol precursors of INP.

In Chapter 7, the impact of INP on climate sensitivity is discussed, by presenting an overview of feedback pathways involving aerosols and clouds. The limitations of current analytical models and the necessity of using an on-line model that calculates meteorological variables and simulates more accurately the interactions between aerosols and clouds are discussed. The implementation in the atmospheric component of the Earth System Model – EC-Earth3 of a new ice nucleation scheme, which is sensitive to both aerosols and temperature, is

presented and the improvement in the accuracy of the simulation of cloud properties and their impacts on Earth's radiation budget is evaluated. Preliminary results of the model simulations are presented.

Chapter 8 briefly outlines the thesis results on the current level of scientific understanding of INP based on available INP observations, INP parameterizations, aerosol observations, and aerosol modeling for different particle sources contributing to atmospheric INP. Finally, the requirement to further improve the description of aerosols in climate is highlighted, with a particular focus on the aerosol sources of INP, for which the current level of understanding is low, and suggests modeling and experimental approaches to address this issue.

3. Methodology ¥

3.1 Model description

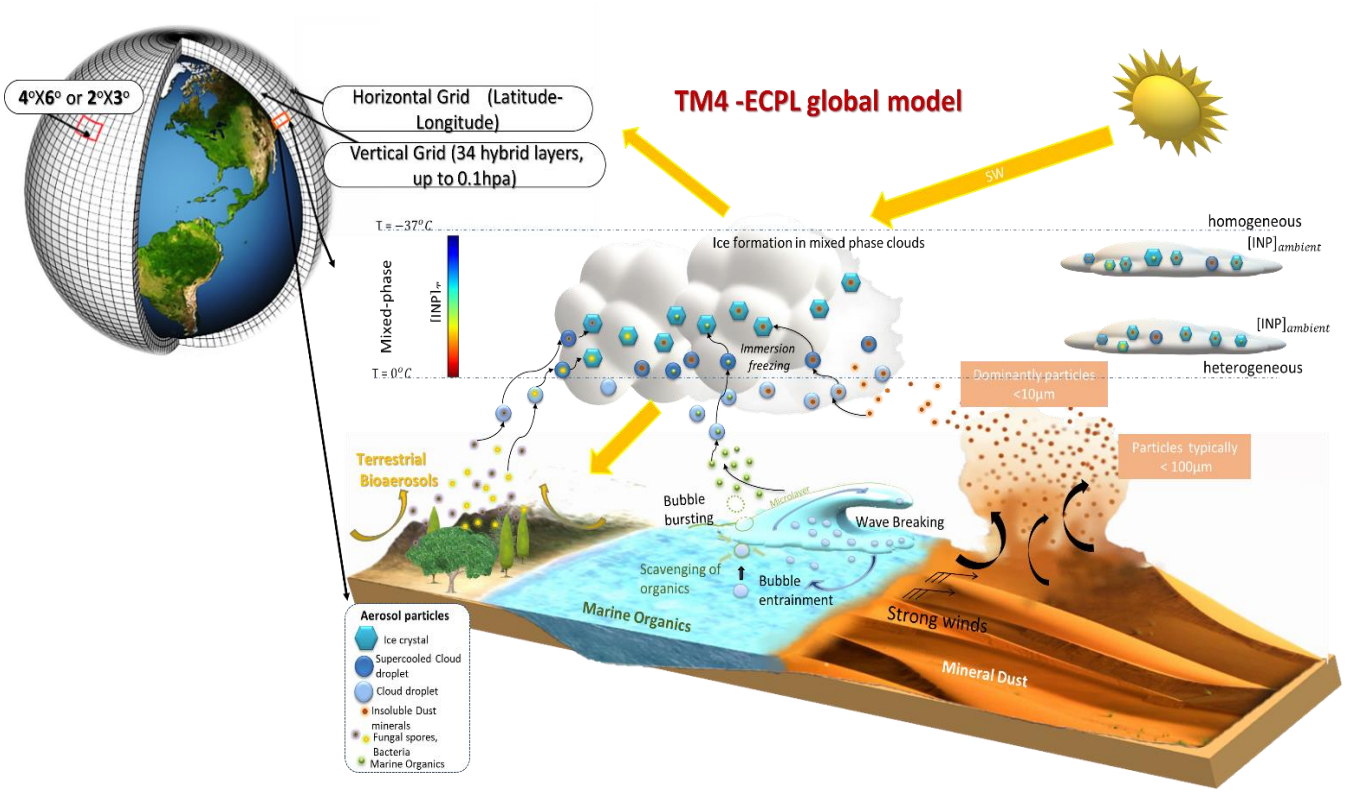

Figure 19: Illustration of the formation of INP from mineral dust aerosol and the two ways in which we display INP concentrations in the present study: [INP]$_{ambient}$ calculated at ambient model temperature relevant to non-deep convective mixed-phase clouds (right part of the figure), and [INP]$_T$ calculated at a fixed temperature relevant for vertically extended clouds as deep-convective systems (left part of the figure). The temperature color scale from 0 to -37°C is provided to the left. Figure modified from Chatziparaschos et al. (2023).

¥ A part of this chapter has been published in the journal Atmospheric Chemistry and Physics Chatziparaschos et al., 2023. https://doi.org/10.5194/acp-23-1785-2023

For the present study, we use the global 3-dimensional chemistry-transport model TM4-ECPL (Daskalakis et al., 2016, 2022; Myriokefalitakis et al., 2016, 2015; Kanakidou et al., 2020) driven by ERA-interim reanalysis meteorological fields produced with the European Centre for Medium-Range Weather Forecasts (ECMWF) meteorological model (Dee et al., 2011). This model version has a horizontal resolution of 3^o longitude by 2^o latitude with 25 hybrid pressure vertical levels from surface up to 0.5hPa (about 56 km) (Table 4) and uses a model time step of 30 minutes. This results to a total of 270,000 grid boxes for the high resolution and 67,500 grid boxes for the low resolution. At the polar region the model has one single grid box with a radius equal to the latitudinal model resolution.

Table 4: Model levels height (top of the level) and pressure (bottom of the level) for the equator over sea.

Levels	Geopotential height (m)	Pressure (hPa)	Levels	Geopotential height (m)	Pressure (hPa)
1	*26.20*	*1004.64*	**14**	*9795.95*	*303.48*
2	*107.54*	*995.45*	**15**	*11367.12*	*243.24*
3	*260.32*	*978.43*	**16**	*13024.78*	*189.93*
4	*506.89*	*951.53*	**17**	*14770.92*	*143.81*
5	*862.64*	*913.89*	**18**	*16622.27*	*105.17*
6	*1338.43*	*865.63*	**19**	*18687.95*	*73.95*
7	*1942.34*	*807.71*	**20**	*21081.16*	*49.89*
8	*2678.56*	*741.73*	**21**	*25100.73*	*28.20*
9	*3547.34*	*669.77*	**22**	*30686.72*	*11.97*
10	*4547.41*	*594.19*	**23**	*36599.49*	*5.06*
11	*5678.44*	*517.49*	**24**	*44073.66*	*1.97*
12	*6937.47*	*442.08*	**25**	*56742.60*	*0.48*
13	*8314.76*	*370.15*			

A total of 256 thermal and 46 photolysis gas phase and 43 aqueous phase reactions are considered in the model. These reactions involve 146 tracers of which 37 are aerosol species and 109 gaseous species (Myriokefalitakis et al., 2011; Myriokefalitakis et al., 2008). Biogenic emissions come from the MEGAN—MACC Biogenic Emission Inventory for the year 2008 (Sindelarova et al., 2014). Soil NOx and oceanic CO and VOCs emissions are taken from POET (Granier et al., 2005) inventory database. Oceanic emissions of primary organic aerosol, isoprene, terpenes and sea—salt particles are calculated online driven by meteorology following Myriokefalitakis et al. (2010). In Table 5 the emission databases used in TM4- ECPL are provided together with their spatial and temporal resolution. All these emissions are converted to the model resolution for use in the model.

Table 5: Emission and emission proxy datasets used in the TM4-ECPL model.

Dataset	Spatial resolution	Temporal resolution	Reference
Natural emission datasets			
MEGANv2.1*(vegetation)	0.5°x0.5	Monthly	Sindelarova et al. (2014)
POET2000 (soils/oceans)	1°x1°	Monthly	Ito and Penner (2004)
AEROCOM (dust)		Daily	Dentener et al. (2006)
MODIS/SeaWIFS (chlorophyll)	1°x1°	Monthly	Myriokefalitakis et al. (2010)
Anthropogenic emission datasets			
ACCMIP-interpolated*	0.5°x0.5	Monthly	Lamarque et al. (2013)
ECLIPSE**	0.5°x0.5	Monthly	Klimont et al. (2013)
Biomass burning emission datasets			
ACCMIP-interpolated*	0.5°x0.5°	Monthly	Lamarque et al. (2013)
GFEDv2***	1°x1°	Monthly	van der Werf et al. (2006)
GFEDv3.1***	0.5°x0.5°	Monthly	van der Werf et al. (2010)
FINN[F]	1km	Daily	Wiedinmyer et al. (2011)
GUESS-ES*	1°x1°	Monthly	Knorr et al. (2012)

* *downloaded from http://eccad.sedoo.fr/*
** *downloaded from http://www.eclipse.nilu.no/*
*** *downloaded from http://globalfiredata.org/*

The model considers lognormal aerosol distributions in fine and coarse modes (as listed in the Table 6) and allows hygroscopic growth of particles, as well as removal by large-scale and convective precipitation and gravitational settling. In-cloud and below-cloud scavenging are parameterized in TM4-ECPL as described in detail by Jeuken et al. (2001).

Table 6: Size, density and standard deviation of lognormal distribution for various aerosol types that considered for this study and used by TM4-ECPL model.

Type	*Radius (m)*	*Density kg m^{-3}*	*Sigma*
Marine Primary Organic Aerosols	Accumulation mode: radius_ssa = 0.09e-6 (number median radius) Coarse mode: radius_ssc = 0.794e-6 (number median radius)	mpoa_density = 1300	Accumulation mode: 1.59 Coarse mode: 2.0
Dust	Accumulation mode: mmr_dua = 0.37e-6 (mass median radius) Coarse mode: mmr_duc = 1.75e-6 (mass median radius)	dust_density = 2650	Accumulation mode: 1.59 Coarse mode: 2.00
Bacteria	mmr_bct = 0.5e-6 (mass median radius)	bct_density = 1000	1 (monodisperse)
Fungal spores	mmr_fng = 1.5e-6 (mass median radius)	fng_density = 1000	1 (monodisperse)

3.1.1 Deposition

Removal of gaseous and particulate atmospheric constituents from the atmosphere depends on their chemical and physical properties. It occurs through dry and wet deposition or sedimentation (gravitational settling) for coarse particles. The change in the concentration of the chemical tracers due to their deposition is calculated each model time step. Coarse particle sedimentation is calculated with an internal time step that is half the model general time step. Chemical compounds are removed from the atmosphere when they are dissolved in cloud droplets or through below-cloud scavenging during precipitation.

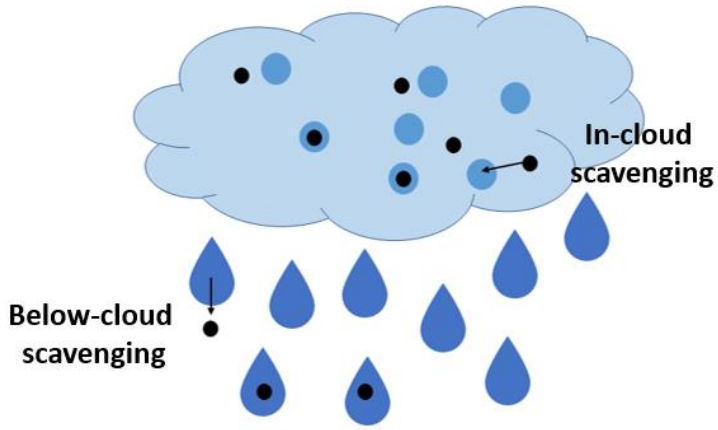

Figure 20: Aerosol removal by scavenging either in cloud or below cloud.

Aerosol removal by scavenging either in cloud or below cloud. With regard to the wet deposition parameterizations, chemical compounds are separated in four categories:

1. The insoluble and low solubility gases that are not removed by wet deposition.
2. Those that are removed because of complete dissolution in the cloud droplets.
3. Those that are partially dissolved in the cloud droplets based on Henry's law.
4. Those that are removed by scavenging (mostly particles).

Dry deposition reduces the concentration of the compounds depending on the deposition velocity (vd) which is calculated based on the approximation of electrical resistances in line that was developed by Ganzeveld and Lelieveld (1995) based on the work by Wesely (1989):

$$v_d = \frac{1}{r_a + r_b + r_c}$$

Where, as resistances we consider the aerodynamic resistance (ra), the resistance of the compound on the thin layer between the atmosphere and the deposition surface (quasi laminar layer resistance) (rb) and resistances because of the characteristics of the surface where deposition takes place (rc) like humidity, depth of snow, vegetation, wind etc. All these resistances depend on each compounds properties (molecular weight, Henry value, reactivity) and the surfaces on which the deposition will take place. The values of these parameters derived from the climate model ECHAM4 that has been developed from the ECMWF atmospheric model.

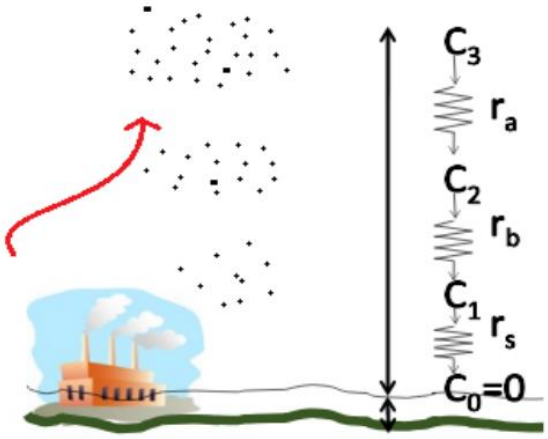

Figure 21: Resistances model for the dry deposition simulation in the atmosphere where r_a the aerodynamic resistance, r_c the quasi-luminal layer resistance and r_s the resistances caused by the surface. $C_{0\text{-}3}$ are the particle concentrations.

The model also takes into account the gravitational settling of particles. For coarse particles with diameters larger than 1μm, such as sea salt or mineral dust, their mass leads to quick removal from the atmosphere because of gravitational forces. Important role in the effectiveness of this procedure plays the adsorption of water by particles that leads to increase in their diameters (hydroscopic growth). The model calculates the fall velocity as a function of pressure, temperature and air and particle density.

3.1.2 Advection

The movement of air in all three spatial directions is taken into account in order to simulate the advection of air-masses. The model recalculates the air-mass in each box after the advection is applied, ensuring mass conservation. Deviations below 0.01% are considered acceptable, and the simulation stops if negative concentrations are calculated. The slopes scheme is used to parameterize the advection of tracers in the model, as described in Russell and Lerner (1981) (and references therein). The convective transport is parameterized based on the Tiedtke (1989) and Olivié (2004) scheme, while the vertical diffusion follows the parameterization method detailed in Louis (1979). The model calculates the fast vertical air-masses movements (induced convection) for each time step. At the end of this process the model checks for negative concentrations. After these calculations the iterative cycle of processes restarts from the beginning.

3.1.3 Emissions

3.1.3.1 Emissions of K-feldspar and quartz

Dust emissions are calculated online as described by Tegen et al. (2002) and implemented as in Van Noije et al. (2014). Dust aerosol (including feldspar and quartz) emissions are represented by lognormal distributions in fine and coarse modes with dry-mass median radii (lognormal standard deviation) of 0.34 (1.59) and 1.75 µm (2.00), respectively, and particle density is assumed equal to 2650 kg m^{-3} (Ginoux et al., 2004; Tegen et al., 2002). All aerosols are considered as externally mixed. Typical lognormal distribution equations are used to convert mass to number concentrations of aerosols in each grid box of the model.

To calculate the quartz and K-feldspar emissions, we used the global soil mineralogy atlas of Claquin et al. (1999), including the updates proposed in Nickovic et al. (2012) (Figure 23). The atlas of Claquin et al. (1999) provides mineral fractions for eight major minerals, including quartz and feldspar, in arid and semi-arid regions for two soil size fractions: clay (up to 2 µm) and silt (from 2 to 50 µm). Claquin et al. (1999) exclusively apportion feldspar to the silt size fraction, but feldspar is also observed in the smaller sizes, both in the soil (e.g., Journet et al., 2014) and the airborne dust (e.g., Kandler et al., 2009). Following Atkinson et al. (2013), we added feldspar in the clay size fraction of the soil by scaling the feldspar fraction in the silt size

fraction of the soil with the clay-to-silt ratio of quartz. Since Claquin et al. (1999) only estimated total feldspar, based on observations, we also assumed that K-feldspar represents 35 % of feldspar (Atkinson et al., 2013). Atkinson et al. (2013) calculated the emission of K-feldspar as the product of dust emission flux and the soil fractions of K-feldspar. Here, we additionally account for the known differences between soil and emitted mineral fractions. The soil samples that constitute the basis of soil mineralogical atlases are subject to destructive analytical techniques. As a result, the aggregates originally present in the soil are more effectively disturbed than through wind erosion processes, hence overemphasizing the fine fraction of clay minerals compared to their actual abundance at emission (Perlwitz et al., 2015).

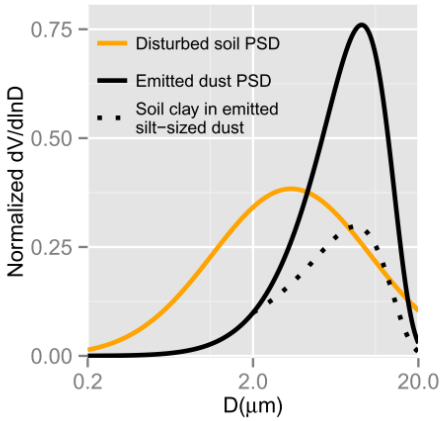

Figure 22: Size distribution of emitted dust (black line) and orange curve describes the arid dispersed soil represented by a monomodal log-normal distribution with a volume median diameter of 3.4 µm and geometric standard deviation of 3.0. The dotted line represents the contribution of dispersed soil clay particles to silt- sized dust aggregates.(Perlwitz et al., 2015)

We calculated the emitted mass fractions of quartz and K-feldspar in the fine and coarse modes based on brittle fragmentation theory (BFT) from Kok (2011). BFT proposes that repeated collisions between soil aggregates mobilized by saltation, will result in emitted aggregate diameters that are mostly smaller than a scale λ.

According to this theory, the number concentration N of emitted particles varies inversely with the square of the diameter D:

$$\frac{dN}{dlnD} \propto \frac{1}{C_N D^2} \exp\left[-\left(\frac{D}{\lambda}\right)^3\right] \int_0^D p(D_s) dD_s \qquad for\ D > x_0, \qquad \text{Eq. 2}$$

where the exponential is an upper bound on the emitted size range near diameter λ. The inverse-square dependence in Eq. 2 remains valid for diameters as small as x_0 which is the indivisible scale, where the material comprising the aggregates resist further disintegration. C_N is a normalization factor and $p(D_s)dD_s$ is the distribution of wet-sieved diameters.

BFT restores soil clay-sized minerals (mainly illite, kaolinite, and smectite), created by wet sieving, into emitted coarse aggregates. As a consequence, the fractional contributions of quartz and K-feldspar in the emitted coarse dust are reduced relative to their fractions in the silt size of the soil (Pérez García-Pando et al., 2016; Perlwitz et al., 2015). Finally, the corresponding accumulation and coarse-mode emission of each mineral is calculated by applying the respective mineral-emitted mass fractions to the dust emission flux.

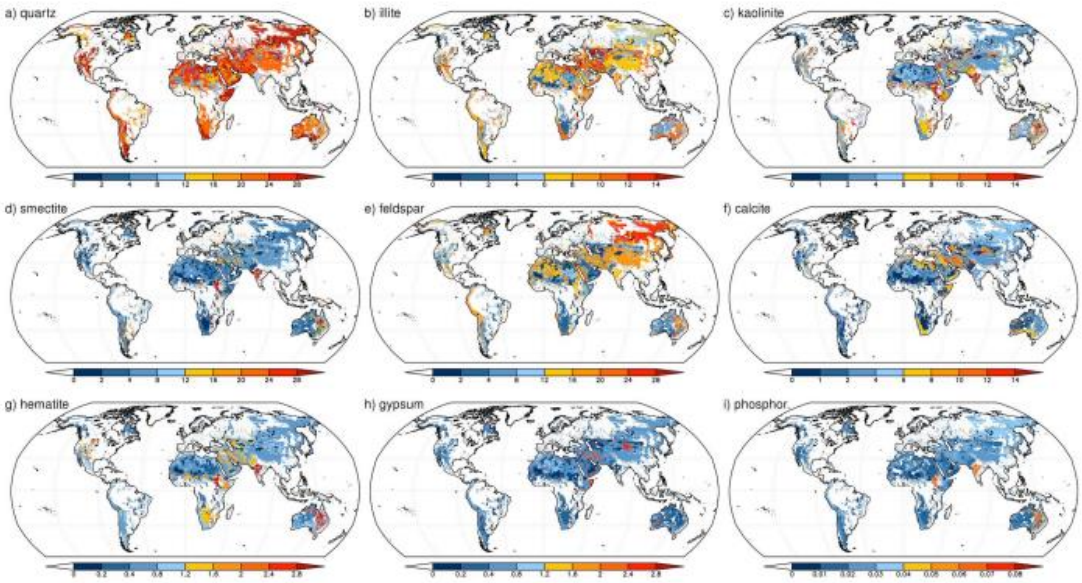

Figure 23 : Global distribution of the effective percent mineral content in soil in percentages for (a) quartz, (b) illite, (c) kaolinite, (d) smectite, (e) feldspar, (f) calcite, (g) hematite, (h) gypsum and (i) phosphorus. The mineral fraction is weighted with the clay and silt content in soil. For minerals that are present in both clay and silt, the weighted values are summed (Nickovic et al., 2012).

3.1.3.2 Marine Primary Organic emissions

The marine primary organic aerosols are calculated by the model considering the partitioning between insoluble organics and sea salt using a parameterization developed by O'Dowd et al. (2008) and modified by Vignati et al. (2010):

$$\%\ organic\ mass = 43.5 * Chla\ [mgm^{-3}] + 13.805, \quad Chla < 1.43\ mgm^{-3} \qquad \text{Eq. 3}$$

assuming internally mixed sea spray, Chla is chlorophyll-a concentration. The relation between % OM and Chla is valid for chlorophyll concentrations below 1.43 mg m^{-3} and for larger values the percentage is kept constant to 0.76% (Vignati et al., 2010). This parameterization calculates the MPOA as a fraction of the submicron sea-salt aerosol that is based on the chlorophyll-a present on the ocean surface. Chlorophyll-a concentrations are satellite-derived monthly average MODIS observations at a resolution of 1°x1°. The density of water insoluble organic mass has been chosen as 1 g cm^{-3} (Vignati et al., 2010) and of dry sea salt = 2.165 g cm^{-3}. The insoluble organic matter is they are put into the insoluble accumulation mode. Sea-salt emissions are parameterized as suggested by Gong, 2003 and adapted by Vignati et al. (2010) accounting for particles radius increase due to the added organic material from the oceans:

$$D_m = 0.09\ x\left(1 + 0.5\frac{Chla[mgm^{-3}]}{1.126}\right) \qquad \text{Eq. 4}$$

where D_m is the final accumulation mode diameter of the mixture of organic matter with sea salt, using the same threshold Chla as for Eq. 3. This function allows the calculation of the variation in accumulation mode modal diameter with both season and location.

It is assumed that submicron MPOA is entirely insoluble and mixed with sea-salt, in contrast to terrestrial primary organic aerosol (POA) from combustion and fossil fuels which are assumed to be emitted as 50% hydrophilic (Cooke et al., 1999). The aging of insoluble POA of continental origin is taken into account as described by Tsigaridis and Kanakidou (2003), with a global mean turnover time of approximately one day. Additionally, based on research by Facchini et al. (2008), we have adopted a coarse mode MPOA source as suggested by Gantt et

al. (2009). The implementation of this source in TM4-ECPL model is presented in (Myriokefalitakis et al., 2010).

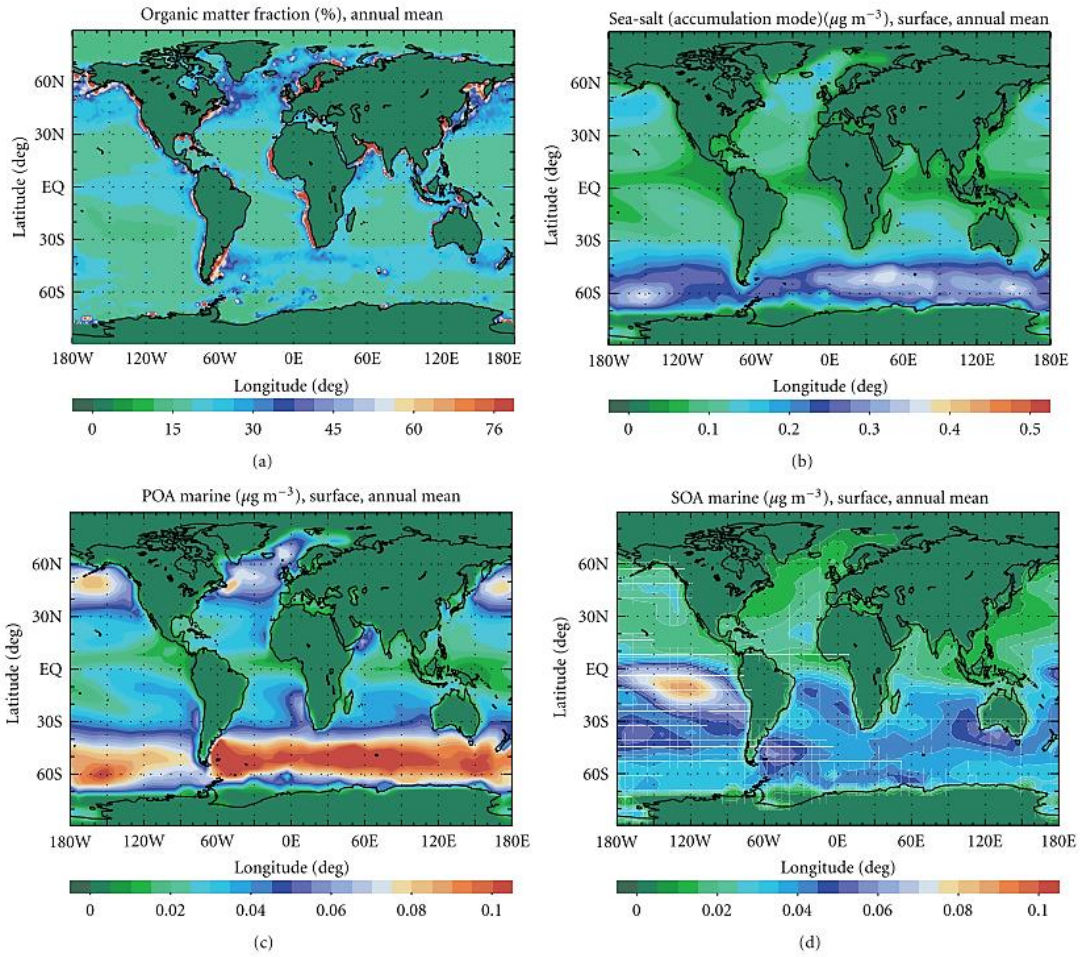

Figure 24: Annual mean surface distributions of (a) mass fraction of organic matter to submicron sea-spray aerosol calculated based on Chl-a as described by Vignati et al. (2010) *(b) sea-salt in the accumulation mode; (c) MPOA; (d) total marine secondary organic aerosol (from MS–isoprene and monoterpenes); in μgm^{-3} ,* (Myriokefalitakis et al., 2010)

3.1.3.3 Terrestrial primary biological aerosol emission

Primary biological aerosol particles emissions in TM4-ECPL are described in Myriokefalitakis et al. (2017) and (Myriokefalitakis et al., 2016).

Bacteria (BCT) emissions are parameterized as in Burrows et al. (2009). Burrows et al. (2009) used a number of near-surface observations and model simulations to provide best-fit estimates of BCT flux rates for particles of 1 μm diameter based on different ecosystems (coastal, crops, wetlands, land-ice, grassland and shrubs) (Figure 25). The original land types

on the 0.5°x0.5° by Olson Global Ecosystem Database is lumped to 10 ecosystem groups as proposed by Burrows et al. (2009b) (Figure 25). The number fluxes f_i (see table in Figure 25) are used here, weighted by the area fraction of the respective ecosystems in the gridbox (a_i).

$$F_{BCT} = \sum_{\iota=1}^{10} \alpha_i \, . \, f_i \qquad \textit{Eq. 5}$$

Here the index i runs over the up to ten ecosystems with nonzero bacterial emissions.

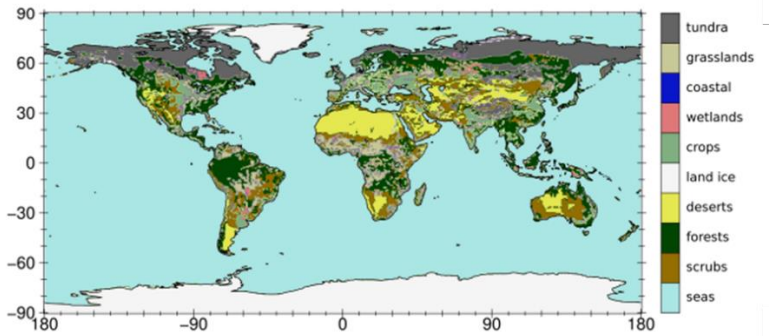

Ecosystem	Area (10^6 km^2)	F_i (m^{-2} s^{-1}) in simulations PBAP and PBAP-intermediate
Coastal	0	900
Crops	22.7	704
Deserts	19.1	0
Forests	30.3	0
Grasslands	32.9	648
Land-ice	15.5	7.7
Seas	362.6	0
Shrubs	20.3	502
Tundra	7.0	0
Wetlands	4.2	196

Figure 25: Lumped ecosystem classes, based on the Olson World Ecosystems (Olson, 1992). The table depicts bacterial emission fluxes (best-fit and 95th percentiles of emission estimates by Burrows et al (2009a)), and ecosystem area.

Fungal (FNG) fluxes linearly depend on the leaf area index (LAI) and the specific humidity (q), based on near-surface mannitol observations fraction as suggested by Hummel et al. (2014) with a mean diameter of 3 µm:

$$F_{FNG} = 20.426 \cdot (T - 275.82K) + 3.93 \cdot q \cdot LAI \qquad \textit{Eq. 6}$$

The grid cell mean LAI is given by the model CLM (Community Land Model) and undergoes month-to-month variations (Bonan et al., 2002).

Bioaerosol sizes in the model range from fine to coarse and their shapes are not accurately known, for the present work PBAP are assumed to be monodisperse spherical particles with

1 g cm^{-3} density (Hummel et al., 2015). The organic matter to organic carbon (OM:OC) ratio of all PBAPs is set equal to 2.6 and the molecular weight equal to 31 g mol^{-1} , as suggested by (Heald and Spracklen, 2009). BCT here are emitted as insoluble aerosols (Ariya et al., 2009) while fungal spores emissions are assumed to be 50 % soluble (Fanourgakis et al., 2019; Mahowald et al., 2008a). However, in TM4-ECPL, all PBAPs can be transferred to the soluble mode during atmospheric aging (Ariya et al., 2009), with the same rate as all primary organic matter in the model.

3.1.2 *Ice nucleation parameterizations*

Mineral dust: The effect of mineralogy on INP concentration is constrained by using the singular approximation of ice-nucleating activities of aerosols and based on laboratory-derived active site parameterizations for K-feldspar and quartz minerals provided by Harrison et al. (2019). The parameterizations for temperature ranges and standard deviation for log(ns(T)), where n_s is in units of cm^{-2} and T is in Celsius, are as follows:

$$\text{Quartz}: \log\left(n_s(T)\right) = -1.709 + (2.66 \times 10^{-4} T^3) + (1.75 \times 10^{-2}\, T^2) + (7 \times 10^{-2} T), \quad \text{Eq. 7}$$

$$(for\ T\ from\ -10.5\ to\ -37.5\ \ ^{\circ}C\ ;\ 0.8)$$

$$\text{K-feldspar}: \log\left(n_s(T)\right) = -3.25 + (-0.793T) + (-6.91 \times 10^{-2} T^2) + (-4.17 \times 10^{-3} T^3) + (-1.05 \times 10^{-4} T^4) + (-9.08 \times 10^{-7} T^5), \quad \text{Eq. 8}$$

$$(for\ T\ from -3.5\ to\ -37.5\ ^{\circ}C;\ 0.8)$$

The parameterization for K-feldspar is valid between -3.5°C and -37.5°C, while for quartz between -10.5 and -37.5°C temperature range.

In order to estimate aerosol surface area, we assume that each mineral dust particle is spherical and externally mixed (Atkinson et al., 2013; Vergara-Temprado et al., 2017). The ice nucleation active surface site density that is derived by the spectrum of ice-nucleating properties and for a polydisperse aerosol sample is given by the Poisson distribution:

$$INP_{mineral\ dust}(T) = \sum_i \sum_j n_{i,j} \left\{ 1 - e^{[-S_{i,j}\, n_s(T)]} \right\} \quad \text{Eq. 9}$$

Where INP is the ice number concentration formed on the aerosol based on parameterizations provided in Harrison et al. (2019), $n_{i,j}$ is the total aerosol number concentration (per m^{-3}), indexes i, j correspond to aerosol type (quartz or K-feldspar) and size mode (accumulation or coarse mode), respectively. $S_{i,j}$ is the individual aerosol particle mean surface (cm^{-2}) area in size mode *j*.

Marine organic aerosols*:* The parameterization of sea spray INP based on material collected from the sea surface microlayer was developed by Wilson et al. (2015) to predict INP based on total organic carbon and ice-nucleating temperature. Wilson et al. (2015) expresses the spectrum of active sites density per unit mass of total organic carbon (TOC) contained in insoluble marine organic aerosols at temperature range between −6°C to −27°C. A factor of 1.9 is used for the conversion of MPOA to organic carbon in TM4-ECPL (Burrows et al., 2013). The number of marine INP is calculated following the equation below.

$$INP_{marine} = TOC_{marine}\, e^{[11.2186 - (0.44593 \cdot T)]} \quad \text{Eq. 10}$$

where TOC is the total organic carbon (gr) in marine particles and (*T)* temperature in Celsius.

Terrestrial bio-aerosols: To simulate the number concentrations of INP active under mixed-phase cloud conditions derived from terrestrial bio-aerosols (bacteria and fungal spores), the parameterization of Tobo et. (2013) is used. This parameterization is a modified version of the parameterization proposed by DeMott et al. (2010), who demonstrated that INP parameterizations that account only for dependence on temperature could be improved by taking account of dependence on the number concentration of aerosol particles with diameters larger than 0.5µm. Tobo et al. (2013) refined this parameterization to calculate INP number concentration at the temperature ranging from about -34°C to -9°C and the number concentrations of ambient fluorescent biological aerosol particles with diameters larger than 0.5 µm, as follows:

$$INP_{PBAPs} = (N_{PBAPs,>0.5\mu m})^{\alpha'(273.16-T)+\beta'} e^{\gamma'^{(273.16-T)}+\delta'} \quad \text{Eq. 11}$$

Where, α′ =-0.108, β′ = 3.8, γ′ = 0, and δ′ = 4.605, N_{PBAPs} number concentration of PBAPs with diameter larger than 0.5μm and temperature (*T*) in Kelvin.

3.1.3 The simulations performed

In Table 7, a comprehensive overview of the TM4-ECPL model setup is presented. It includes details about the period of the simulations, the model resolution and meteorology that is used by the model. Additionally, two different soil mineralogy datasets were incorporated and tested in the model, enabling evaluation of the sensitivity of the model results to the used soil mineralogy. The emissions parameterizations used in the simulations for each aerosol type, are also outlined. The simulated tracers, precursors of INP are also listed, indicating the specific variables and components tracked by the model. Lastly, the table provides insights into the model's physical and dynamical processes.

Table 7 :TM4-ECPL model set up.

	TM4-ECPL	
Years	2009 -2016	
Resolution	horizontal resolution of 3◦ in ***longitude***, by 2◦ in ***latitude*** 25 hybrid layers in the vertical, from the surface up to 0.1 hPa model time step of 30 min	
Meteorology	ECMWF (European Center for Medium-Range Weather Forecasts) Interim re-analysis project (***ERA-Interim***) (Dee et al., 2011)	
Mineralogy	1.Claquin et al. (1999) based on brittle fragmentation theory (BFT) by Kok (2011) (*base case*)	2. Journet et al. (2014) based on brittle fragmentation theory (BFT) by Kok (2011)
Emissions	***MPOA-SS*** (accumulation-coarse mode) (Vignati et al., 2010; Gong, 2003; Facchini et al., 2008) ***Mineral Dust (K-feldspar, quartz)*** (accumulation-coarse mode) (Tegen et al., 2002) ***PBAPs (bacteria, Fungal spores)***	

	(monodisperse) (Burrows et al., 2009b; Hummel et al., 2015)
Tracers	***INP _mpoa*** (Wilson et al., 2015) ***INP _Kfeld , INP _qua*** (Harrison et al., 2019) ***INP _fngl, INP _bct*** (Tobo et al., 2013)
Model's physical and dynamic processes	***Convection*** (Tiedke, 1989) ***Diffusion*** (Louis ,1979) Wet deposition: ***In-cloud, below-cloud scavenging*** (Jeuken et al., 2001) ***Dry deposition*** (Tsigaridis et al., 2006) ***Gravitational settling*** (Seinfeld and Pandis, 1998)

3.2 Data used for model evaluation

3.2.1 Dust aerosol data

Observations of INP and their precursor aerosols have been used to evaluated model results. These are:

1. dust observations from stations in areas suitable for studying emissions of Saharan dust and its atmospheric transport. Four stations (M'Bour, Bambey, Cinzana, and Banizoumbou) are located at the edge of the Sahel, the major natural dust source of the region (Lebel et al., 2010), three stations (Miami, Barbados and Cayenne) are on the American continent downwind the dust Atlantic transport (Zuidema et al., 2019; Prospero et al., 2020) and two stations, Finokalia (Crete, Greece) (Mihalopoulos et al., 1997; Kalivitis et al., 2007) and Agia Marina (Cyprus) (Kleanthous et al., 2014; Pikridas et al., 2018) lie on the dust transport route crossing the Mediterranean (Figure 27).

2. climatological annual means of dust surface from the Rosenstiel School of Marine and Atmospheric Science (RSMAS) of the University of Miami (Arimoto et al., 1995;

Prospero, 1999) and the African Aerosol Multidisciplinary Analysis (AMMA) (Marticorena et al., 2010).

3. observations for modern climate compiled by Albani et al. (2014) from 110 different locations. Both the dust deposition fluxes and the constrained mass fraction for particles with a diameter lower than 10μm conformed to the range of simulated sizes of dust (Figure 26).

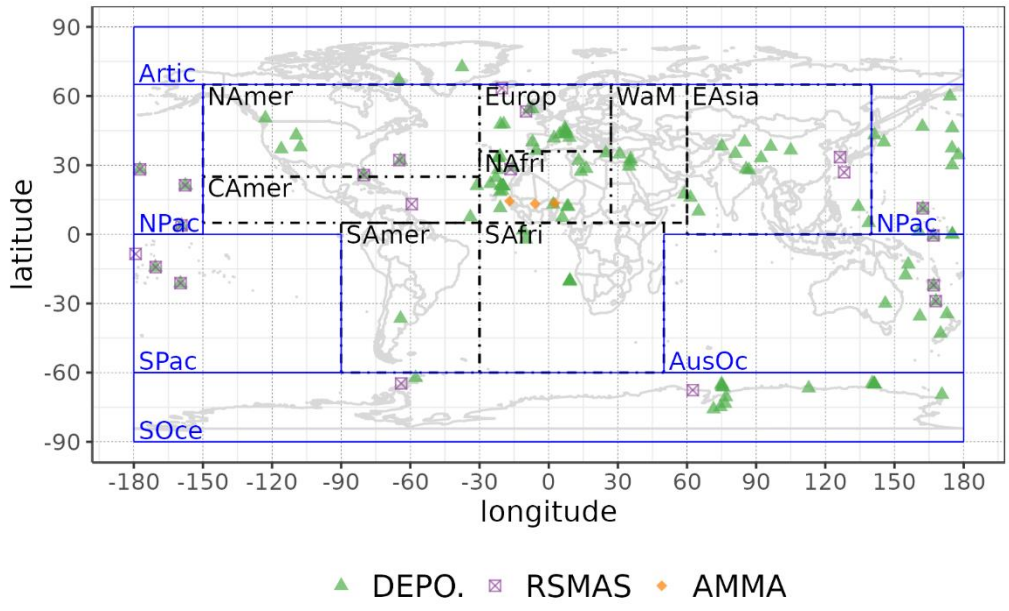

Figure 26: Site location map of observations dust surface concentration (RSMAS, purple squares; AMMA, orange diamonds), and dust deposition rates (several sources compiled in Albani et al.,2014, green triangles) (Chatziparaschos et al., 2023).

3.2.2 Methodology to derive the dust content of atmospheric aerosols

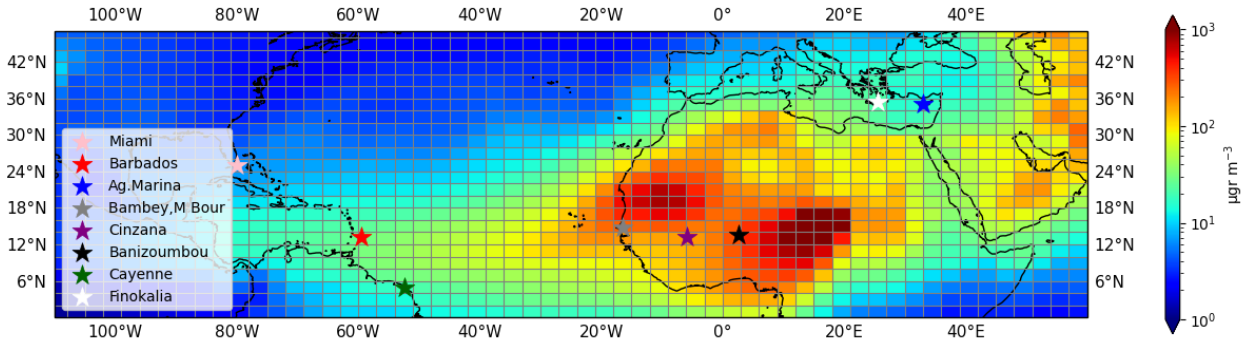

Figure 27: The location of the 8 stations used for the model validation, plotted over the dust concentration field simulated by TM4-ECPL model for summer 2015. Note that the two stations, M'Bour and Bambey, are so close to each other that they are superimposed on the map. The grey grids correspond to the model gridding in 3◦ x2◦ resolution (Chatziparaschos et al., 2023).

Air masses from Africa transported over the open sea were selectively sampled at Miami and Barbados stations. The mineral dust fraction was then calculated from the aluminium (Al) content in the ash residue of the burned sample (assuming an 8% Al content) (Zuidema et al., 2019). At the location of Cayenne, the dust load is calculated by subtracting a regional background from the PM_{10} concentrations measured by the ATMO-Guyane organizations using TEOM (tapered element oscillating microbalance) instrumentation (Prospero et al., 2020). For the Sahel stations, the reported measurements are for total PM_{10}. As the stations are close to the dust emission source, dust concentration can be estimated by omitting in the calculation of the monthly averages the air masses originating from areas containing a significant amount of aerosols from other sources (mainly, biomass burning for Banizoumbou and Cinzana, sea salt and urban pollution for M'Bour and Bambey) (Reid et al., 005; Lebel et al., 2010; Kok et al., 2021). Filtering the observations according to wind direction might lead, however, to an overestimation of the real dust concentrations, as even dust-rich air masses coming from the source regions may contain aerosols other than dust. For the stations of Banizoumbou (Niger, 13.54°N, 2.66°E) and Cinzana (Mali, 13.28°N, 5.93°W), we filtered out southerly air masses during the dry season (December to February) to avoid the interference of biomass burning aerosols (Cavalieri et al., 2010). For the M'Bour (Senegal, 14.39°N, 16.96°W) and Bambey (Senegal, 14.70 °N, 16.47 °W) stations, we excluded the air masses rich in sea-salt and pollutants associated with wind sectors originating from marine and urban areas. Following Kok et al. (2021), we accounted for the correction from geometric to aerodynamic diameter when comparing the model dust concentration with the Sahel

measurements. To do so, we used the result of Huang et al. (2020), who calculated that for desert dust, a geometric diameter of 6.8 μm corresponds to an aerodynamic diameter of 10 μm. For the stations of Agia Marina (35°N, 33.06°E) (Pikridas et al., 2018) and Finokalia (25.67°N, 35.34°E), the dust concentration is calculated from measurements of total PM load following the methodology developed by Escudero et al. (2007), using air mass origin characterization based on air mass back-trajectories.

3.2.3 INP data

The INP concentrations calculated by the TM4-ECPL model with available INP observations from the databases of BACCHUS (Impact of Biogenic versus Anthropogenic emissions on Clouds and Climate: towards a Holistic UnderStanding) (http://www.bacchus-env.eu/in/index.php, last access on March 2019) and Wex et al. (2019) (https://doi.pangaea.de/10.1594/PANGAEA.899701, last access on February 2022). For this comparison, $[INP]_T$ concentrations are calculated at the temperature at which measurements were performed. All model results are compared to observations for the specific month and year of the observations, except the observed dataset by Yin et al. (2012), which covers temporally scattered measurements (between 1963 to 2003) (Figure 28).

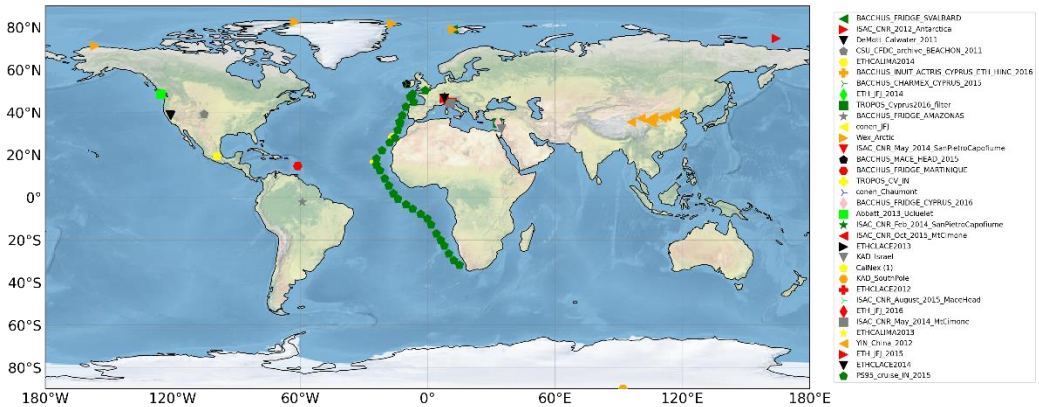

Figure 28: Location of the data used for comparison in Figure 37. (Chatziparaschos et al., 2023)

Table 8: Data sets used for this study. Campaign/data

Campaign/data set	*Location*	*References*
Arctic station Barrow/Utqiagvik	Arctic	(Wex et al., 2019)
Alert (Canadian Arctic Station)	Arctic	
Arctic station Ny-Ålesund	Arctic	
Station_Nord (Villum Research Station)	Arctic	
PS95 Atlantic Cruise 2015	Atlantic	(Welti et al., 2020)
KAD_Israel	Tel Aviv	(Ardon-Dryer and Levin, 2014)
KAD_South_Pole	South Pole	(Ardon-Dryer et al., 2011)
Conen_ Chaumont	Jungfraujoch and Chaumont	(Conen et al., 2015)
CYPRUS BACCHUS/CHARMEX 2015	Forestry Department site, Agia Marina	(Ansmann et al., 2019)
BACCHUS_FRIDGE AMAZONAS	Amazonian Tall Tower Observatory	(Schrod et al., 2020)
CalWater	Coastal California, Airborne	(Fan et al., 2014)
Conen_JFJ	Jungfraujoch	(Conen et al., 2015)
CLACE2014	Jungfraujoch	(Lacher et al., 2021, 2018, 2017) (Boose et al., 2016c)
CLACE2013	Jungfraujoch	
CLACE2012	Jungfraujoch	
CalNex	California	(Wang et al., 2012)
CALIMA 2014	Izana observatory, Tenerife	(Boose et al., 2016c)
CALIMA 2013	Izana observatory, Tenerife	(Boose et al., 2016)
ISAC-CNR MaceHead BACCHUS Campaign	Mace Head Observatory, Carna, Galway, Ireland	(Rinaldi et al., 2016)
ISAC-CNR SanPietro_Capofiume BACCHUS Campaign	San Pietro Capofiume (BO, Italy)	(Belosi et al., 2017)
ISAC_CNR_MtCimone BACCHUS Campaign	mountain observatory Mt. Cimone	(Rinaldi et al., 2017)
ISAC-CNR Antarctica BACCHUS Campaign	Mario Zucchelli Station, Terranova Bay, Antarctica	(Belosi et al., 2014)

BACCHUS_FRIDGE_SVALBARD Campaign	Zeppelin Observatory, Svalbard/Spitzbergen	(Schrod et al., 2020)
BACCHUS_FRIDGE_MARTINIQUE	Volcanic and Seismologic Observatory, Fonds-Saint-Denis, Martinique, Caribbean	(Schrod et al., 2020)
CSU_CFDC_archive_BEACHON	Manitou Experimental ForestObservatory (MEFO)	(Tobo et al., 2013)
ETH_JFJ_2014	Jungfraujoch High Altitude Research Station	(Lacher et al., 2017)
ETH_JFJ_2016	Jungfraujoch High Altitude Research Station	(Lacher et al., 2017, 2018)
ETH_JFJ_2015	Jungfraujoch High Altitude Research Station	(Lacher et al., 2017)
TROPOS_Cyprus2016	Agia Marina, Xyliatou, Cyprus	(Ansmann et al., 2019; Schrod et al., 2017)
TROPOS_CV_IN	Cape Verde	(Welti et al., 2018)
Yin_China	China	(Yin et al., 2012)
NETCARE_2013	Coastal (West coast of Canada)	(Mason et al., 2015)

3.3 Statistical indicators for model evaluation

Table 9 summarizes the statistical parameters used to validate the model, and the locations (and regions) of the various observations are depicted in Figure 30. The correlation coefficient (*R*) reveals the linear relationship between model results and observations, while the normalized mean bias (nMB), and the normalized root-mean-square error (nRMSE) are the measure of the mean deviation of the model from the observations due to random and systematic errors. All the equations that are used for the statistical analysis of model results are provided below (Eqs. 11–13):

$$R = \left[\frac{\frac{1}{N}\sum_{i=1}^{N}(O_i - \bar{O})(P_i - \bar{P})}{\sigma_o \sigma_P}\right] \quad \textit{Eq. 12}$$

$$NMB = \frac{\sum_{i=1}^{N}(M_i - O_i)}{\sum_{i=1}^{N}(O_i)} x100 \quad \textit{Eq. 13}$$

$$nRMSE = \frac{\sqrt{\frac{1}{N}\sum_{i=1}^{N}(P_i - O_i)^2}}{\sum_{i=1}^{N} O_i} \quad \textit{Eq. 14}$$

where O_i and P_i stand for observations and predictions, respectively, and N is the number of pairs (observations, predictions) that are compared.

4. Evaluation of dust and PBAPs

4.1 Dust

Airborne dust concentration is of paramount importance to this work, since dust affects directly the amount of INP in the atmosphere. Consequently, we evaluate modelled dust by comparing with monthly averaged dust observations from stations that are in the outflow of Saharan desert and with worldwide climatological observations. The climatological annual means comparison allows us to validate the geographical distribution of sources and transported dust regions, while the monthly means comparison reveals if the intra-annual variability can be well captured by the model.

We first evaluate the dust mass simulations against monthly averaged dust observations at nine ground-based stations between 2000 and 2017. Figure 27 shows the location of these stations plotted over the simulated dust concentration for summer 2015. Figure 29 depicts the comparison of model dust aerosol concentrations with observations on a monthly mean basis (correlation coefficient, R=0.81).

The mean bias between model and observations is 8.3 $\mu g \cdot m^{-3}$. The total average dust concentration observed at the selected locations and during the studied period 2000-2017 is approximately 43.3 $\mu g \cdot m^{-3}$. Thus, the mean bias corresponds to 5% of the total concentration. The relative error increases with decreasing concentrations, and only a few outliers are not within one order of magnitude of the observations in Figure 29, mainly corresponding to observations at the Caribbean and American stations.

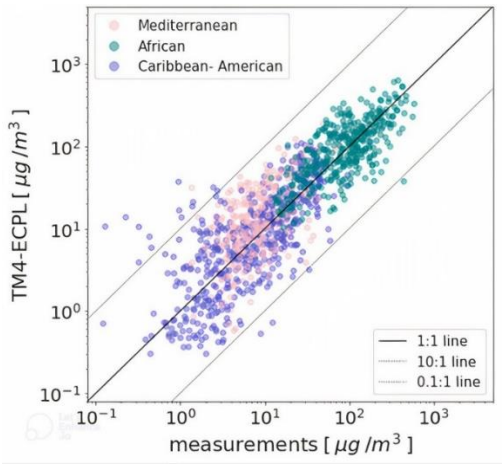

Figure 29: Monthly averaged model-simulated dust concentration versus observed at selected locations in μg·m^{-3}. The continuous black line is the 1:1 line, while the dashed lines are the 10:1 and 1:10, top and bottom lines, respectively. The stations are geographically grouped: African stations in green (M'bour, Bambey, Cinzana, Banizoumbou), American stations in violet (Miami, Barbados, Cayenne), and Mediterranean stations in pink (Agia Marina and Finokalia). Simulations were run with a 3°x2° spatial resolution (Chatziparaschos et al., 2023).

.

We further evaluate modelled dust by comparing with climatological globally distributed observations of dust surface concentration and deposition for the years from 2009 to 2016 when we also perform the comparison between observed and modelled INP concentrations. The observations are compared with the multi-annual model mean surface dust concentration (Figure 30a). We also compare the modelled deposition dust fluxes with observations from Albani et al. (2014) (Figure 30b).

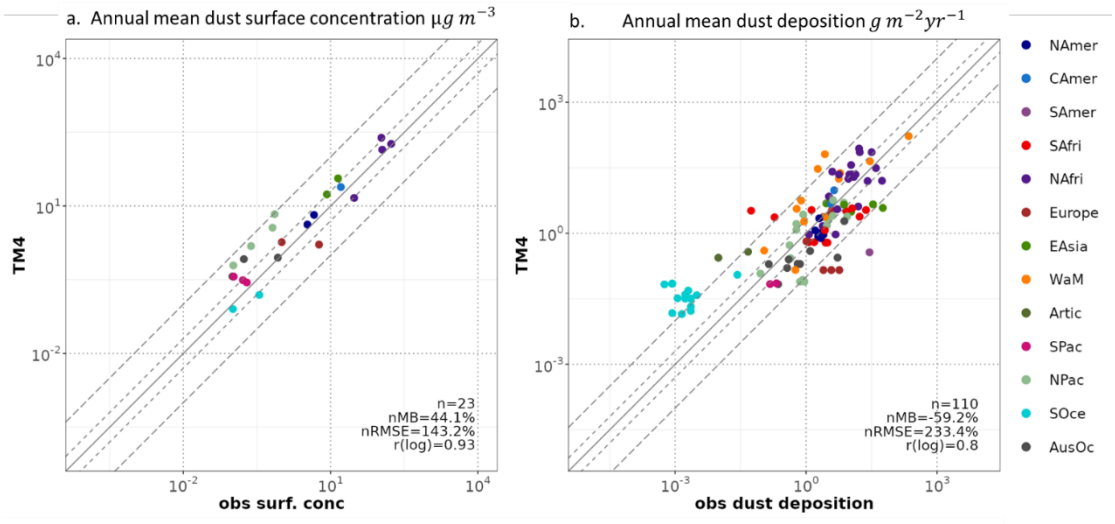

Figure 30: Comparison of (a) the modeled annual mean dust surface concentration for the years 2009–2016 against climatological mean values from RSMAS sites and AMMA campaign, and (b) modeled annual dust deposition flux

averaged for the same period against observations compiled by Albani et al. (2014) from several sources. The solid line represents the 1 : 1 correspondence, the long dashed lines show the 10 : 1 and 1 : 10 relationships, and short dashed lines correspond to a factor of 2, respectively. Colors indicate measurement locations listed in the figure legend (Chatziparaschos et al., 2023).

The geographical distribution of the available concentration stations (23 in total) in Figure 30a covers locations close to emission sources (AMMA stations over the Sahelian dust transect), and in both transport and remote regions (RSMAS). The overestimation of the dust surface concentration already shown at the monthly scale is also observed in the comparison with annual mean climatological observations, with an overall normalized mean bias of 44.1%. Errors are generally larger after transport to remote regions, particularly over the North Pacific, than over source regions (Figure 30a). When it comes to deposition, the errors are larger than in the representation of the surface concentration fields, particularly overestimations are found over the Southern Ocean and Arctic, than downwind sources (Figure 30b); while concentrations over Europe and South America are largely underestimated. They are, however, kept within the one-order of magnitude differences, except for those points located over the Southern Ocean, where overestimations are significant. The aerosol concentrations and deposition fluxes in such remote regions are usually low and thus, small differences are emphasized in relative terms. There may be multiple causes for the discrepancy between modelled and observed fluxes (e.g., an excessive modelled fine fraction of aerosols, differences in the wet deposition fluxes caused by differences in precipitation, differences in the observed and modelled period, or uncertainties associated to the observations themselves). The main purpose of this comparison is to assess the ability of the model to reproduce the geographical distribution of dust in the atmosphere, which is found satisfactory, and exploring further the issues behind the deviation in a particular remote region is out of the scope of this work.

Table 9: Summary of statistics for all points and per region for the evaluation of (a) the modelled annual mean dust surface concentration for 2009– 2016 compared to climatological mean values from RSMAS sites and AMMA campaign, and (b) the modelled annual dust deposition flux averaged for the same period against observations as compiled in Albani et al. (2014) from several sources. The number of stations (n), the Pearson correlation coefficients (R) between the simulated and measured monthly mean concentrations, the normalized mean bias (nMB), and the normalized root-mean-square errors (nRMSEs) are indicated for the TM4-ECPL simulation.

	n	*R*	*nMB(%)*	*nRMSE (%)*		*n*	*R*	*nMB(%)*	*nRMSE (%)*
Dust surface concentration					**Dust Deposition rates**				
N. America	1		35.66	38.54	Arctic	2		1032.05	1038.09
C. America	2		50.60	50.60	N. America	6		-83.42	107.81
Europe	2		-48.92	88.03	C. America	2		-44.25	68.06
N. Africa	4		37.97	66.62	S. America	1		-99.35	99.35
E. Asia	2		138.61	150.95	Europe	13		-74.28	129.73
Australian oceans	3		87.83	111.26	N. Africa	23		-54.33	143.07
S. Pacific Ocean	3		105.04	115.32	S. Africa	5		-77.39	92.66
N. Pacific Ocean	4		630.89	803.67	W. Asia and M. East	5		-94.72	163.86
Southern Ocean	2		-48.25	61.84	E. Asia	12		-31.93	190.09
All Points	23	**0.93**	44.10	143.20	Australian oceans	9		-94.62	195.95
					S. Pacific Ocean	2		-60.99	63.05
					N. Pacific Ocean	15		-30.02	79.72
					Southern Ocean	15		1290.20	1475.04
					All Points	110	**0.80**	-59.20	233.40

4.2 PBAPs

Based on PBAPs parameterizations used in the model, annual emissions of PBAPs for the year 2008 estimated by TM4-ECPL, include 0.79 Tg yr^{-1} of bacteria in the fine aerosol mode, about 76 Tg yr^{-1} of fungal spores and about 47 Tg yr^{-1} of pollen (Table 10). Altogether, PBAP emissions in the model are estimated to equal about 123 Tg yr^{-1} and a global mean lifetime of about 2.8 days is calculated for PBAPs.

Using a mean OM:OC mass ratio of 2.6 as earlier discussed, these emissions correspond to 47.5 Tg-C yr^{-1} that is comparable to the amount of primary particulate OC (46.3 Tg-C yr^{-1}) injected into the atmosphere by anthropogenic emissions. Table 10 also summarizes the simulated bioaerosol emissions strengths and atmospheric burden and compares them to previous studies. This evaluation for TM4-ECPL has been done by Myriokefalitakis et al. (2017).

Table 10: Bioaerosol (PBAP) emissions and burdens and the calculated contributions from bacteria, fungal spores and pollen [a](Hoose et al., 2010), [b] (Burrows et al., 2009a), [c] (Jacobson and Streets, 2009), [d] (Heald and Spracklen, 2009), [e](Mahowald et al., 2008b), [f] (Elbert et al., 2007)

Bioaerosol	TM4-ECPL emissions (Tg yr^{-1})	Literature values for emissions (Tg yr^{-1})	TM4-ECPL burden (Gg)	Literature values for burden (Gg)
Bacteria	0.79	0.75[a], 0.1–1.8[b], 28[c]	11.6	4.3[a], 8.7[b]
Fungal spores	75.8	31[a], 186[c], 28[d], 50[f]	773.4	94[a], 180[d]
Pollen	47	47[a], 84[b]	6.2	22[a]
PBAPs (total)	123.5	78[a], 296[c], 186[e]	791.2	121[a]

5. Global distributions of INP from mineral dust

5.1 K-feldspar and quartz contributions to the global INP distribution from dust

Figure 31a presents the simulated distributions of K-feldspar and quartz particles present at modelled pressure level of 600 hPa that are able to freeze in the immersion mode at -20°C and form ice crystals, hereafter called $[INP]_{-20}$. These conditions are representative of mixed-phase clouds' glaciation and allow both quartz and K-feldspar to activate and act as INP.

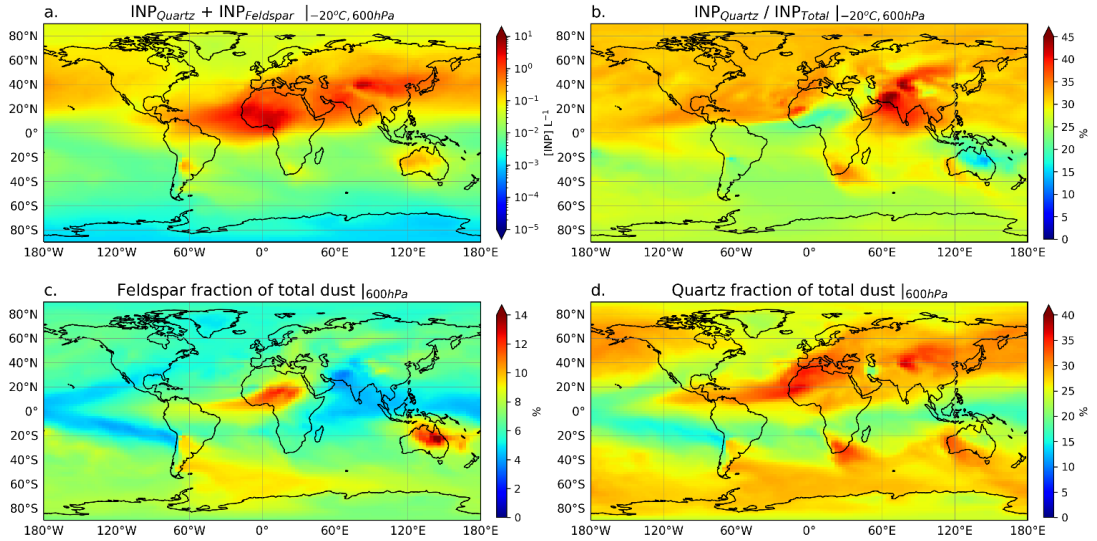

Figure 31: Annual mean distributions calculated by TM4-ECPL for the year 2015 of (a) INP concentrations for an activation temperature of −20°C based on K-feldspar and quartz at a pressure level of 600 hPa, (b) ratio of INP from quartz over total INP from dust (K-feldspar and quartz) at the same conditions, (c and d) mass ratios of feldspar (c) and quartz (d) in percentages over total dust mass at 600hPa. Figure form (Chatziparaschos et al., 2023)

$[INP]_{-20}$ distributions are of interest for their impact on clouds formed in deep-convective systems experiencing large vertical velocities (Figure 19). They are mainly observed in subtropical and tropical regions. $[INP]_{-20}$ concentrations derived from K-feldspar and quartz (Figure 31a) contribute much more to mid-latitude, mid-level mixed-phase clouds in the Northern Hemisphere (NH) than in the Southern Hemisphere (SH) due to the location of dust sources and long-range atmospheric transport patterns that favour dust concentration in the NH. However, there are also dust-related INP sources in the SH, such as those from Patagonia,

South Africa and west Australia, that yield considerable $[INP]_{-20}$ concentrations (larger than 10^{-2} L^{-1}).

To investigate the spatial variability of the contribution of each mineral to potential primary ice crystals concentration at -20°C, we also present the ratio of INP from quartz ($[INP]_{quartz}$) to the INP derived from both quartz and K-feldspar ($[INP]_{total}$ at that temperature (Figure 31b). This analysis shows regions at the pressure level of 600hPa and temperature of -20°C where $[INP]_{quartz}$ has the potential to significantly contribute to the total ice crystals concentration derived by immersion freezing on dust particles. In particular we attribute to quartz 30% of the total $[INP]_{total}$ over North Atlantic, south USA and more than 40% over India and Eurasia.

The areas most affected by ice crystals derived from quartz are the regions of the South Saudi Arabian Peninsula, India, North Indonesia and Eurasia (Figure 31b), where high ratios of quartz minerals to dust mass (Figure 31d) and high concentrations of derived ice crystals of about 0.5 L^{-1} are simulated (Figure 31a). The mass contribution of quartz to the dust particles originating from Saudi Arabia and the Gobi Deserts exceeds 35% (Figure 31d). At the same time, the quartz contribution to ice crystals formed by immersion freezing on dust particles is 35-40% (Figure 31b). When the mass of quartz is six times that of feldspar (Figure 32), the quartz derived ice crystal concentration ($[INP]_{quartz}$) constitutes more than 35-45% of total ice crystals concentration derived from dust (Figure 31b). Furthermore, the North Atlantic and, generally, the NH are likely affected by ice formation from both quartz and K-feldspar. In contrast, the South Atlantic is affected by K-feldspar INP originating from the Patagonia desert since 75% of ice crystals potentially formed at -20°C are derived from K-feldspar, and the remaining 25% is from quartz (Figure 31b). Additionally, high percentages of quartz minerals and low feldspar (about 6%) in terms of mass are calculated over South Africa originating from the Kalahari

Desert. There, 35% of the total INP concentrations (around $10^{-2}L^{-1}$) originate from quartz particles (Figure 31c-d).

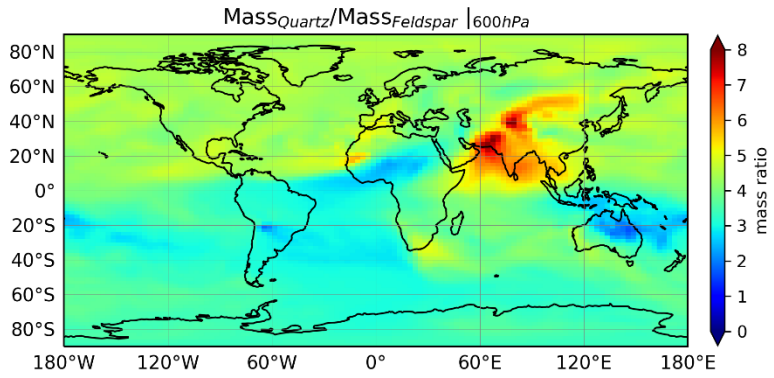

Figure 32: Ratio of quartz to feldspar minerals masses in dust as calculated by dividing quartz mass by feldspar mass.

As expected, concentrations of primary ice crystals derived from dust at the model temperature, $[INP]_{ambient}$, follow the air temperature distribution, showing the highest modelled values roughly poleward of 50 degrees in both hemispheres (Figure 33 for model dust concentrations and temperature at 600 hPa). The contributions of both minerals to primary ice crystals are comparable (Figure 33c-d); $[INP]_{quartz}$ appears as important as $[INP]_{feldspar}$ around 40° and poleward of 70°. Overall, the number concentration of primary ice formed by immersion freezing on dust particles strongly depends on the ambient temperature and the mass concentrations of these minerals, with positive dependence on mass and negative dependence on temperature.

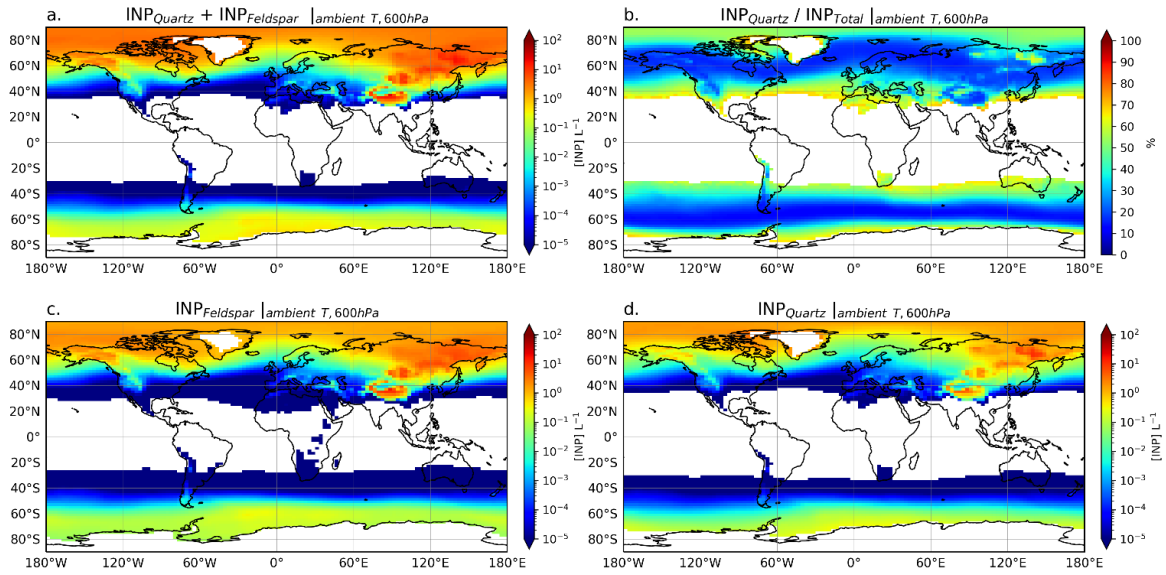

Figure 33: Annual mean distributions of ice-nucleating particles number concentrations $[INP]_{ambient}$ calculated by TM4-ECPL at ambient (model's) temperature and 600 hPa based on the presence both of K-feldspar and quartz (a). Ratio of INP from quartz over total INP from K-feldspar and quartz under the same conditions (b). Panels (c-d) show the corresponding INP concentrations derived individually from each mineral: K-feldspar (c) and quartz (d).

Figure 34a shows the annual zonal mean distribution of primary ice crystals derived from both minerals. Total primary ice crystals ($[INP]_{total}$) maximize approximately at 600-500 hPa below -25 °C in mid-latitudes at local model temperature (Figure 34a), with K-feldspar-derived ice crystals accounting for the largest fraction (Figure 34b). This behaviour is attributed to the high ice activity of K-feldspar and its temperature dependence. However, at lower altitudes and below -12°C, low $[INP]_{total}$ concentrations ($<10^{-2}L^{-1}$) are calculated and are mainly derived from quartz dust particles (60%) (Figure 34b). This outcome is attributed to quartz's high number concentration between 30-40°N at and below 700 hPa, partially associated with higher local quartz than feldspar emissions from Asian dust sources (Claquin et al., 1999; Nickovic et al., 2012). At temperatures below −25 °C, the quartz contribution becomes increasingly important with increases in INP concentration when the temperature decreases, reaching up to 50 % at −35 °C (Figure 34b). These findings agree well with Ilić et al. (2022) and Boose et al. (2016), who showed that quartz could significantly contribute to [INP] at temperatures between the homogeneous freezing limit and −33°C. Overall, $[INP]_{quartz}$

dominates at the lowest and the highest altitudes of dust-derived INP (Figure 34b; reddish colours).

This is clearly demonstrated in Figure 35 for Eurasia where at the range of 700-900hPa and around 450 hPa model pressure levels the contribution of $[INP]_{quartz}$ to total ice crystals from immersion freezing on dust particles exceeds 60%. Figure 36 shows that in the South Hemisphere quartz contribution to total INP is about 40%. Consequently, $[INP]_{feldspar}$ is expected to affect mid-altitude clouds, while $[INP]_{quartz}$ is expected to affect both the low-altitude clouds and the high-altitude cold clouds. The present study emphasizes that INP concentrations could be significantly affected not only by K-feldspar, as generally thought, but also by quartz. The evaluation of the climate impact of these INP is a subject of ongoing research. It requires the incorporation of parameterizations, such as those used here, into a climate model able to simulate ice formation and its interactions within the climate system.

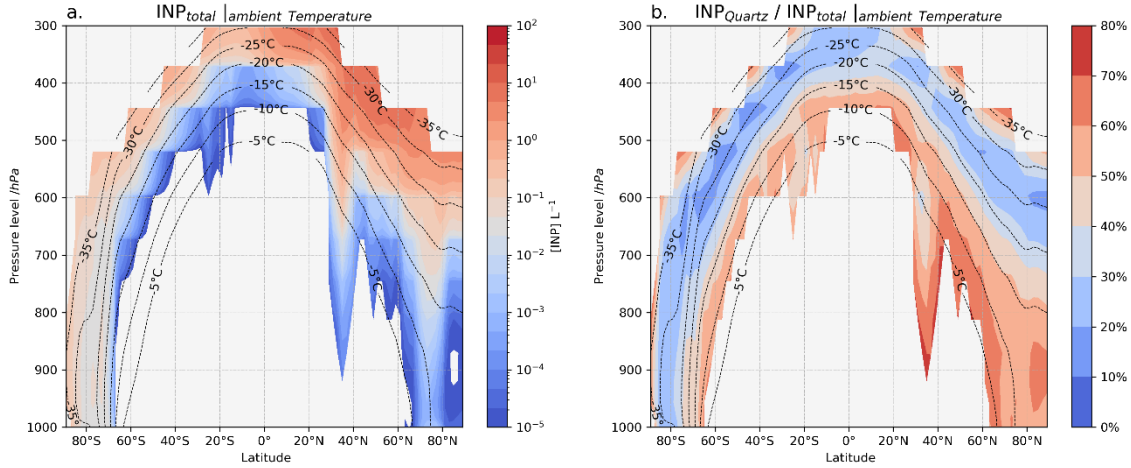

Figure 34: Annual zonal mean profiles of $[INP]_{ambient}$ number concentration for 2015, calculated by TM4-ECPL and accounting for K-feldspar and quartz. The black contour dashed lines show the annual mean temperature of the model. The color map shows the INP concentration derived from feldspar and quartz dust aerosols $[INP]_{total}$ (a) and the ratio of INP from quartz to the total INP from both minerals (b).

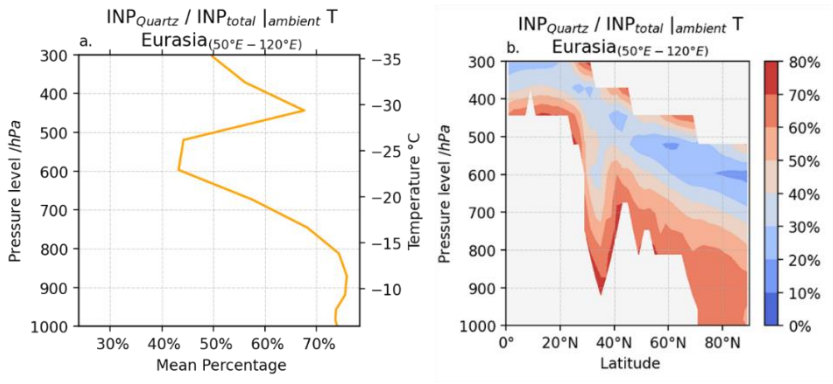

Figure 35: (a) Profile of the mean percent contribution of INP from quartz minerals over Eurasia (50°E-120 °E, 30 °N-66°N). (b) Annual zonal mean over Eurasia, this figure is related to Figure 34.

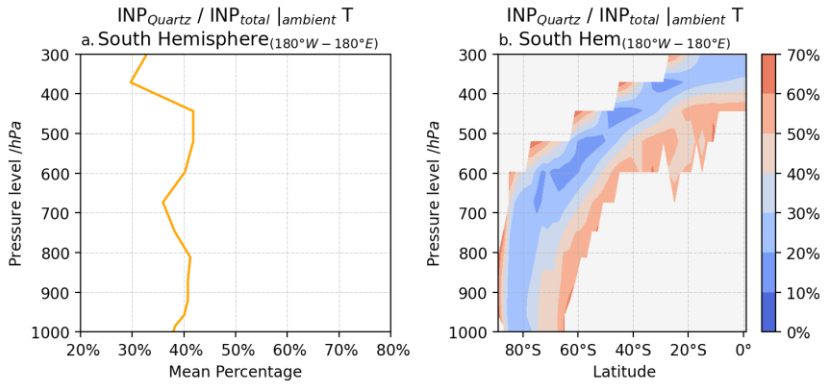

Figure 36: (a) Profile of mean percent contribution of INP from quartz minerals in the South Hemisphere. (b) Annual zonal mean of the percent contribution of INP $_{quartz}$ to the total INP from dust in the South Hemisphere. This figure is related to Figure 34.

5.2 Evaluation of mineral dust INP

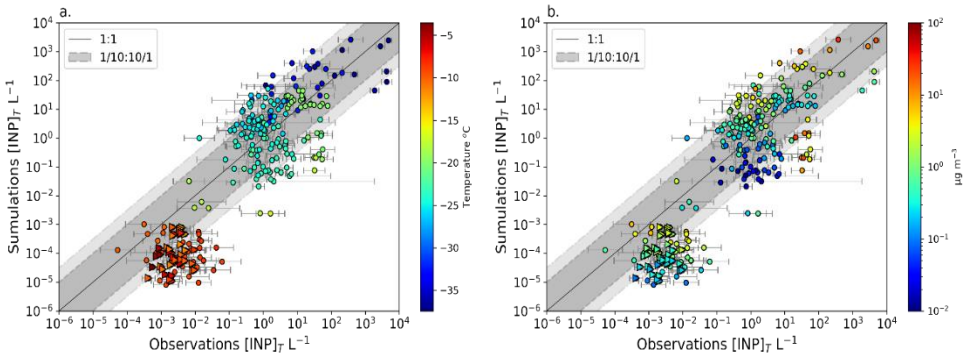

Figure 37: Comparison of $[INP]_T$ concentrations calculated at the temperature of the measurements against observations (locations provided in Table 8). Circle markers correspond to the BACCHUS database and triangles to Wex et al. (2019) database. The dark grey dashed lines represent one order of magnitude of difference between modelled and observed, and the light-grey dashed lines 1.5 orders of magnitude. The simulated values correspond to monthly mean concentrations, and the error bars correspond to the observed error of monthly mean INP values. The color bars show the corresponding instrument temperature of the measurement in Celsius (a) and the modelled dust aerosol mass concentration in µg m^{-3} (b) (Chatziparaschos et al., 2023).

In Figure 37 we compare the INP concentrations calculated by the TM4-ECPL model with available INP observations from the databases of BACCHUS. These data span the years 2009 to 2016 and originate from different campaigns (locations are shown in Figure 28). For this comparison, $[INP]_T$ concentrations are calculated at the temperature corresponding to the instrument temperature of the measurement. All model results are compared to observations for the specific month and year of the observations, except the observed dataset by Yin et al. (2012), which covers temporally scattered measurements (between 1963 to 2003). This dataset is compared to the modeled multi-annual monthly mean INP concentration considering the years 2009 to 2016. The color bar shows the corresponding temperature at which the measurement is performed (Figure 37a) or the modeled dust aerosol mass concentration (Figure 37b). These different color bars allow us to determine if the bias of the model can be correlated with the temperature of the observed INP (e.g., highly active INP, reddish symbols in Figure 37a) or with modelled dust mass (e.g., low modelled dust mass, blueish symbols in Figure 37b). The model agrees reasonably well with observations of INP (R=0.84, Table 11) at the full temperature range of the measurements when dust is present in significant amounts (dust concentrations larger than 10^{-1} µg m^{-3}), (Figure 37b) and at temperatures lower than -10°C (Figure 37a). Overall, the model reproduces about 51% of the

observations within an order of magnitude and about 69% within one and a half orders of magnitude (Table 11).

The model is not efficient enough in simulating highly ice-active INP observed in both Wex (triangles) and BACCHUS (circles) databases (Figure 37a, red spots corresponding to high temperatures). The temperature range of these measurements is very close to the temperature limits of the Harrison et al. (2019) parameterization. Since the quartz parameterization temperature limit is at -10.5°C, INP observations measured between -3.5 °C and -10.5°C are compared with simulated INP derived from K-feldspar only.

Table 11: Statistical performance of the simulations assuming different minerals as INP precursors in the model. Pt_1 and $Pt_{1.5}$ are the percentages of data points reproduced within an order of magnitude and 1.5 orders of magnitude in the temperature range of every parameterization. R_1 and $R_{1.5}$ are the correlation coefficient on related to Pt_1 and $Pt_{1.5}$ percentages. The number of data points used for calculating these values is shown under the data points column. The correlation coefficients have been calculated with the logarithm of the values.

Parameterization: (Harrison et al., 2019)	*Temperature range*	Pt_1	R_1	*Data point*	$Pt_{1.5}$	$R_{1.5}$	*Data points*	*R*
Quartz	-10.5 to -37.5 °C	45%	0.74	119	58%	0.63	153	
K-feldspar	-3.5 to -37.5 °C	50%	0.93	132	66%	0.91	172	
K-feldspar and quartz		51%	0.94	135	69%	0.92	181	
All points							263	0.84

Figure 37b reveals that the observed high concentrations of INP correspond to high dust mass concentrations. Additionally, the observed low concentrations of INP correspond to particles that activate at relatively high temperatures (higher than -10°C; reddish symbols in Figure 38c) and low mass dust concentration (blueish symbols in Figure 37b). Thus, our model underestimates measurements corresponding to low dust mass concentrations (blueish symbols in Figure 37b). As shown in Figure 37a, these low-dust mass points correspond to measurements performed at temperatures around -20°C and -25°C. Therefore, these INP observations, not reproduced by our model when accounting only for dust-originating INP, are probably not solely affected by airborne mineral dust, pointing to other aerosol sources contributing to INP as discussed below.

Figure 38 depicts the comparison to observations using quartz and K-feldspar separately. This figure reveals that INP from quartz can improve the comparison with observations at low temperatures, which corroborates the suggestion the experimental study by Boose et al. (2016) that for temperatures between -33°C to -37°C, quartz can be a significant contributor to INP concentration. Figure 38d clearly shows that consideration of quartz together with K-feldspar INP improves the comparison with observations by moving the respective points closer to the 1:1 line. This is particularly true for high INP concentrations at low temperatures (below -30°C) and for relatively low INP concentrations at temperatures around -20°C. Overall, about 3% more data points are within 1.5 orders of magnitude from the observations when accounting for quartz INP in addition to feldspar INP (Figure 38).

Additionally, modeled INP concentrations are strongly underestimated compared to observations for temperatures above -25°C. Thus, above that temperature other aerosols types might contribute to INP (Figure 38c). In agreement with our findings, Si et al. (2019) pointed out that mineral dust was a major contributor to the INP population at temperatures lower than -25°C. They also found that, for three coastal sites, modeled INP concentrations based on K-feldspar as the only INP precursor agreed well with INP measurements at -25°C, but measurements at −15°C were underestimated. Both our results and Si et al. (2019) indicate a source of INP other than dust that activates at temperatures higher than -25°C, as can be seen in Figure 38c.

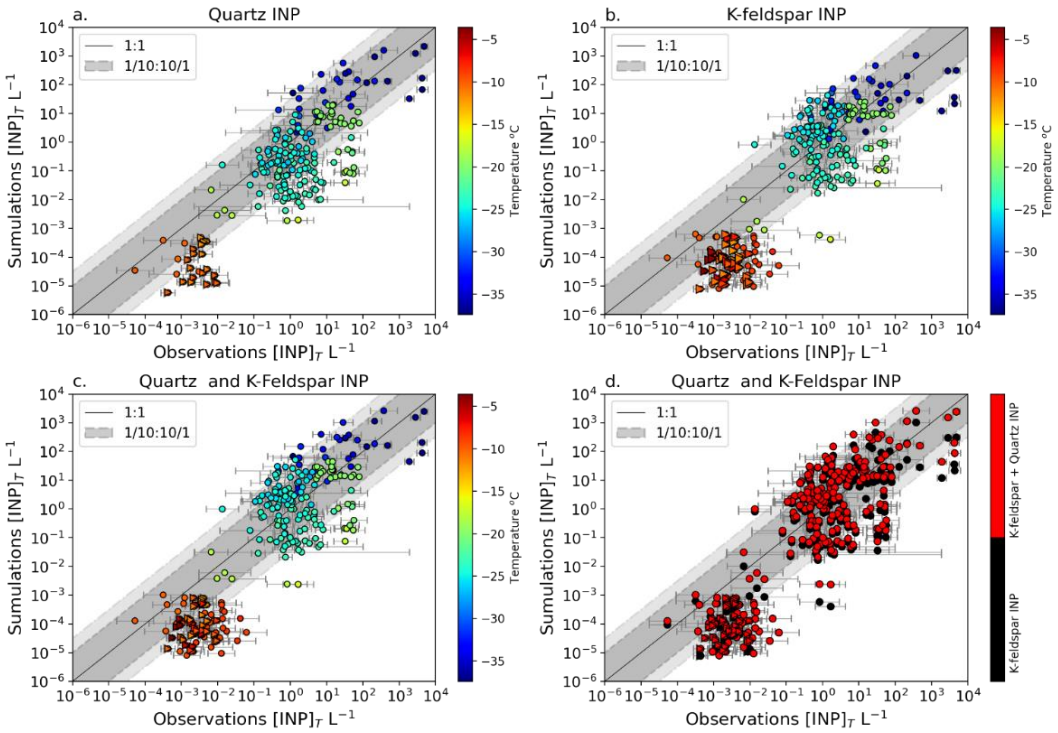

Figure 38: Comparison of $[INP]_T$ concentrations calculated at the temperature of the measurements against observations. (a) simulating only quartz derived INP, (b) simulating only K-feldspar derived INP and (c) simulating both quartz and K-feldspar derived INP (d) simulating only feldspar INP (black circles) and both quartz and K-feldspar INP (red circles). This figure is related to Figure 37.

Figure 39 provides a global view of the regions and months where TM4-ECPL model overestimates (blueish) and underestimates (reddish) INP observations. Improving the representation of the dust cycle could reduce the bias of INP simulations. The model underestimate of the dust surface concentrations observations over Europe and Southern Ocean and the dust deposition fluxes over South Africa and Western Asia, discussed in section 4.1, may at least partly explain the underestimation by the model of the observed INP concentrations (close to 2 orders of magnitude, reddish points) in these regions. Additionally, model deviation from measurements could be attributed to potential inaccuracies in the simulated content of quartz and K-feldspar due to uncertainties in the dust cycle and in the emitted mineral fractions (Perlwitz et al., 2015; Pérez García-Pando et al., 2016). Furthermore, the boxes in Figure 39 depict the climatological monthly mean bias (observations –model) at specific regions (Arctic, Europe, China, North America, Central America, North Africa, South Africa and West Asia-Middle East). This analysis shows that observed INP concentrations are underestimated by 2 orders of magnitude over Europe during autumn and over West Asia-Middle East during autumn and winter. However, the model captures the seasonality of INP

at Arctic region, simulating well INP between February to July. This is attributed to higher dust emissions that occurred during this period (Werner et al., 2002).

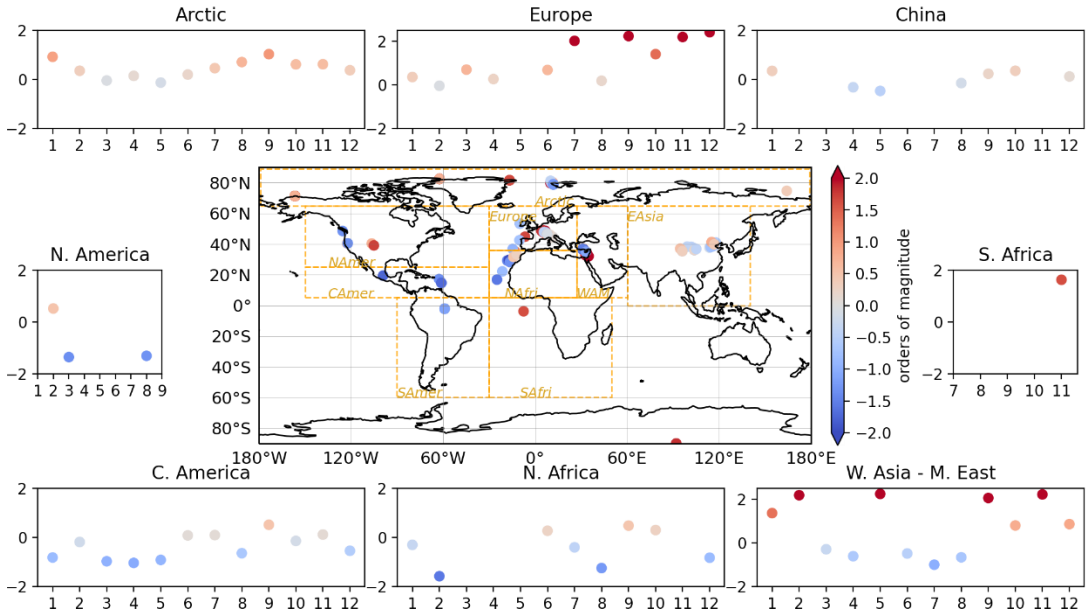

Figure 39: Shows the locations where model overestimates (blueish) and underestimates (reddish) INP observations by ±2 orders of magnitude (color-bar). The location of the points with same coordinates have been moved randomly (1-4° degrees) in the plot for purpose of visualization so it can be seen when the bias affects a single data point. The plots surrounding the map show the climatological monthly mean of the deviations between modelled and observed INP concentration for specific regions. Y-axis shows the bias between model results and observations calculated as the difference log10(observations)-log10(model) while the x-axis indicates the corresponding month or the year.

The overall agreement between the model results and observations is reasonable (see Figure 37, Table 11) but there are significant discrepancies. These differences between model results and observations could be attributed to several factors, such as the omission of the contribution of marine organic (Wilson et al., 2015) and terrestrial biogenic aerosols (Myriokefalitakis et al., 2021; Spracklen and Heald, 2014). Ice nucleation at temperatures in the vicinity of zero is typically related to macromolecules from biogenic entities such as bacteria, fungal spores, pollen, and marine biota. These ice-active macromolecules nucleate ice from just below 0°C down to roughly −20°C (O'Sullivan et al., 2018; Kanji et al., 2017; Murray et al., 2012). Indeed, based on air mass back-trajectories analysis, Wex et al. (2019) (triangles in Figure 37a) suggested that both terrestrial locations in the Arctic and the adjacent sea were possible source areas for highly active INP derived from material of biogenic origin. In addition, mineral dust particles likely only become ice active at low temperatures (see section 5.1), but they may be carriers of biogenic ice-active macromolecules (O'Sullivan et al.,

2014; Hill et al., 2016; O'Sullivan et al., 2016), which enhance dust nucleation activity at higher temperatures. Thus, although some biological nanoscale fragments could be attached to mineral dust particles (Fröhlich-Nowoisky et al., 2015; Violaki et al., 2021; O'Sullivan et al., 2016), their effect on the ice nucleating activity of dust was not considered here. Furthermore, errors may be partly due to atmospheric processes such as ageing, resulting in ice ability degradation (leading to positive model bias) or a possible underestimation of the concentration of these transported aerosol species (leading to negative model bias). These processes are currently neglected in our model but the sensitivity of the INP simulations to these uncertainties is the subject of an ongoing complementary study.

5.3 Sensitivity of simulated INP concentrations to soil mineralogy

We further investigate the sensitivity of the contribution of dust minerals, K-feldspar and quartz, to INP calculated by the global chemistry transport model TM4-ECPL (Chatziparaschos et al., 2023) to the soil mineralogy by using two different soil mineralogy atlases in the model (Claquin et al., 1999 and Journet et al., 2014). The fractions of minerals emitted in the accumulation and coarse insoluble modes of the model are calculated based on these soil mineralogy atlases and the brittle fragmentation theory (Kok, 2011).

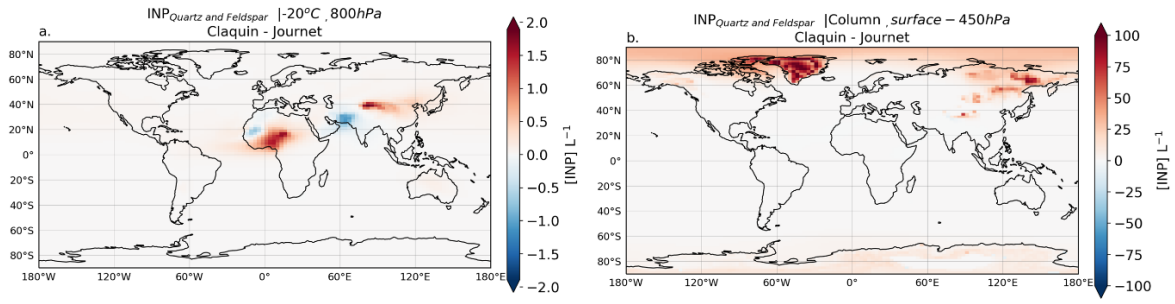

Figure 40: Difference of annual mean distributions calculated by TM4-ECPL based on mineral dust atlases by Claquin et al. (1999) and Journet et al. (2014) a) of INP concentrations for activation temperature of −20°C at a pressure level of 800 hPa and b) of the column INP concentration at model/ambient temperature from surface up to 450hPa.

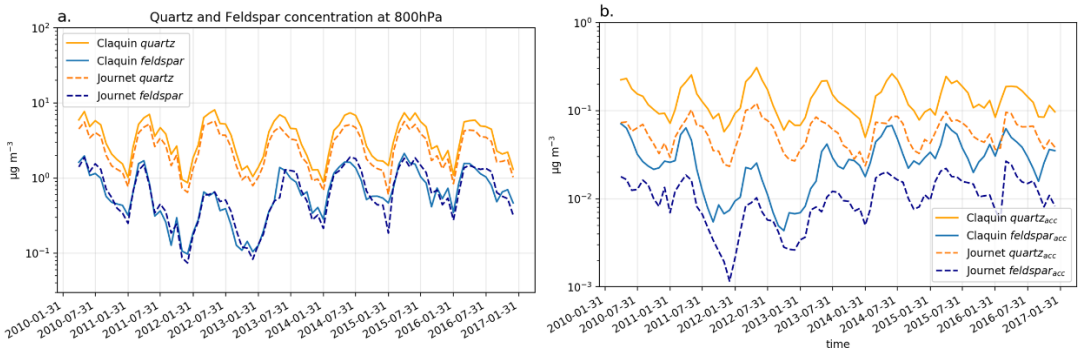

Figure 41: Interannual variability of modelled concentrations from feldspar and quartz based on mineral dust atlases by Claquin et al. (1999) and Journet et al. (2014) for the years 2010 to 2016, a) sum of accumulation and coarse modes b) accumulation mode.

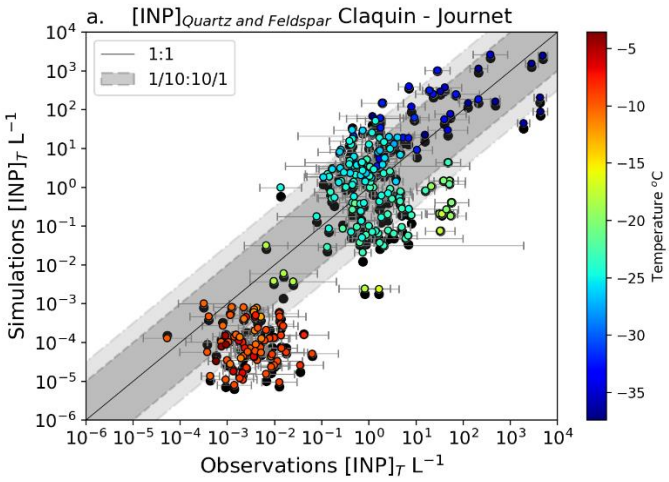

Figure 42: Comparison of INP concentrations calculated at the temperature of the measurements based on mineral dust atlases by Claquin et al. (1999) (coloured spots) and Journet et al. (2014) (black spots) against observations from the BACCHUS database and the Wex et al. (2019) database. The dark grey dashed lines represent one order of magnitude of difference between modelled and observed concentrations, and the light-grey dashed lines 1.5 orders of magnitude. The color bar shows the corresponding instrument temperature of the measurement in Celsius.

Simulations considered both K-feldspar and quartz minerals of dust as major contributors to ice nucleating particles in the global atmosphere. When the model's emission fluxes are calculated by applying the respective mineral emitted mass fractions by Claquin et al. (1999) atlases, quartz and feldspar concentrations are higher especially at accumulation mode (Figure 41). Additionally, when considering the number of points that are out of 1 or 1.5 orders of magnitude and the correlation with observation of the model results that are within the grey areas, no significant difference in the performance of the two datasets is found. Comparison of simulated INP concentrations with observations (Figure 42) does not show any significant difference in the performance of the two mineral's atlases Claquin et al. (1999) and

Journet et al. (2014), although there are differences in the computed columns as shown in Figure 40b. The difference between the column modelled concentration of INP based on these mineral atlases reveals a strong variability of INP concentrations especially over the poles, where it is well known that models have difficulties to properly represent atmospheric transport.

Overall, the simulated concentrations of INP from two-dust components agree with the observational data from the BACCHUS and Wex et al. (2019) databases within one and a half orders of magnitude. Statistical analysis of the comparison of the modeled annual mean dust surface concentration has shown that the model underestimates dust concentration over Europe and the Southern Ocean, potentially explaining part of the bias between modeled and observed INP concentrations. Furthermore, the omission of marine and terrestrial biological INP sources, dust mineralogy uncertainties and atmospheric processes such as ageing and in-cloud removal could also explain the model's discrepancies. As importantly, the heterogeneously formed ice crystals could trigger secondary ice production processes, such as the Hallett – Mossop process, which usually takes place around -5^{o}C and could probably improve our comparison at high temperatures. These processes are not considered in our study. However, they are known to further increase the number concentration of ice crystals (Sotiropoulou et al., 2020) and their subsequent climate impact.

We conclude that dust particles appear to be important precursors of INP, able to account for most of the observed INP number concentration globally. K-feldspar contributes globally most of the INP associated with desert dust because it is more ice-active and less sensitive than quartz to ageing processes that reduce the ice-nucleating activity of the particles (Harrison et al., 2019). However, our simulations showed that although quartz particles have lower ice active density, they are more abundant in airborne dust than K-feldspar, thus partly compensating for their lower ice nucleating activity with respect to K-feldspar. We find that $[INP]_{quartz}$ dominates at lower altitudes over locations with abundant dust emissions but low INP concentrations. There are regions of the atmosphere, in particular over mid-and high-latitudes of Asia, where quartz contributes over 60% (at ambient model temperature) to the total INP concentration derived from dust aerosols represented by quartz and K-feldspar. The quartz contribution increases when temperature is decreasing, resulting in high INP concentrations at temperatures below about −30°C and high altitudes. Consideration of quartz-derived INP improves the comparison with observations for high INP concentrations at low temperatures (below about -30^{o}C) and relatively low INP concentrations at temperatures

around -20^{o}C. These results highlight the important role of quartz in increasing INP concentrations, mainly over the mid-to-high latitudes of both hemispheres.

Improving the representation of INP thus requires further constraining the abundance of quartz and K-feldspar in arid soil-surfaces along with their abundance, size distribution and mixing state in the emitted dust atmospheric particles at global scale. Also, additional experimental studies on the ice-nucleating ability of mineral dust particles must be performed to investigate the impact of atmospheric ageing and the presence of biological fragments attached to dust on the ice-nucleating activity of dust particles.

In the present thesis in order to reconcile observations with model results we investigate the contribution of other aerosol types of INP concentration. In particular, in the next Chapter we examine the contribution of organic aerosols to the global INP distributions.

6. Contribution of Organic aerosols to global INP distribution

6.1 Contributions of INP from various precursor aerosols

Figure 43 depicts annual zonal mean profiles of INP number concentration derived from (a) mineral dust, (b) fungal spores and bacteria, and (b) marine organic aerosols and their percentage contribution to the total INP concentration (d-f). INP from mineral dust (Figure 43a) present considerable concentrations (>10^{-2} L^{-1}) at temperatures, T <-15°C (Hoose and Möhler, 2012). However, they readily act as INP at higher temperatures depending on, among other factors, the type and amount of feldspar and quartz fraction (Chatziparaschos et al., 2023; Harrison et al., 2019), particle size, particle concentration per droplet in the immersion mode (Augustin-Bauditz et al., 2016), and biological nanoscale fragments that could be attached to mineral dust particles (Violaki et al., 2021).

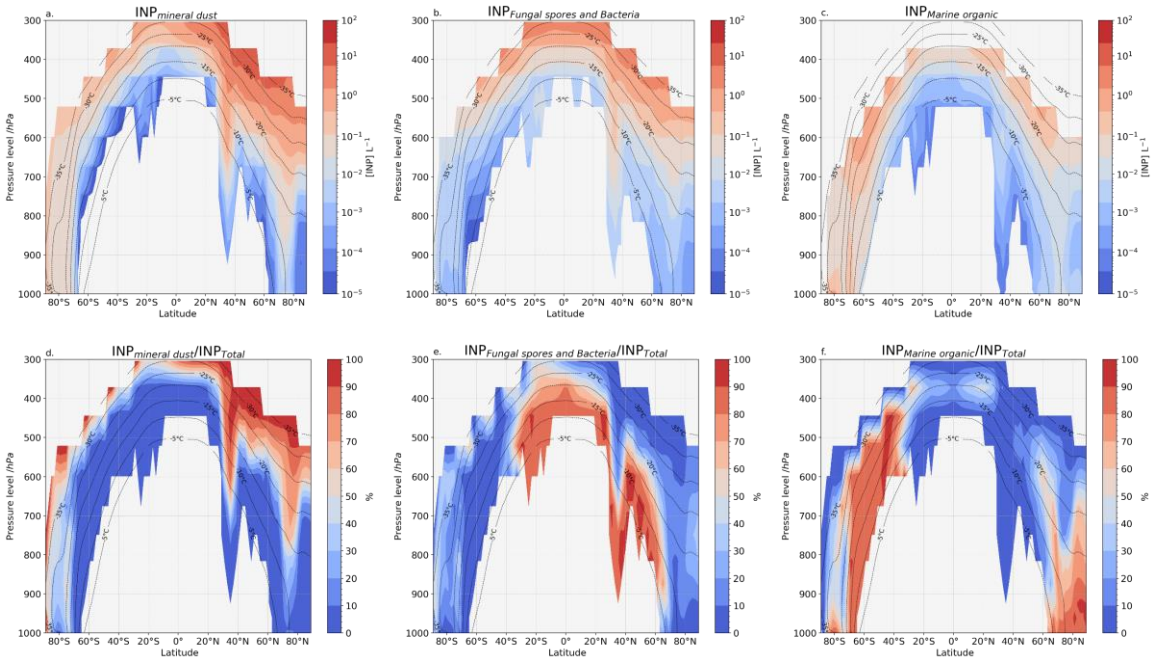

Figure 43: Annual zonal mean profiles of $[INP]_{ambient}$ number concentration calculated by TM4-ECPL, accounting for (a) mineral dust, (b) fungal spores and bacteria, and (c) marine organic aerosols. The black contour dashed lines show the annual mean temperature of the model. Figures (d-f) depict the percentage contribution of each species to the total INP concentration. The color map shows the INP concentration (a-c) and the ratio of INP from each aerosol type to the total INP (d-f).

The contribution of mineral dust acting as INP (Figure 43d) dominates at high altitudes (low-pressure levels) all over the globe in all seasons (see further 5.1) except between 0°-20°S where the contribution of INP from PBAPs is competitive due to South America and Africa large tropical forests which are significant sources of PBAPs.

The high contribution of mineral dust over extra-tropics at low modelled pressure levels would possibly control the ice formation in mid-level clouds or marginally high-level clouds. The present work focuses on immersion freezing that affect primary MPCs regime and the temperature limits of the parameterizations here used (e.g., -10.5°C to -37°C for dust) fall within the range of temperatures for mixed phase clouds. Our simulations show that mineral dust is the most prevalent aerosol in ice formation at low pressure levels. This would possibly impact not only mid- but also high-level clouds with different freezing pathways (e.g., deposition freezing). The results partially agree with a recent study by Froyd et al. (2022), who combining global-scale dust observations in the upper troposphere with a cirrus-formation model found that throughout the NH extra-tropics 75–93% of cirrus clouds glaciation is initiated by dust particles, depending on the season.

Figure 43 shows that at higher model pressure levels (600 hPa), INP from dust minerals dominate in the NH (Chatziparaschos et al., 2023) where the major sources of dust minerals, such as Sahara and Gobi deserts, are located. Between 20°-40°N the concentrations of INP are constrained only by mineral dust and PBAPs (Figure 40 left and middle columns). INP derived from PBAPs are important at low model pressure levels between 30°S to 60°N, where they present considerable concentrations ($>10^{-2}L^{-1}$) and their contribution is more than 70% since PBAPs are more active than mineral dust at relatively high temperatures (Figure 43 middle column) (Murray et al., 2012; Tobo et al., 2013; Harrison et al., 2019). These results suggest that PBAPs derived from forest biota could play an important role in constraining atmospheric INP populations near these ecosystems, especially at warmer temperatures, potentially leading to ice initiation in nearby mixed-phase clouds as also suggested by Tobo et al. (2013). Our results confirm that terrestrial bioaerosols dominate the INP population at relatively warm temperatures, in agreement with previous experimental (Tobo et al., 2013, 2014; Huffman et al., 2013; Pöschl et al., 2010) and modeling studies (Hoose et al., 2010; Paukert and Hoose, 2014). At temperatures colder than about T<-15°C, non-biological aerosol particles like mineral dust can act as effective INP (Murray et al., 2012; Si et al., 2019) and thus may dominate the INP population (Tobo et al., 2013).

In contrast to the above, INP from MPOA (Figure 43c, f) dominate between 40°-70°S and the simulated low INP number concentrations (10^{-1} -10^{-2} L^{-1} at 800hPa, 10°C) are consistent with the concentration range calculated by Vergara-Temprado et al. (2018). Despite the relatively large sources of marine organic aerosols in the SH, a region covered mostly by sea, the resulting INP concentrations remain lower than those simulated over continental areas in the NH, where dust dominates. This pattern of low INP concentration agrees with observations in the Southern Ocean (Chubb et al., 2013) and could suppress cloud droplet freezing, reduce precipitation, and enhance cloud reflectivity, explaining why the models show a strong radiation bias mainly in this remote region away from major sources of INP (Vergara-Temprado et al., 2018). Vergara-Temprado et al. (2018) proposed a correlation between INP concentration and liquid water path and consequently cloud-reflected SW radiation. They suggest that the low INP concentrations derived from MPOA present a negative relationship with SW radiation up to about INP concentration of 1 L^{-1}, above which the reflected radiation drops sharply as the ice processes become more efficient and deplete most of the liquid water. Figure 43(d-f) reveals that in all modelled pressure levels in the Antarctic, INP concentrations are affected by mineral dust and MPOA since the annual mean contribution of PBAPs is less than 20%.

Additionally, in the Arctic (66.5°- 90°N) the dominant types of INP have been shown to consist of mineral and biological materials, originating from land (e.g., dust minerals (Chatziparaschos et al., 2023)) and the ocean (e.g., sea spray (Demott et al., 2016) and biological productivity (Creamean et al., 2019)). Also, earlier studies found that at relatively warm temperatures (above −15 °C) that are common in central Arctic clouds, the majority of INP are typically of biological origin (Creamean et al., 2022). At lower temperatures, INP are dust particles from sources in Siberia, Eastern Europe, and Northern Canada (Creamean et al., 2022).These findings are in agreement with our results since as depicted in Figure 43 (d-f), the simulated concentrations of INP over this region originate from dust minerals and MPOA. More specifically at high modelled pressure levels (i.e., near-surface) and relatively high temperatures (about -10°C) INP from MPOA are dominant with percentage contribution >70% to the total INP concentrations. While at low temperatures and modelled pressure levels INP from dust minerals prevail, resulting in high concentrations of INP ($0.1L^{-1}$, 600hPa, -25°C). The contribution of PBAPs to INP concentration in this region is limited to 10 % - 30 % (Figure 43e) at 800hPa and -15°C.

Figure 44 presents the simulated distributions of INP at 600 hPa pressure level calculated for temperature at -20°C. These are glaciation conditions in deep-convective systems (shown in

Figure 19) which are mainly observed in subtropical and tropical regions. Mineral dust (see section 5.1) contributes much more to $[INP]_{-20}$ concentrations in the mid-latitudes of the NH than in the SH due to the location of dust sources and long-range atmospheric transport patterns that favour dust concentration in the NH. However, there are also dust-related INP sources in the SH, such as those from Patagonia, South Africa and west Australia (Chatziparaschos et al., 2023). The soil composition of dust, which comprises K-feldspar and quartz, plays an important role in the simulated levels of INP over dust source regions (Chatziparaschos et al., 2023).

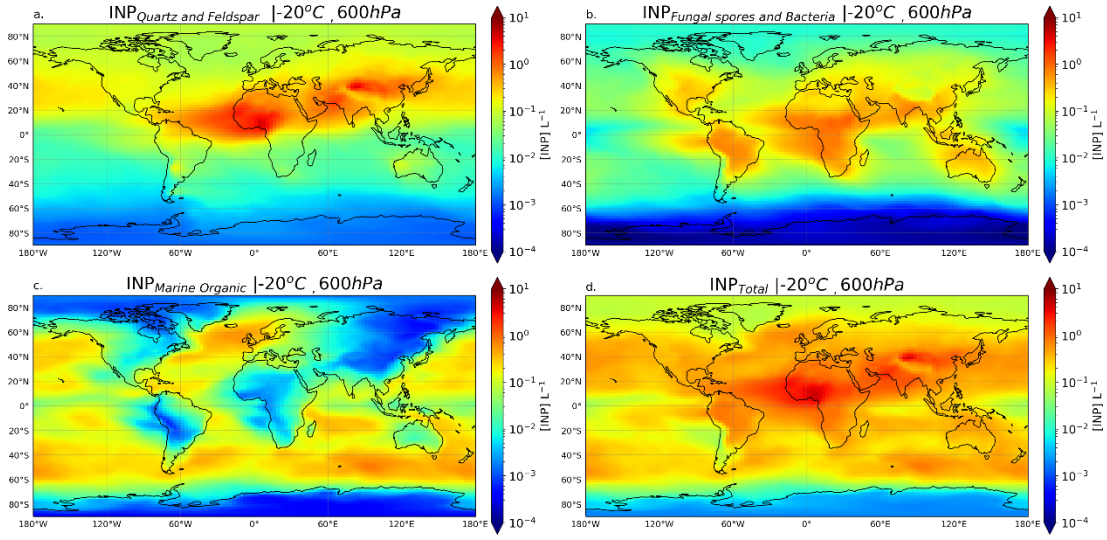

Figure 44: Annual mean distributions calculated by TM4-ECPL for the year 2015 of INP concentrations based on (a) K-feldspar and quartz, (b) fungal spores and bacteria, (c) marine organic aerosols, and (d) the sum of the aforementioned INP for an activation temperature of −20°C at a pressure level of 600 hPa.

In the SH, MPOA is the most important contributor to $[INP]_{-20}$ concentration. Comparison between panels a, b and c of Figure 44 reveals that INP from mineral dust far outnumber INP from MPOA and PBAPs throughout much of the low latitudes and midlatitudes of NH, while marine organics are becoming more important over the world's remote oceans, such as the Southern Ocean (Vergara-Temprado et al., 2017). $[INP]_{-20}$ that are estimated based on PBAPs concentrations, affect INP population over continental sites and are dependent on vegetation, suggesting the important role of PBAPs as a major INP source, at least in these ecosystems (Tobo et al., 2013). However, there are coastal regions in the South Atlantic Ocean, such as the South West coast of Africa in the tropics at the outflow of the continental air (Figure 44) in the middle and high troposphere (Figure 43e), where terrestrial bioaerosol has the potential to form ice crystals, enhancing INP concentrations in marine environments. INP derived from PBAPs such as fungal spores, have a relatively large size, which could lead to quick

sedimentation. However, it is worth noting that factors such as shape, air temperature, and humidity can also influence their sedimentation rate.

Finally, Figure 44 presents the total distribution of INP at 600 hPa that apparently varies depending on the different sources of the INP. $[INP]_{-20}$ concentration in NH is shown to be higher compared to that in the SH. This is consistent with several studies (e.g. Boose et al., 2016; Atkinson et al., 2013; Vergara Temprado et al., 2016; Murray et al., 2012b). However, the distribution of INP is complex and dynamic, and it is influenced by a variety of factors such as source regions, atmospheric transport, weather patterns, location and season. Thus, the SH could have higher concentrations of INP in certain regions or during certain periods of the year. Therefore, more research is needed to understand the factors that influence INP concentrations in different regions of the world and to provide a comprehensive global picture of INP concentration.

The analysis of INP seasonality as depicted in Figure 45 suggests that terrestrial bioaerosols affect more the NH than the SH, contributing to higher INP concentrations in the NH than in the SH. Dust-derived INP dominate all seasons and altitudes worldwide. In the NH, during MAM and DJF INP concentrations originate mainly from MPOA and dust aerosol, while in JJA dust and PBAPs dominate the simulated INP concentrations.

The zonal mean representation can describe satisfactorily the vertical contribution of INP that is obtained by averaging the variables over all longitudes at a given latitude. But this projection can obscure or distort information about variability in the east-west direction, smoothing down features that vary rapidly with longitude.

To take this analysis one step further, the contribution of each INP precursor to the total INP average column by season is depicted in Figure 46. The atmospheric column covering the model hybrid levels from surface to level 10 that is approximately 500hPa (~4.5 km altitude, at 0^{o}N, 0^{o}E) was considered. For each INP precursor, the seasonal mean column INP content has been calculated by averaging the respective months' total INP absolute number in the atmospheric column. The total number of INP from each precursor aerosol has been calculated as the sum of the product of the INP concentration by the volume for each grid box of the column. Then, the mean column concentration has derived by dividing the calculated total column number with the total volume of the column.

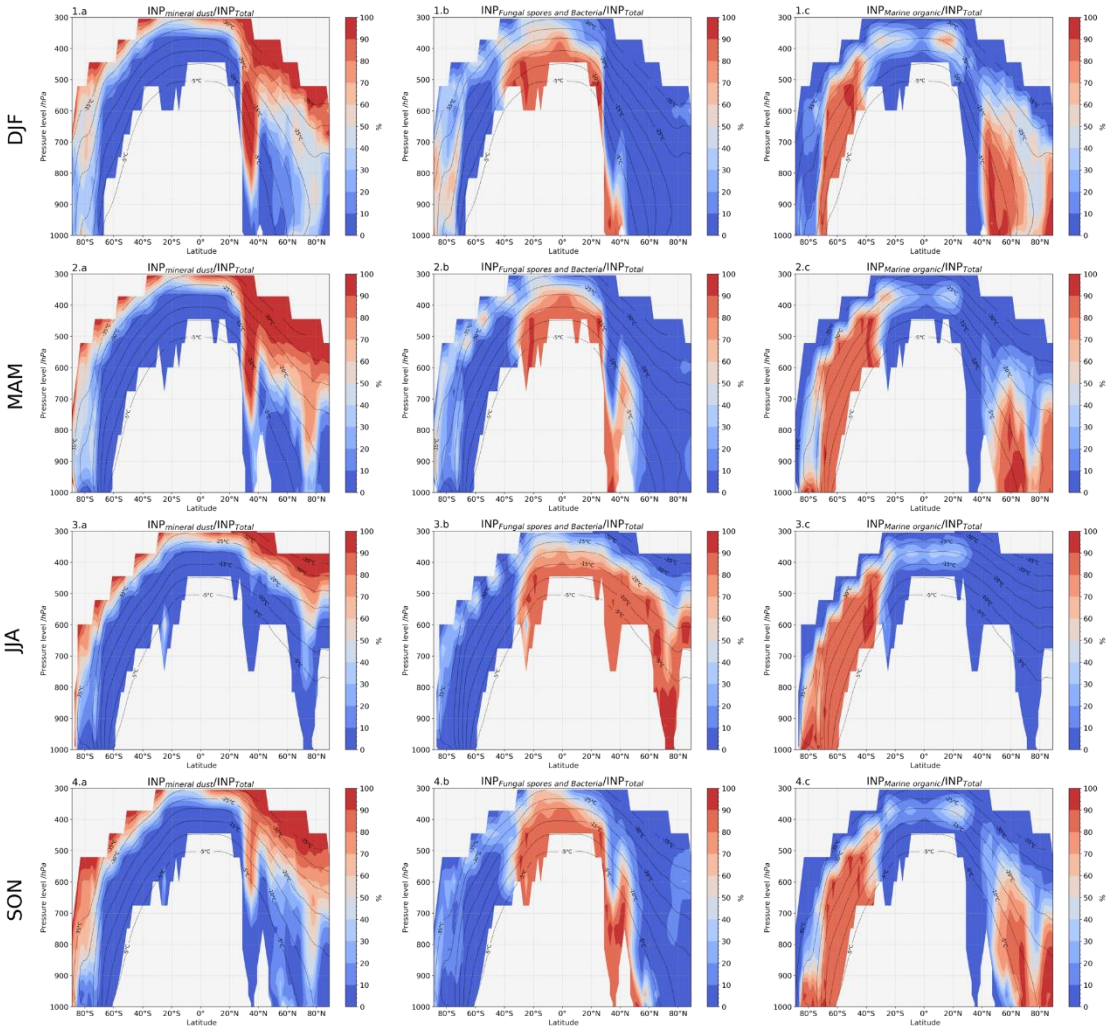

Figure 45: Seasonal variation of the percentage contribution of INP from a) mineral dust (b) fungal spores and bacteria and (c) marine organic aerosols to the total $[INP]_{ambient}$ concentration as calculated by TM4-ECPL and plotted only where the total $[INP]_{ambient}$ concentration is larger than 0.01 m^{-3}. The black contour lines represent seasonal mean isotherms in ^{o}C.

Figure 46 displays a clear pattern of dust-derived $INP_{ambient}$ across all seasons, with a prominent peak in the NH during winter (DJF and MAM). During winter and spring in the SH (JJA and SON), the contribution of the Patagonia desert to INP can be readily observed. On the other hand, INP derived from PBAPs show a strong contribution (around 70%) around 30°S in SH spring and summer (SON and DJF) and their contribution to the INP column in the NH is significant in NH spring and summer when it extends to the entire NH (>50%). This is attributed to the influence of large continental vegetation areas such as the Amazon and Asian forests, which release PBAPs that can act as efficient INPs in the atmosphere. The highest contribution of MPOA-derived INP is found over the Southern Ocean, dominating in all seasons.

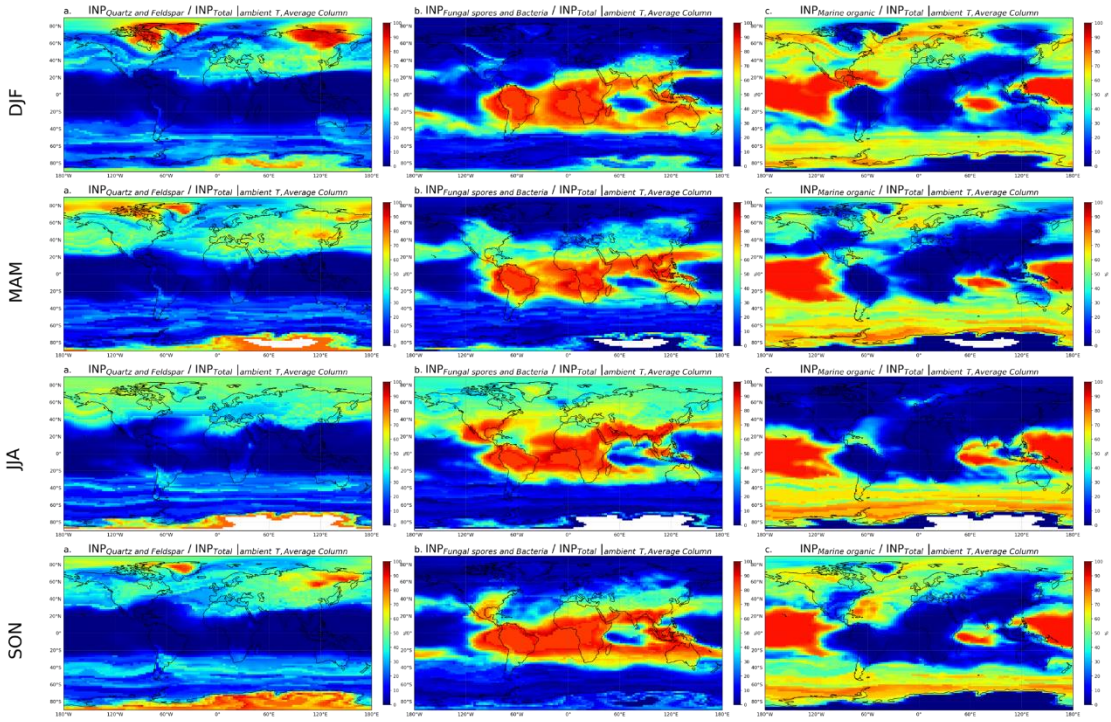

Figure 46: Seasonal average percentage contribution of the tropospheric column up to about 500 hPa (first 10 model levels) of INP from mineral dust (left column), PBAPs (mid column) and MPOA (right column) to the total number of $[INP]_{ambient}$ in the column for each season.

In summary, Figure 46 indicates that at low latitudes closer to the equator, the contribution of biological aerosols (PBAPs and MPOA) to the formation of INP is notably high. This underscores the importance of biological aerosols in influencing cloud formation and atmospheric processes in tropical and equatorial regions but also over the Southern Ocean, and highlights the need for further investigation.

In order to gain a more nuanced understanding of the contribution of different INP, and establish a correlation between the percentage contribution of each species and the concentration ranges of INP, we present Figure 47. We have separated the northern and southern hemispheres and calculated the seasonal percentage contributions, as presented in Figure 47a-f. This analysis reveals that mineral dust is the dominant INP precursor in the NH, accounting for an average contribution of about 56%, followed by PBAPs and MPOA with contributions of about 19% and 25%, respectively (Figure 47 a,b). Notably, during the NH summer season (JJA), PBAPs emerge as the primary source of INP, which strongly correlates with vegetation. In the SH (Figure 47 d,e), the dominant source of INP is MPOA (about 48%), followed by dust (about 29%) and PBAPs (about 23%), which partially explains the generally low concentration of INP in this region, in agreement with earlier findings by (Vergara-Temprado et al., 2018).

Additionally, Figure 47 (c, f) depicts the percentage contribution of INP precursors over the North and South Poles extended areas (75°-90° in the respective hemisphere). The analysis reveals that mineral dust is the dominant source of INP. Dust is significantly influencing INP column in the South Pole extended area during summer when however, the INP levels are low (Figure 47, central panel). This is attributed to the low fraction of K-Feldspar and quartz minerals on dust particles emitted from the Patagonia desert (Nickovic et al., 2012). MPOA-derived INP are the main type of INP at the South Pole in winter.

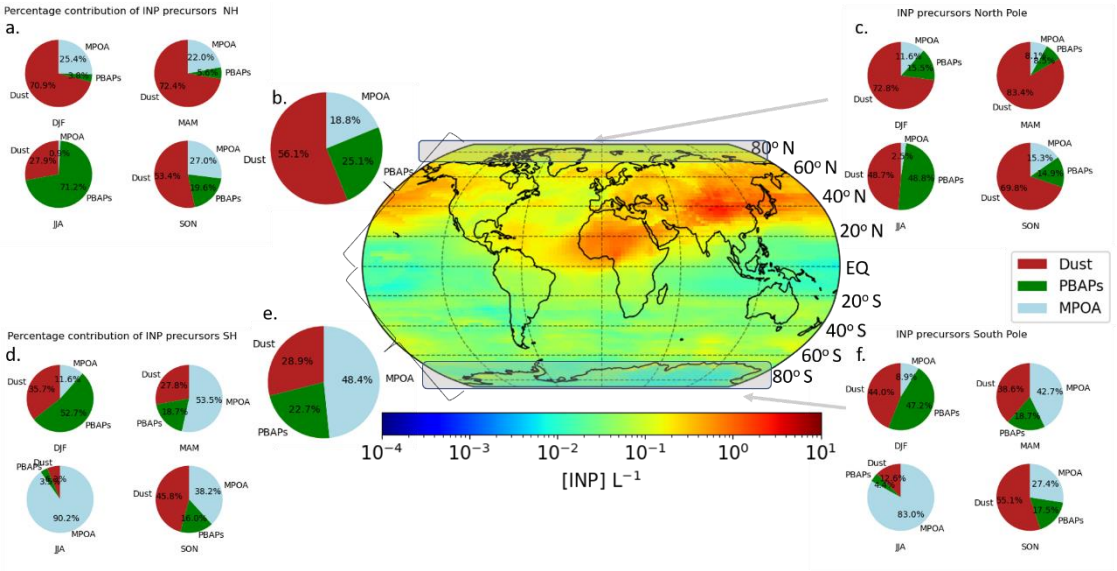

Figure 47: Annual mean column of the total INP number (central panel) considering all INP precursors. Side plots depict the percentage contribution of each species on the total concentration of INP for every season separating for (a) NH (d) SH, (c) and (f) the North and South Pole, respectively. Pie plots b and e are the averages correlated to the panels a and d. Column is calculated by summing of INP number from surface to approximately 500 hPa (~4.5 km for 0°N, 0°E), weighted by the volume of each model's grid box.

6.2 Evaluation of simulated INP

We further compare the available INP observations, from the databases presented in section 3.2.2 and already used in section 5.2, to the INP concentrations calculated by the TM4-ECPL model (Figure 48) considering mineral dust only (a), mineral dust and MPOA (b) mineral dust, MPOA and PBAPs (c). This observational dataset is compared to the modelled multi-annual monthly mean INP concentration considering the years 2009 to 2016. The color bar shows the corresponding temperature at which the measurement was performed (Figure 48a-c), allowing to correlate the model's bias with the temperature of the observed INP (e.g., highly active INP is shown with reddish symbols in Figure 48).

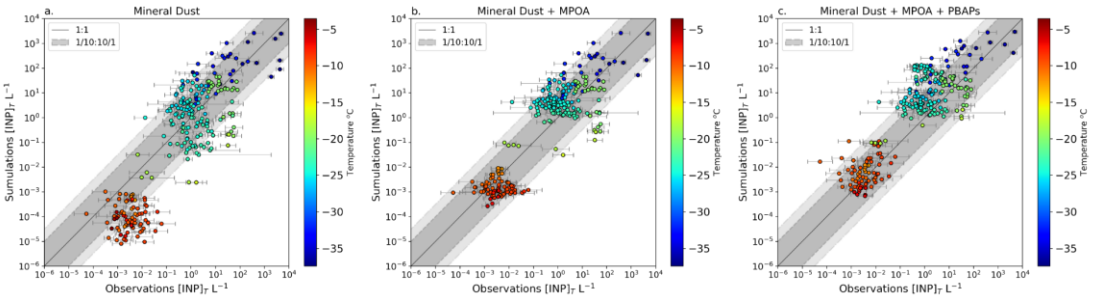

Figure 48: Comparison of $[INP]_T$ concentrations calculated at the temperature of the measurements against observations considering mineral dust only (a), mineral dust and MPOA (b), and mineral dust, MPOA and PBAPs (c). For each observation, the INP concentration is calculated at the temperature corresponding to that of the measuring instrument. Circle markers correspond to the BACCHUS database and triangles to Wex et al. (2019) database. The dark grey dashed lines represent one order of magnitude of difference between modelled and observed, and the light-grey dashed lines 1.5 orders of magnitude. The simulated values correspond to monthly mean concentrations, and the error bars correspond to the observed error of monthly mean INP values. The color bars show the corresponding instrument temperature of the measurement in Celsius (a-c).

The model reasonably agrees (R=0.87 for log-log regression of all data, Table 12) with the INP observations when it considers all of the putative tracers (mineral dust, MPOA, and PBAPs) of INP (Figure 48c). However, the simulated INP considering only mineral dust and MPOA (Figure 48b) show better predictive ability of the model especially at high temperatures (-6>T>-25°C) where MPOA shows high INP activity (red points in Figure 48b). Indeed, the model results neglecting PBAPs show better agreement with observations (Figure 48b, Figure 49, and Table 12) since the model reproduces about 70% of the observations within an order of magnitude and about 84% within one and a half orders of magnitude (Figure 49).

Consideration of INP derived from PBAPs in the simulations leads to an overestimation of measurements and reduces the accuracy of the model's predictions (Figure 48, Table 13). The

overestimation can be attributed to the parameterization used to constrain PBAPs as INP (Tobo et al., 2013). In particularly, the assumption of using the parameterization of fluorescent biological aerosol particles (FBAPs) to simulate the INP contribution of bacteria could lead to an expected overestimation, since bacteria cannot be associated sufficiently or even at all with any FBAPs type (Negron et al., 2020).

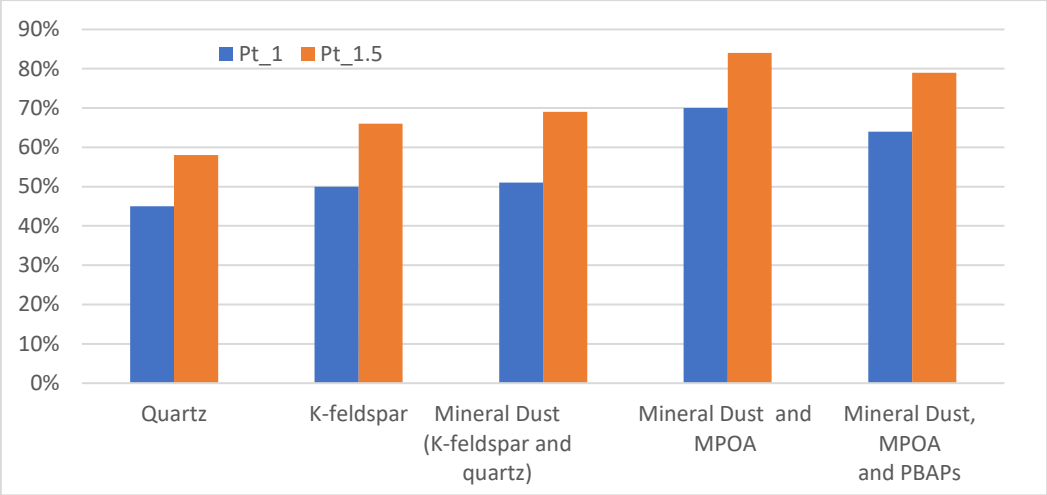

Figure 49: Graphical illustration of Pt_1 and $Pt_{1.5}$ percentages of data points reproduced by the different simulations within an order of magnitude and 1.5 orders of magnitude in the temperature range of each parameterization specific for the different INP precursors.

These findings could suggest that the main INP sources globally are mineral dust and marine organic aerosols. The model validation reveals that ice nucleation at temperatures in the vicinity of zero is typically related to biogenic sources (O'Sullivan et al., 2018; Kanji et al., 2017) and that mineral dust particles likely only become ice active at low temperatures (Chatziparaschos et al., 2023). However, there are large uncertainties in this hypothesis since dust minerals may be carriers of biogenic ice-active matter (Hill et al., 2016; O'Sullivan et al., 2016), which enhances dust ice-nucleation activity at higher temperatures. Such process is not included in our model and could partially explain the overestimate of the observations when PBAPs are considered. Thus, the current representation of INP from bioaerosols in particular PBAPs that can co-exist with mineral dust aerosols requires dedicated studies and improved parameterizations. Furthermore, model bias may be attributed to atmospheric processes such as ageing, resulting in degradation of ice nucleation activity or to the simulated transported tracers. In our model, we neglect these processes but the sensitivity of mineral dust-derived INP simulations to dust mineralogy has been further investigated in our previous studies (Chatziparaschos et al., 2023).

Table 12: Statistical performance of the different INP simulations. Pt_1 and $Pt_{1.5}$ are the percentages of data points reproduced within an order of magnitude and 1.5 orders of magnitude in the temperature range of each parameterization. R_1 and $R_{1.5}$ are the correlation coefficients that correspond to the Pt_1 and $Pt_{1.5}$ percentages, i.e., accounting only the data reproduced within the respective interval. The number of data points used for calculating these values is shown under the data points column. The correlation coefficients have been calculated with the logarithm of the values. Parameterizations are based on (Harrison et al., 2019; Wilson et al., 2015; Tobo et al., 2013).

Parameteri -zations	*Temperature range*	*R All data*	*p-value*	*Standard error*	Pt_1	R_1	*Data point*	$Pt_{1.5}$	$R_{1.5}$	*Data points*
Quartz	-10.5 to -37.5 °C	0.63	4.21E-29	0.119	45%	0.74	119	58%	0.63	153
K-feldspar	-3.5 to -37.5 °C	0.79	5.99E-72	0.023	50%	0.93	132	66%	0.91	172
Mineral Dust (K-feldspar and quartz)	-10.5 to -37.5 °C -3.5 to -37.5 °C	0.84	1.00E-75	0.022	51%	0.94	135	69%	0.92	181
Mineral Dust and MPOA	-10.5 to -37.5 °C -3.5 to -37.5 °C -6 to -27.5 °C	0.86	4.48E-78	0.027	**70%**	**0.95**	**184**	**84%**	**0.92**	**221**
Mineral Dust, MPOA and PBAPs	-10.5 to -37.5 °C -3.5 to -37.5 °C -6 to -27.5 °C -9 to -34 °C	0.87	7.82E-80	0.028	64%	0.96	170	79%	0.93	208
All points									**263**	

Table 13: Statistical performance of the different INP species. Pt1 and Pt1.5 are the percentages of data points reproduced within an order of magnitude and 1.5 orders of magnitude in the temperature range of every parameterization. Slope, Intercept, R-value, P-value, Standard Error and Number of points correspond to the related Pt1 and Pt1.5 percentages. All the statistical values have been calculated with the logarithm of the values.

INP Species	*Mineral Dust and MPOA*		*Mineral Dust, MPOA and PBAPs*	
One order of magnitude	Pt_1	$Pt_{1.5}$	Pt_1	$Pt_{1.5}$
Slope	0.847	0.808	0.918	0.887
Intercept	-0.188	-0.231	-0.264	-0.359
R-value	0.956	0.926	0.957	0.931
P-value	1.11E-98	1.72E-94	2.42E-92	4.43E-92
Standard Error	0.019	0.022	0.021	0.024
Number of data points ***(total 263)***	184	**221**	170	208

6.3 Summary and conclusions

In this study, we performed global model simulations of mineral dust, marine organic aerosols, bacterial and fungal spore concentrations investigating their contribution to atmospheric ice nucleation, using laboratory-derived parameterizations based on the singular description. The simulated distribution of ice nucleating particles varies depending on the source of the INP. We found that at relatively warm temperatures (above −15 °C) the majority of INP has typically biological origins while at lower temperatures and high altitudes INP from mineral dust prevail globally. Marine-derived INP are primarily found over ocean and coastal areas and dominate between 40°-70°S (Southern Ocean), with higher concentrations in regions of high sea spray and phytoplankton activity. Marine organic INP dominate primary ice nucleation below 600 hPa over the SH, while dust INP are more abundant elsewhere. Generally, the concentration of INP is mainly affected by mineral dust (both feldspar and quartz) and marine organics since the contribution of PBAPs is 20% at the same pressure level (600 hPa). Mineral dust-derived INP show higher concentrations in regions of high dust emissions such as the Sahara Desert, Gobi Desert and the Arabian Peninsula, contributing to high INP concentrations in NH. Primary terrestrial biological aerosol particles such as fungal spores that are found at low model pressure levels between 30°S to 40°N, could play an important role in constraining atmospheric IN populations at warmer temperatures but their concentrations vary depending on the season and regional weather patterns. To the simulated INP under mixed-phase cloud relevant conditions, INP from dust contribute more in mid-latitude of the NH than in the SH due to the location of dust sources and the long-range atmospheric transport patterns. In the SH, marine organics are more prevalent in affecting INP concentrations and could be assumed as the main and only source of INP there. However, INP from terrestrial bioaerosols have the potential to form ice crystals in the NH subtropics at the outflow of the continental air.

Comparison of observed INP concentrations to those simulated by the TM4-ECPL model, using data from 2009 to 2016 and considering the above-mentioned precursors of INP, shows better agreement when considering only mineral dust and MPOA, and the model overestimates observations when including PBAPs. The study suggests that mineral dust and marine organic aerosols may be the main global sources of INP, and that INP from PBAPs may only affect concentrations locally, near source regions. However, this study also highlights the uncertainties in the potential co-existence and relationship between dust and biogenic matter as sources of INP, and the potential impact of atmospheric processes on INP concentrations.

Concluding, the assumption that INP concentrations globally can be calculated individually by mineral dust, marine organic and terrestrial bioaerosols is a good approximation for simulating INP close to emission sources. However, far from their source regions, simulating INP must take into consideration that INP precursors would be a mixture of different INP species, such as dust minerals that could be carriers of biogenic ice-active macromolecules (O'Sullivan et al., 2016) or coating (sulphate and/or nitrate (Iwata and Matsuki, 2018) with pollutants, enhancing or depleting their ice-activation. The efficiency of ice-nucleating parameterizations is subject to the assumption that particles are either internally or externally mixed (Atkinson et al., 2013), as well as how the parameterization is applied after atmospheric aging. A more complete understanding of these factors is necessary for accurate modeling of the impact of INP in the atmosphere. The investigation of the impact of these processes on INP is beyond the scope of the present study. Overall, the global distribution of INP is complex and dynamic, influenced by a variety of factors including emissions, atmospheric transport, and weather patterns. Therefore, it is important to use a combination of observational data and modeling to understand the distribution and the factors that affect INP concentrations and their impact on climate and weather in different regions of the world.

7. Impact on cloud properties and radiation

Figure 50 presents an overview of the forcing and feedback pathways involving greenhouse gases, aerosols, and clouds. Forcing agents, such as aerosols and greenhouse gases, are shown in the green and dark blue boxes, respectively, with straight green and blue arrows indicating the mechanisms through which they exert their forcing. Focusing on Aerosols-Cloud interaction (aci) (green line), when aerosols are emitted into the atmosphere, they can affect cloud formation and properties. This, in turn, due to albedo changes can affect the amount of solar radiation that reaches the Earth's surface, adjusting state variables such as temperature, moisture and wind speed that leads to changes in emissions, distribution and transport of aerosols in the atmosphere.

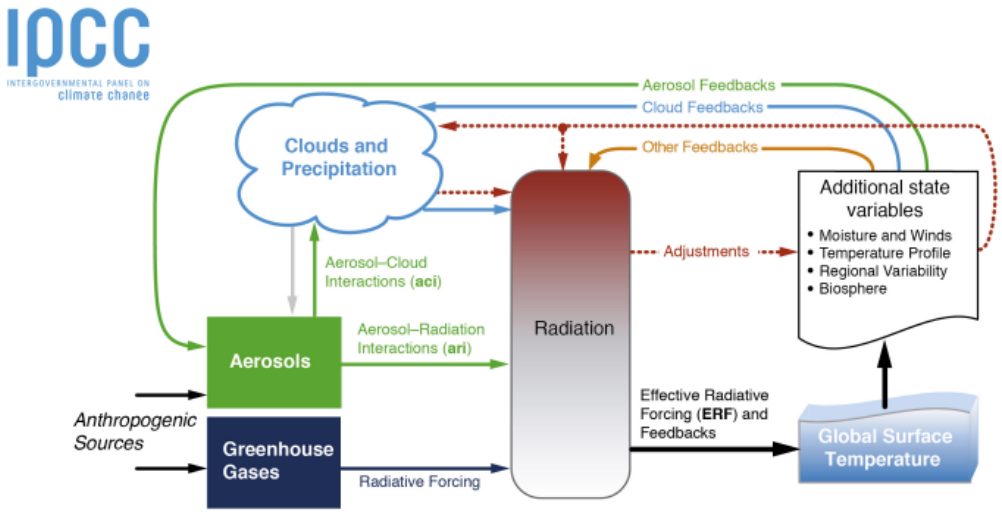

Figure 50: Overview of forcing and feedback pathways involving greenhouse gases, aerosols and clouds. Forcing agents are in the green and dark blue boxes, with forcing mechanisms indicated by the solid green and dark blue arrows. The forcing is modified by rapid adjustments whose pathways are independent of changes in the globally averaged surface temperature and are denoted by brown dashed arrows. Feedback loops, which are ultimately rooted in changes ensuing from changes in the surface temperature, are represented by curving arrows (blue denotes cloud feedbacks; green denotes aerosol feedbacks; and orange denotes other feedback loops such as those involving the lapse rate, water vapour and surface albedo). The final temperature response depends on the effective radiative forcing (ERF) that is felt by the system, that is, after accounting for rapid adjustments, and the feedbacks, (IPCC, 2021).

This feedback loop between aerosols and clouds can be highly complex and dynamic. To gain a comprehensive understanding of the lifecycle of aerosols, including their emission, transport, and deposition, as well as their properties such as size, mixing state, composition, and optical properties, it is necessary to employ an analytical model that can accurately

simulate the complex interactions between aerosols and clouds. In particular, the simulation of INP occurrence in the atmosphere requires a model that combines cloud simulations with a transport model.

Such a model can provide valuable insights into the dynamics of the aerosol-cloud system, including the impact of aerosol emissions on cloud formation, precipitation patterns, and radiative forcing. Furthermore, it can help to constrain the sources and sinks of aerosols and to accurately predict their distribution in the atmosphere. By improving our understanding of the lifecycle and properties of aerosols, we can develop effective strategies for mitigating their impact on the climate system.

The results presented in the previous sections, suggest that TM4-ECPL is capable of simulating and providing adequate answers to scientific questions regarding the spatial distribution of the major INP sources globally, as well as giving climatological information on the impact of aerosol species on the climate. However, the coarse resolution of the model and its off-line structure, which is reading meteorological variables rather than simulating them, make it difficult for the model to capture the impact of aerosol feedbacks on the climate. In other words, while TM4-ECPL is able to simulate the transport and transformation of atmospheric chemical species, as an off-line model, it cannot represent the feedback mechanisms that occur between aerosols and meteorological variables (Figure 51), such as changes in cloud albedo, precipitation, water liquid path and ice water path.

In order to capture the complex feedback mechanisms between aerosols and meteorological variables, it is necessary to use an on-line model that calculates the meteorological variables, like the Integrated Forecasting System (IFS) (Forbes et al., 2012). While TM4-ECPL is a valuable tool for simulating atmospheric chemistry and understanding the sources and transport of pollutants and greenhouse gases, it is not adequate for capturing the full complexity of atmospheric aerosols-cloud interactions. Unlike TM4-ECPL, which relies on meteorological input data from external sources, IFS calculates meteorological variables such as wind speed and direction, temperature and humidity internally and, includes a state-of-the-art cloud scheme as part of its numerical weather prediction system (Figure 51).

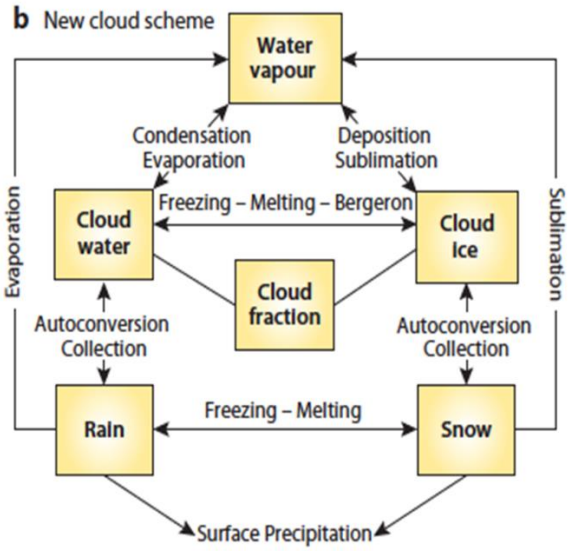

Figure 51: The IFS cloud scheme with six moisture related prognostic variables Yellow boxes indicate prognostic variables (Forbes et al., 2012)

By incorporating the calculations of both atmospheric chemistry and meteorological variables within a single model, IFS is able to provide a more comprehensive and accurate representation of the interactions between aerosols and meteorology, including the feedback mechanisms that occur between them. This can lead to more accurate predictions of weather patterns, air quality, and climate change.

Therefore, to better understand the complexity of aerosol-cloud interactions, we transferred the parameterizations tested in TM4-ECPL to the TM5 model that is the atmospheric chemistry component of the EC-Earth3 Earth System Model (van Noije et al., 2021). Unlike TM4, TM5 includes M7, an aerosol microphysics module that takes into account aerosol microphysics, i.e., the complex processes that affect the formation and growth of aerosol, considering a wide range of aerosol properties such as size, composition, and mixing state. M7 includes detailed representations of aerosol nucleation, condensation, coagulation, in order to simulate aerosol-cloud interactions, based on modal representation of aerosol sizes. M7 is one of the aerosol microphysics modules currently available and is used in a wide range of global atmospheric models to study the impact of aerosols on weather and climate. TM5 can be coupled with IFS, the meteorological model of the EC-Earth3, to calculate realistic meteorological variables. Therefore, it is possible to simulate the complex interactions between aerosols, clouds, and meteorology, providing valuable insights into the impact of aerosols on air quality and climate. The combination of TM5 and IFS (EC-Eeath3) represents

an important step forward in atmospheric modeling and has the potential to improve our understanding of the Earth's atmosphere for this study.

EC-Earth3 is a state-of-the-art climate model developed by the European Centre for Medium-Range Weather Forecasts (ECMWF) in collaboration with several research institutions across Europe (van den Hurk et al., 2009; Döscher et al., 2022). The model is a fully coupled Earth System Model (ESM) able to simulate the interactions between the atmosphere, oceans, land surface, and cryosphere, providing a comprehensive representation of the Earth's climate system. EC-Earth3 includes advanced physical parameterizations and high-resolution grids, enabling it to accurately simulate past and present climate conditions, as well as to make reliable projections of future climate change under different greenhouse gas emission scenarios (van Noije et al., 2020). The model is widely used in climate research and policy-making, providing important insights into the drivers and impacts of climate change, and informing strategies for mitigating and adapting to its effects.

Our collaboration with the Barcelona Supercomputing Center (BSC), enabled the fast incorporation in the EC-Earth3 model of our parameterization schemes of INP that we have successfully implemented in the TM4-ECPL model. The INP parameterization schemes, have been further refined and validated, leading to more accurate simulations of aerosol-cloud interactions and their impact on the climate system. The exchange of knowledge and expertise between ECPL and BSC research groups has been invaluable in advancing our understanding of the Earth's climate and its complex processes. In the following sub-section, we will present briefly some preliminary model results obtained with the atmospheric component of the Earth System Model EC-Earth3 (IFS-TM5).

7.1 Preliminary results

The simulated ice crystal concentrations in mixed-phase cloud are affected by uncertainties in the INP concentrations, leading to discrepancies in the climate sensitivity of the models (Murray et al., 2021). Aiming to reduce the uncertainty in climate projections we focused on aerosols-cloud interactions and on the improvement of the representation of clouds in the CMIP6 ESM EC- Earth3-AerChem (van Noije et al., 2021). This was achieved by updating the heterogeneous ice nucleation representation by replacing the commonly used ice nucleation scheme based only on temperature (Meyers et al, 1992) by the state-of-the-art scheme sensitive to both aerosol and temperature that was used in TM4-ECPL. Thus, we further

developed the Earth3-AerChem to account for INP concentrations derived from mineral dust (quartz and feldspar) and marine organic aerosols in the atmosphere using the state-of-the-art parameterizations we have been tested in TM4-ECPL. We have implemented in IFS-TM5 a new tracer of Primary Marine Organic Aerosol parameterized as referred in Vignati et al. (2010) and Myriokefalitakis et al. (2010) and using Wilson et al. (2015) ice nuclei parameterization. This affects INP concentrations especially over remote oceans, leading to more realistic cloud projections globally. This development enabled the study of the behavior of dust-sensitive ice deposition nucleation schemes for cirrus clouds and dust, organic-sensitive immersion freezing schemes for mixed-phase clouds in the model, and investigate the sensitivity of the simulated liquid and ice water content and the atmospheric radiative fluxes (Costa-Surós et al., in prep., 2023)

The new ice nucleation parameterizations in EC-Earth3 have yielded some promising preliminary results, showing a strong correlation between the simulated ice crystal number concentrations and the INP sources included in the model. These results demonstrated the effectiveness of the implemented INP parameterization schemes and their potential for improving climate simulations.

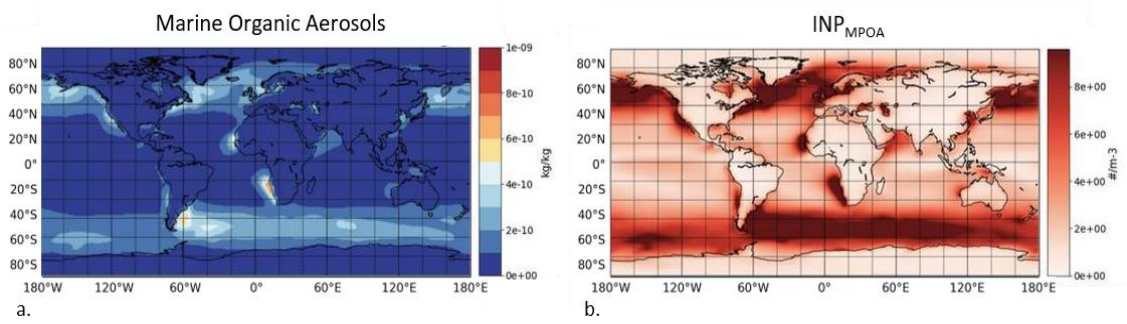

Figure 52: Annual mean of modelled distribution of marine organic aerosols in accumulation soluble mode (a) and ice number concentration derived from marine organics activated at -15 ºC (b) (IFS first level, surface for the year 1990)

The impact of the newly implemented ice nucleation parameterizations can be observed in Figure 52, which displays the simulated annual mean near-surface marine organic aerosols and the calculated ice number concentration (Figure 52b), using an activation temperature of -15°C. These conditions (-15ºC) provide a good approach for comparison between simulated concentrations of INP and measurements. Calculated INP simulations at modelled temperature indicate that the consideration of INP marine source exerts a noticeable influence in liquid water path (LWP) and shortwave (SW) radiation at high latitudes over remote oceans (changes by -1.39 Kg m^{-2} and 4.87 W m^{-2}, respectively). Figure 53 depicts the

differences in LWP and incoming SW radiation at the top of the atmosphere between ice-nucleating particles derived from mineral dust and marine organic aerosols. The figure shows the difference in the effects of these two types of INP, with the INP calculated accounting for dust and organic-derived INP and those derived from only mineral dust. It is calculated by subtracting the respective results of two different simulations performed with IFS-TM5: One accounting for both mineral dust INP from feldspar and quartz and from primary marine organic aerosol (MPOA) and the other one accounting only for dust INP. Simulations were using the parameterizations by Harrison et al. (2019) for immersion freezing of mineral dust and Ullrich et al. (2017) for deposition nucleation together with those of Wilson et al. (2015) for immersion freezing of MPOA. By doing so, the figure highlights the relative contributions of marine source of INP to the Earth's energy balance. The marine-derived INP lead to increased formation of ice crystals, which has the potential to reduce the amount of water in the form of hydrometeors in clouds. This, in turn, can lead to a decrease in the liquid water path of the clouds causing a slight decrease in the shortwave radiation at the top of the atmosphere (TOA) (Figure 53).

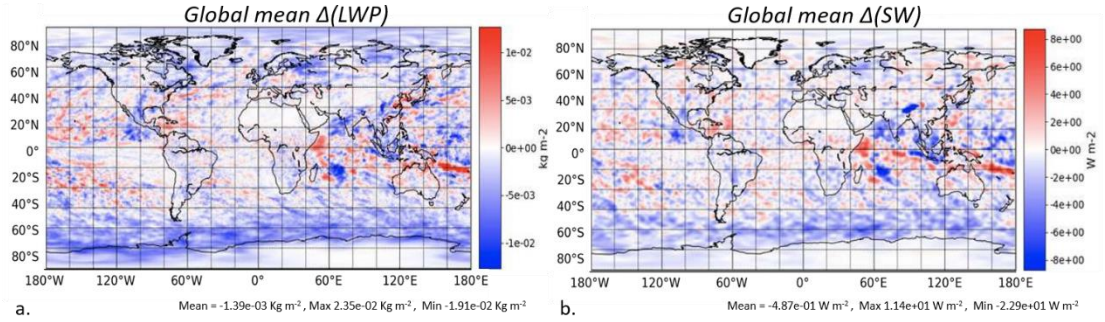

Figure 53: Annual differences in (a) LWP and (b) SW radiation at the top of the atmosphere (TOA) due to the consideration of INP derived from marine organic aerosols in the model (Harrison et al. 2019 (immersion freezing of mineral dust) + Ullrich et al. 2017(deposition nucleation) + Wilson et al. 2015(immersion freezing of MPOA)) – (Harrison et al. 2019 + Ullrich et al. 2017)

The model results become even more interesting when comparing the temperature-dependent ice nucleation parameterization with the aerosol-sensitive parameterizations. These parameterizations are a combination of Harrison et al. (2019), Ullrich et al. (2017) and Wilson et al. (2015) for primary ice and Georgakaki et al. (in prep.), for secondary ice and they show a significant improvement in simulating ice crystal number concentrations in the atmosphere. The use of these parameterizations could lead to a more realistic representation of aerosol-cloud interactions, increasing the accuracy of the simulation of cloud properties

and their impacts on the Earth's radiation budget. Further research is, however, needed on this topic.

Figure 54 shows the differences between aerosol-sensitive and temperature-dependent parameterizations for cloud cover, IWP (Ice Water Path), surface temperature and LW(Longwave) radiation. The results show negative Δ(LW) change in LW radiation at the top of the atmosphere in mid-latitudes (i.e. more LW radiation is trapped into the atmosphere, (Figure 49d)). Therefore, they indicate that the aerosol-dependent parameterization tends to warm the high-latitude regions, correcting part of the cold bias detected in previous climate modeling studies over large parts of the Northern Hemisphere land regions and the Arctic (Döscher et al., 2022). However, for Antarctica, the new parameterization appears to further increase the existing warm bias reported by Döscher et al. (2022), (Figure 49c). Since the warm bias over the Southern Ocean and Antarctica has been linked to biases in shortwave cloud radiative effects, it is likely that modifications in the cloud cover (Figure 49a) will help to alleviate them.

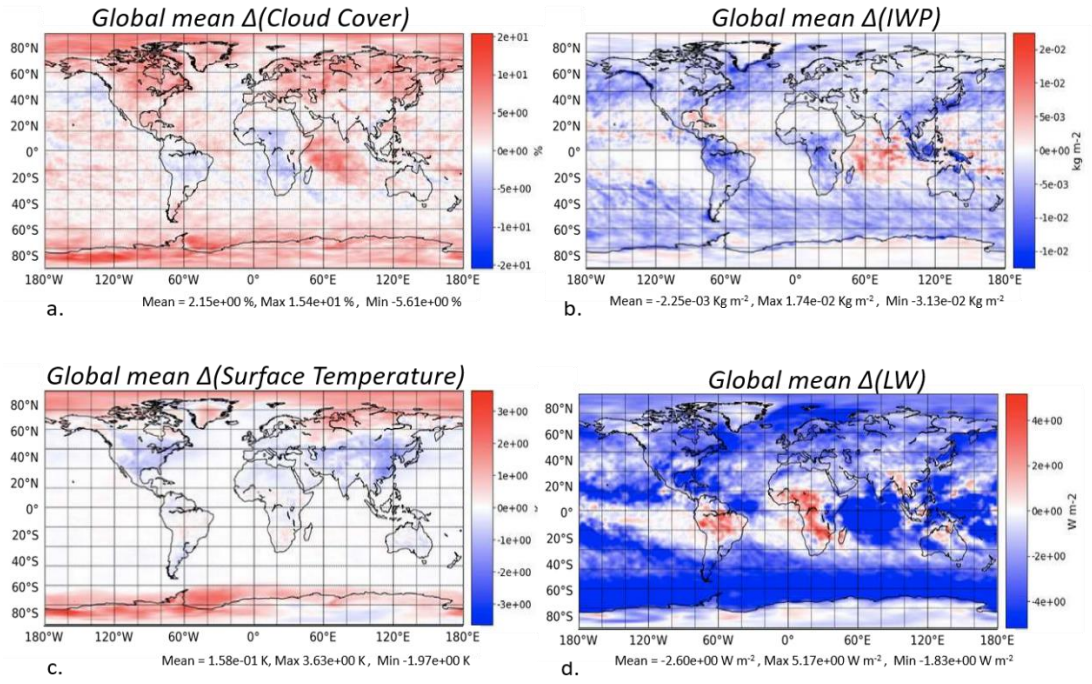

Figure 54: Differences in (a) Cloud Cover, IWP (b), surface temperature (c) and LW radiation (d) between aerosol-sensitive and temperature-dependent parameterizations. (Harrison et al. 2019 + Ullrich et al. 2017+ Wilson et al. 2015) (aerosol-dependent parameterizations) - Meyers et al. (1992) (aerosol-independent).

8. Conclusions and Future Work

Our simulations with TM4-ECPL have shown the dominance of dust particles on INP global distribution. We have also demonstrated the need to account not only for feldspar-dust minerals but also for quartz containing dust, which can be significant INP precursors in the global atmosphere (Chapter 5). Furthermore, the importance of organics both of terrestrial and marine origin as INP precursors has been investigated and demonstrated by TM4-ECPL model results and their comparison to available observations (Chapter 6). While consideration of INP from marine organic aerosol improves the comparison with observations in particular those at relatively high temperatures (close to zero), incorporation of INP from terrestrial bioaerosol in the model seems to lead to a slight overestimate of the observations. This result points to the need for further experimental investigations to improve the parametrizations of INP from terrestrial bioaerosol and from dust taking into account their potential co-existence in the atmosphere, as well as that atmospheric aging that affects INP activity of aerosols. The use of the suggested parameterizations in the EC-Earth3, Earth System Model and in particular in the IFS, its meteorological component, enabled to calculate the impact of these INP on cloud cover, ice water path, surface temperature, and shortwave and longwave radiation at the top of the atmosphere (Collaboration with BSC) (Chapter 7).

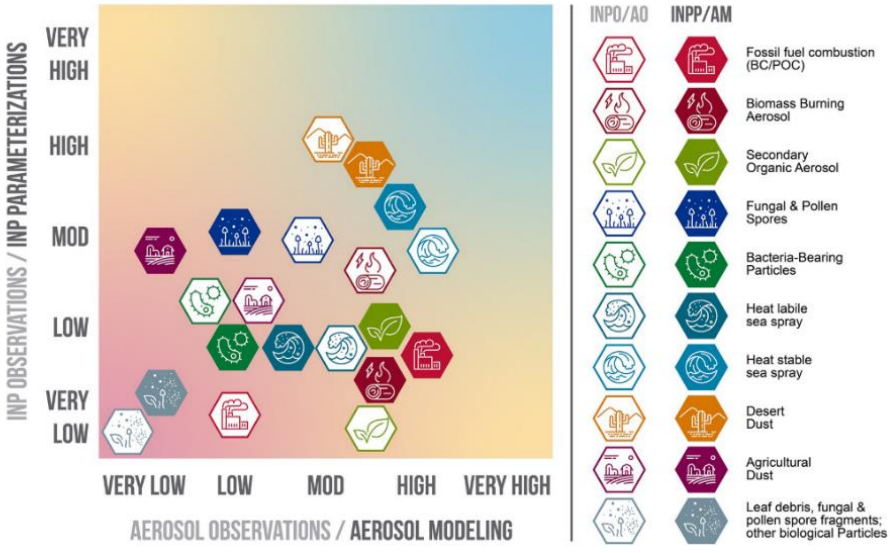

Figure 55: Summary of the relative level of scientific understanding based on available INP observations, INP parameterizations, aerosol observations, and aerosol modeling for different particle sources contributing to atmospheric INP . INPO, Ice-nucleating particle observations; AO, Aerosol Observations; INPP, Ice-nucleating particle parameterizations; AM, Aerosol Modeling (Burrows et al., 2022).

The results presented in Chapter 7 are part of the preliminary findings of Costa-Surós et al. (in prep., 2023), and although they are promising, further improvements and refinements of the aerosol-dependent parameterization are required and planned. One of the main goals is to better represent the ice formation processes in the Earth System Model by including other INP as precursors of ice crystals, such as pollen, fungal spores, and bacteria (Tobo et al., 2013) that have been tested in TM4-ECPL. Additionally, the implementation of another immersion freezing parameterization based on sea spray, and not only on organic matter, as proposed by McCluskey et al. (2018), will be considered in the future. The secondary ice process (SIP) parameterization will be further tested with the added primary IN parameterizations to assess its behavior (work in collaboration with EPFL and CSTACC). Furthermore, the simulation period will be extended to climatological scales to evaluate the variability of the results over longer periods. The aerosol-sensitive ice nucleation parameterization proposed based on dust and marine organic aerosol is now integrated with other developments from the EU FORCeS Horizon program into the EC-Earth model to improve the representation of aerosols and their interactions with warm and cold clouds in the CMIP6 (the sixth Phase of the Coupled Model Intercomparison Project) simulations. Therefore, the results that are briefly presented here are just the beginning of ongoing efforts to refine and improve our understanding of aerosol-cloud interactions importance on climate.

The current predictions of models fail to clarify whether clouds dampen or amplify climate warming. The primary factor contributing to this uncertainty is how models estimate the concentration of INP (Murray et al., 2021) in clouds, particularly in the mixed-phase cloud regime. The dynamics and properties of these clouds are among the largest uncertainties in climate models (Fan et al., 2016). To address this issue, it is essential to improve the description of aerosols in models, with a particular focus on the aerosol sources of INP, for which the current level of understanding is low to very low.

It is widely known that a variety of particle types can act as INP, including particles found in agricultural soils (Suski et al., 2018; Tobo et al., 2014), the boundary layer and free troposphere (Twohy et al., 2021; Prenni et al., 2009), biomass burning particles (Barry et al., 2021; McCluskey et al., 2014), and nascent sea spray (McCluskey et al., 2018; Wilson et al., 2015). However, accurately representing the emission fluxes of these particle types, including the processes of wet scavenging, dry deposition, and the relevant chemistry, remains a key challenge. This requires the development and evaluation of emission parameterizations that are linked to variables in large-scale models, as well as a thorough understanding of the importance of vertically resolved INP concentrations and precursor aerosol types. To better

understand these complex processes, it is essential to compare model results with measurements and to carefully evaluate and refine emission parameterizations.

Figure 55 summarizes the relative level of scientific understanding based on available INP observations, INP parameterizations, aerosol observations, and aerosol modeling for different particle sources that are known to contribute to atmospheric INP globally. Despite **desert dust** is relatively well understood in comparison to other INP sources, most current climate models neglect or poorly represent dust mineralogy, super-coarse dust, dust shape, and the variability of its optical properties, which are key parameters to constrain dust-cloud interactions (Chatziparaschos et al., 2023). Ice activity of dust aerosols depends on particles' surface, thus coarse particles have high efficiency in ice nucleation. However, climate models miss most of the coarse dust in the atmosphere (Adebiyi and Kok, 2020), resulting in underestimation of INP concentration. Furthermore, it is essential for models to incorporate dust INP parameterizations that consider the aging of transported dust aerosols. It has been observed that the ice-nucleating efficiency of these aerosols is reduced when they are coated by acids or water-soluble organics (Iwata and Matsuki, 2018; Jahl et al., 2021; O'Sullivan et al., 2016). This critical process is currently not well-represented in models, and its inclusion could potentially lead to significant changes in simulated INP concentrations.

Organic-rich soil dust is more INP active than inorganic desert dusts in both the immersion and deposition modes (Steinke et al., 2019; Tobo et al., 2014; O'Sullivan et al., 2014). Soils that aerosolized by **agricultural** operations may largely determine local INP concentrations in agricultural regions. Current estimates of dust emissions from agricultural areas in semi-arid regions are subject to significant uncertainty, reaching 25% (Ginoux et al., 2012). However agricultural dust emissions (Penfold et al., 2011) are not yet routinely represented in any climate or Earth system model. This potentially organic-rich fraction is typically not distinguished from desert dust in models. Additionally, organic-rich soils emissions would be affected by climate change via human driven shifts in land use, agricultural management, water usage. It is necessary to develop new tracers for organic-rich dust in agricultural regions, in order to improve the representation of emissions in such areas.

The ice-nucleating activity of **biomass-burning aerosol** is highly variable and often significantly low contributing about 5% to INP populations when accounting also for dust INP on a global average (Schill et al., 2020). In biomass burning plumes there is a variety of types of particles such as soot, organic particles, dust that are commingled and their chemical complexity during transport cannot not be captured by the models. Additionally, even though it has been shown

that biomass burning aerosol components are potentially precursors of INP at relatively warm temperatures (<−25°C), it is unclear whether aging enhances (Jahl et al., 2021) or depletes (Schill et al., 2020) their IN efficiency. Thus, it is important to consider the ash and dust component, in addition to the organic and black carbon from biomass burning aerosol particles, as a potential precursor of relevant ice active species within biomass burning aerosols. We also need to take into consideration atmospheric aging of these particles.

PBAPs derived INP (e.g., bacteria, fungal spores, and pollen) have been studied (Pummer et al., 2012, 2015; Bell, et al., 2018) and introduced in several models (Hoose et al., 2010) susing stochastic or deterministic derived parameterizations as a 'bottom-up'' approach. To better represent **PBAPs** in models, it is necessary to take into account the large variability in INP activity both between and within taxa, as well as in response to environmental conditions. One approach to address this uncertainty is to use correlations between PBAPs IN efficiency and fluorescent biological aerosol particles (Tobo et al., 2013), which can allow for the simulation of INP without the complexity of accounting for species-to-species variability. In addition, global emissions parameterizations for PBAPs, such as bacteria and fungal spores, have been developed based on factors such as **leaf area index** and **flux rates** for different ecosystems. However, future human-driven changes in land use and deforestation or desertification may impact these parameters and need to be considered in model simulations. Therefore, a more accurate representation of PBAPs in models requires the development and evaluation of improved parameterizations that incorporate the variability in INP activity and account for changes in relevant ecosystem parameters due to land use and environmental changes.

Sea Spray (SS) associated with primary marine organic aerosols has been identified as important contributors to INP population and its current level of understanding is moderate to high (Figure 55). Several global modeling studies predict INP concentrations using parameterizations which are based on total organic carbon that is associated with the submicron SS aerosols (Wilson et al., 2015). However, a recent study found that super-micron sea spray particles have high active site densities (Mitts et al., 2021). Omission of these particles when calculating INP would lead to underestimation of INP concentrations in the models. In this aspect, a field-derived parameterization of SS INP activity based on total sea spray aerosol surface area (ns), adequately predicts concentrations of INP in the remote marine boundary (McCluskey et al., 2019). Therefore, to accurately represent INP from marine sources, different emission parameterizations for either SS or MPOA (Vignati et al., 2010; O'Dowd et al., 2008; Rinaldi et al., 2013; Burrows et al., 2014) should be tested and then

different INP parameterizations (Wilson et al., 2015; McCluskey et al., 2018) should be applied, taking into consideration SS size distribution. These results have to be evaluated against available INP observations (Wex et al., 2019)

The effect of **atmospheric acidity** on INP activation has not been sufficiently investigated by models. Sullivan et al. (2010) found that when mineral dust particles are exposed to sulphuric acid, their ice nucleation activity is irreversibly lost. This suggests that atmospheric acidity can play a significant role in determining the concentration and activity of ice nucleating particles. Additionally, Iwata and Matsuki (2018) revealed that nitrate and/or sulfate peaks were detected in 99% of the IN non-active particles. Furthermore, it has been shown that the chemical composition and ice nucleation ability of INP can be influenced by anthropogenic emissions of sulfur dioxide and nitrogen oxides (Cziczo et al., 2013). This underscores the importance of considering the impact of atmospheric acidity on INP in understanding the role of particles in cloud glaciation.

There are still many missing sources of INP that are not well understood or characterized. Creamean et al. (2020) highlights the potential of organic-rich particles from Arctic permafrost as sources of INP. They found that permafrost is a rich source of biologically-derived INP, including heat-labile (probably proteinaceous) and other organic INP of biomolecular origin. The thawing of permafrost due to warmer climate and subsequent mobilization of those soils into the atmosphere, lakes, rivers, and the ocean suggests the possibility of increasing emissions of INP, which could have a significant impact on Arctic cloud glaciation and radiative properties. Since permafrost covers 15% of Northern Hemisphere land, this discovery may become central to predictions of aerosol-cloud-precipitation interactions in Arctic mixed-phase clouds.

Concluding, the level of understanding of the sources and properties of INP is still limited, thus, contributing to in accurate prediction of aerosol-cloud interactions by climate models remains challenging. There is a particular need to improve the description of aerosols in CTM and ESM models, with a focus on INP sources and the processes of INP aging, in addition to wet scavenging and dry deposition. While a variety of particles can act as INP, accurately representing the emission fluxes of these particle types remains a key challenge. Moreover, the ice-nucleating activity of dust and biomass-burning aerosols, as well as PBAPs derived INP, is highly variable and often not well-represented in models. To address these issues, carefully designed modeling and observational experiments are required that will allow to evaluate and refine emission parameterizations.

Acronyms

IN	Ice nucleation
INP	Ice nucleating particles
MPOA	Marine primary organic aerosol
SS	Sea Salt
FBAPs	fluorescent biological aerosol particles
PBAPs	Primary biological aerosol particles
BB	Biomass burning
BC	Black carbon
BrC	Brown carbon
T	Temperature
CNT	Classical nucleation theory
$n_s(T)$	Density of nucleation sites per unit surface area (cm^{-2})
$n_m(T)$	Density of nucleation sites per unit mass (g^{-1})
MPCs	Mixed-phase clouds
MODIS	Moderate-Resolution Imaging Spectroradiometer
ESM	Earth System Model
CTM	chemical transport model
SW	Short wave radiation
LW	Long wave radiation
LWP	Liquid water path
IWP	Ice water path
RFaci	Radiative forcing due to aerosol–cloud interactions
RFari	Radiative forcing due to aerosol–radiation interactions
ERFaci	Effective radiative forcing due to aerosol–cloud interactions
ERFari	Effective radiative forcing due to aerosol–radiation interactions

References:

Abbatt, J. P. D., Benz, S., Cziczo, D. J., Kanji, Z., Lohmann, U., and Möhler, O.: Solid Ammonium Sulfate Aerosols as Ice Nuclei: A Pathway for Cirrus Cloud Formation, Science (80-.)., 313, 1770–1773, https://doi.org/10.1126/science.1129726, 2006.

Adebiyi, A. A. and Kok, J. F.: Climate models miss most of the coarse dust in the atmosphere, Sci. Adv., 6, eaaz9507, https://doi.org/10.1126/sciadv.aaz9507, 2020.

Albani, S., Mahowald, N. M., Perry, A. T., Scanza, R. A., Zender, C. S., G.Heavens, N., V. Maggi, J. F. K., and L.Otto-Bliesner, and B.: Improved dust representation in the CommunityAtmosphere Model, J. Adv. Model. Earth Syst., 6, 92–95, https://doi.org/10.1002/2013MS000279.Received, 2014.

Andreae, M. O. and Merlet, P.: Emission of trace gases and aerosols from biomass burning, Global Biogeochem. Cycles, 15, 955–966, https://doi.org/10.1029/2000GB001382, 2001.

Ansmann, A., Tesche, M., Althausen, D., Müller, D., Seifert, P., Freudenthaler, V., Heese, B., Wiegner, M., Pisani, G., Knippertz, P., and Dubovik, O.: Influence of Saharan dust on cloud glaciation in southern Morocco during the Saharan Mineral Dust Experiment, J. Geophys. Res., 113, D04210, https://doi.org/10.1029/2007JD008785, 2008.

Ansmann, A., Mamouri, R. E., Bühl, J., Seifert, P., Engelmann, R., Hofer, J., Nisantzi, A., Atkinson, J. D., Kanji, Z. A., Sierau, B., Vrekoussis, M., and Sciare, J.: Ice-nucleating particle versus ice crystal number concentrationin altocumulus and cirrus layers embedded in Saharan dust:a closure study, Atmos. Chem. Phys., 19, 15087–15115, https://doi.org/10.5194/acp-19-15087-2019, 2019.

Ardon-Dryer, K. and Levin, Z.: Ground-based measurements of immersion freezing in the eastern Mediterranean, Atmos. Chem. Phys., 14, 5217–5231, https://doi.org/10.5194/acp-14-5217-2014, 2014.

Ardon-Dryer, K., Levin, Z., and Lawson, R. P.: Characteristics of immersion freezing nuclei at the South Pole station in Antarctica, Atmos. Chem. Phys., 11, 4015–4024, https://doi.org/10.5194/acp-11-4015-2011, 2011.

Arimoto, R., Duce, R. A., Ray, B. J., Ellis, W. G., Cullen, J. D., and Merrill, J. T.: Trace elements in the atmosphere over the North Atlantic, J. Geophys. Res., 100, 1199–1213,

https://doi.org/10.1029/94JD02618, 1995.

Ariya, P. a., Sun, J., Eltouny, N. a., Hudson, E. D., Hayes, C. T., and Kos, G.: Physical and chemical characterization of bioaerosols – Implications for nucleation processes, Int. Rev. Phys. Chem., 28, 1–32, https://doi.org/10.1080/01442350802597438, 2009.

Atkinson, J. D., Murray, B. J., Woodhouse, M. T., Whale, T. F., Baustian, K. J., Carslaw, K. S., Dobbie, S., O'Sullivan, D., and Malkin, T. L.: The importance of feldspar for ice nucleation by mineral dust in mixed-phase clouds, Nature, 498, 355–358, https://doi.org/10.1038/nature12278, 2013.

Augustin-Bauditz, S., Wex, H., Denjean, C., Hartmann, S., Schneider, J., Schmidt, S., Ebert, M., and Stratmann, F.: Laboratory-generated mixtures of mineral dust particles with biological substances: characterization of the particle mixing state and immersion freezing behavior, Atmos. Chem. Phys., 16, 5531–5543, https://doi.org/10.5194/acp-16-5531-2016, 2016.

Barry, K. R., Hill, T. C. J., Levin, E. J. T., Twohy, C. H., Moore, K. A., Weller, Z. D., Toohey, D. W., Reeves, M., Campos, T., Geiss, R., Schill, G. P., Fischer, E. V., Kreidenweis, S. M., and DeMott, P. J.: Observations of Ice Nucleating Particles in the Free Troposphere From Western US Wildfires, J. Geophys. Res. Atmos., 126, 1–17, https://doi.org/10.1029/2020JD033752, 2021.

Belosi, F., Santachiara, G., and Prodi, F.: Ice-forming nuclei in Antarctica: New and past measurements, Atmos. Res., 145–146, 105–111, https://doi.org/10.1016/j.atmosres.2014.03.030, 2014.

Belosi, F., Rinaldi, M., Decesari, S., Tarozzi, L., Nicosia, A., and Santachiara, G.: Ground level ice nuclei particle measurements including Saharan dust events at a Po Valley rural site (San Pietro Capofiume, Italy), Atmos. Res., 186, 116–126, https://doi.org/10.1016/j.atmosres.2016.11.012, 2017.

Bentley, R. and Chasteen, T. G.: Environmental VOSCs--formation and degradation of dimethyl sulfide, methanethiol and related materials., Chemosphere, 55, 291–317, https://doi.org/10.1016/j.chemosphere.2003.12.017, 2004.

Bhattarai, H., Saikawa, E., Wan, X., Zhu, H., Ram, K., Gao, S., Kang, S., Zhang, Q., Zhang, Y., Wu, G., Wang, X., Kawamura, K., Fu, P., and Cong, Z.: Levoglucosan as a tracer of biomass burning: Recent progress and perspectives, Atmos. Res., 220, 20–33, https://doi.org/10.1016/j.atmosres.2019.01.004, 2019.

De Boer, G., Morrison, H., Shupe, M. D., and Hildner, R.: Evidence of liquid dependent ice nucleation in high-latitude stratiform clouds from surface remote sensors, Geophys. Res. Lett., 38, n/a-n/a, https://doi.org/10.1029/2010GL046016, 2011.

Bonan, G. B., Levis, S., Kergoat, L., and Oleson, K. W.: Landscapes as patches of plant functional types: An integrating concept for climate and ecosystem models, Global Biogeochem. Cycles, 16, 5–23, https://doi.org/https://doi.org/10.1029/2000GB001360, 2002.

Bond, T. C. and Bergstrom, R. W.: Light Absorption by Carbonaceous Particles: An Investigative Review, Aerosol Sci. Technol., 40, 27–67, https://doi.org/10.1080/02786820500421521, 2006.

Bond, T. C., Doherty, S. J., Fahey, D. W., Forster, P. M., Berntsen, T., DeAngelo, B. J., Flanner, M. G., Ghan, S., Kärcher, B., Koch, D., Kinne, S., Kondo, Y., Quinn, P. K., Sarofim, M. C., Schultz, M. G., Schulz, M., Venkataraman, C., Zhang, H., Zhang, S., Bellouin, N., Guttikunda, S. K., Hopke, P. K., Jacobson, M. Z., Kaiser, J. W., Klimont, Z., Lohmann, U., Schwarz, J. P., Shindell, D., Storelvmo, T., Warren, S. G., and Zender, C. S.: Bounding the role of black carbon in the climate system: A scientific assessment, J. Geophys. Res. Atmos., 118, 5380–5552, https://doi.org/10.1002/jgrd.50171, 2013.

Boose, Y., Welti, A., Atkinson, J., Ramelli, F., Danielczok, A., Bingemer, H. G., Plötze, M., Sierau, B., Kanji, Z. A., and Lohmann, U.: Heterogeneous ice nucleation on dust particles sourced from nine deserts worldwide - Part 1: Immersion freezing, Atmos. Chem. Phys., 16, 15075–15095, https://doi.org/10.5194/acp-16-15075-2016, 2016a.

Boose, Y., Welti, A., Atkinson, J., Ramelli, F., Danielczok, A., Bingemer, H. G., Plötze, M., Sierau, B., Kanji, Z. A., and Lohmann, U.: Heterogeneous ice nucleation on dust particles sourced from nine deserts worldwide – Part 1: Immersion freezing, Atmos. Chem. Phys., 16, 15075–15095, https://doi.org/10.5194/acp-16-15075-2016, 2016b.

Boose, Y., Sierau, B., Isabel García, M., Rodríguez, S., Alastuey, A., Linke, C., Schnaiter, M., Kupiszewski, P., Kanji, Z. A., and Lohmann, U.: Ice nucleating particles in the Saharan Air Layer, Atmos. Chem. Phys., 16, 9067–9087, https://doi.org/10.5194/acp-16-9067-2016, 2016c.

Boucher, O.: Atmospheric Aerosols, in: Atmospheric Aerosols. Springer, Dordrecht, vol. 10, 287–291, https://doi.org/10.1002/cpt1969103287, 2015.

Bougiatioti, A., Argyrouli, A., Solomos, S., Vratolis, S., Eleftheriadis, K., Papayannis, A., and Nenes, A.: CCN Activity, Variability and Influence on Droplet Formation during the HygrA-Cd Campaign in Athens, Atmosphere (Basel)., 8, https://doi.org/10.3390/atmos8060108, 2017.

Brook, R. D., Franklin, B., Cascio, W., Hong, Y., Howard, G., Lipsett, M., Luepker, R., Mittleman, M., Samet, J., Smith, S. C., and Tager, I.: Air Pollution and Cardiovascular Disease, Circulation, 109, 2655–2671, https://doi.org/10.1161/01.CIR.0000128587.30041.C8, 2004.

Burrows, S. M., Elbert, W., Lawrence, M. G., and Pöschl, U.: Bacteria in the global atmosphere – Part 1: Review and synthesis of literature data for different ecosystems, Atmos. Chem. Phys. Discuss., 9, 10777–10827, https://doi.org/10.5194/acpd-9-10777-2009, 2009a.

Burrows, S. M., Butler, T., Jöckel, P., Tost, H., Kerkweg, a., Pöschl, U., and Lawrence, M. G.: Bacteria in the global atmosphere – Part 2: Modelling of emissions and transport between different ecosystems, Atmos. Chem. Phys. Discuss., 9, 10829–10881, https://doi.org/10.5194/acpd-9-10829-2009, 2009b.

Burrows, S. M., Hoose, C., Pöschl, U., and Lawrence, M. G.: Ice nuclei in marine air: Biogenic particles or dust?, Atmos. Chem. Phys., 13, 245–267, https://doi.org/10.5194/acp-13-245-2013, 2013.

Burrows, S. M., Ogunro, O., Frossard, A. A., Russell, L. M., Rasch, P. J., and Elliott, S. M.: A physically based framework for modeling the organic fractionation of sea spray aerosol from bubble film Langmuir equilibria, Atmos. Chem. Phys., 14, 13601–13629, https://doi.org/10.5194/acp-14-13601-2014, 2014.

Burrows, S. M., McCluskey, C. S., Cornwell, G., Steinke, I., Zhang, K., Zhao, B., Zawadowicz, M., Raman, A., Kulkarni, G., China, S., Zelenyuk, A., and DeMott, P. J.: Ice-Nucleating Particles That Impact Clouds and Climate: Observational and Modeling Research Needs, https://doi.org/10.1029/2021RG000745, 16 June 2022.

Cavalieri, O., Cairo, F., Fierli, F., Di Donfrancesco, G., Snels, M., Viterbini, M., Cardillo, F., Chatenet, B., Formenti, P., Marticorena, B., and Rajot, J. L.: Variability of aerosol vertical distribution in the Sahel, Atmos. Chem. Phys., 10, 12005–12023, https://doi.org/10.5194/acp-10-12005-2010, 2010.

Chatziparaschos, M., Daskalakis, N., Myriokefalitakis, S., Kalivitis, N., Nenes, A., Gonçalves Ageitos, M., Costa-Surós, M., Pérez Garc\'\ia-Pando, C., Zanoli, M., Vrekoussis, M., and

Kanakidou, M.: Role of K-feldspar and quartz in global ice nucleation by mineral dust in mixed-phase clouds, Atmos. Chem. Phys., 23, 1785–1801, https://doi.org/10.5194/acp-23-1785-2023, 2023.

Choi, Y.-S., Lindzen, R. S., Ho, C.-H., and Kim, J.: Space observations of cold-cloud phase change, Proc. Natl. Acad. Sci., 107, 11211–11216, https://doi.org/10.1073/pnas.1006241107, 2010.

Chubb, T. H., Jensen, J. B., Siems, S. T., and Manton, M. J.: In situ observations of supercooled liquid clouds over the Southern Ocean during the HIAPER Pole-to-Pole Observation campaigns, Geophys. Res. Lett., 40, 5280–5285, https://doi.org/10.1002/grl.50986, 2013.

Claquin, T., Schulz, M., and Balkanski, Y. J.: Modeling the mineralogy of atmospheric dust sources, J. Geophys. Res. Atmos., 104, 22243–22256, https://doi.org/10.1029/1999JD900416, 1999.

Conen, F., Rodríguez, S., Hüglin, C., Henne, S., Herrmann, E., Bukowiecki, N., and Alewell, C.: Atmospheric ice nuclei at the high-altitude observatory Jungfraujoch, Switzerland, Tellus, Ser. B Chem. Phys. Meteorol., 67, https://doi.org/10.3402/tellusb.v67.25014, 2015.

Cooke, W. F., Liousse, C., Cachier, H., and Feichter, J.: Construction of a 1° × 1° fossil fuel emission data set for carbonaceous aerosol and implementation and radiative impact in the ECHAM4 model, J. Geophys. Res. Atmos., 104, 22137–22162, https://doi.org/10.1029/1999JD900187, 1999.

Creamean, J. M., Cross, J. N., Pickart, R., McRaven, L., Lin, P., Pacini, A., Hanlon, R., Schmale, D. G., Ceniceros, J., Aydell, T., Colombi, N., Bolger, E., and DeMott, P. J.: Ice Nucleating Particles Carried From Below a Phytoplankton Bloom to the Arctic Atmosphere, Geophys. Res. Lett., 46, 8572–8581, https://doi.org/10.1029/2019GL083039, 2019.

Creamean, J. M., Hill, T. C. J., DeMott, P. J., Uetake, J., Kreidenweis, S., and Douglas, T. A.: Thawing permafrost: an overlooked source of seeds for Arctic cloud formation, Environ. Res. Lett., 15, 084022, https://doi.org/10.1088/1748-9326/ab87d3, 2020.

Creamean, J. M., Barry, K., Hill, T. C. J., Hume, C., DeMott, P. J., Shupe, M. D., Dahlke, S., Willmes, S., Schmale, J., Beck, I., Hoppe, C. J. M., Fong, A., Chamberlain, E., Bowman, J., Scharien, R., and Persson, O.: Annual cycle observations of aerosols capable of ice formation in central Arctic clouds, Nat. Commun., 13, 1–12, https://doi.org/10.1038/s41467-022-

31182-x, 2022.

Curci, G., Alyuz, U., Barò, R., Bianconi, R., Bieser, J., Christensen, J. H., Colette, A., Farrow, A., Francis, X., Jiménez-Guerrero, P., Im, U., Liu, P., Manders, A., Palacios-Peña, L., Prank, M., Pozzoli, L., Sokhi, R., Solazzo, E., Tuccella, P., Unal, A., Vivanco, M. G., Hogrefe, C., and Galmarini, S.: Modelling black carbon absorption of solar radiation: combining external and internal mixing assumptions, Atmos. Chem. Phys., 19, 181–204, https://doi.org/10.5194/acp-19-181-2019, 2019.

Cziczo, D. J., Froyd, K. D., Hoose, C., Jensen, E. J., Diao, M., Zondlo, M. A., Smith, J. B., Twohy, C. H., and Murphy, D. M.: Clarifying the Dominant Sources and Mechanisms of Cirrus Cloud Formation, Science (80-.)., 340, 1320–1324, https://doi.org/10.1126/science.1234145, 2013.

Daskalakis, N., Tsigaridis, K., Myriokefalitakis, S., Fanourgakis, G. S., and Kanakidou, M.: Large gain in air quality compared to an alternative anthropogenic emissions scenario, Atmos. Chem. Phys., 16, 9771–9784, https://doi.org/10.5194/acp-16-9771-2016, 2016.

Daskalakis, N., Gallardo, L., Kanakidou, M., Nüß, J. R., Menares, C., Rondanelli, R., Thompson, A. M., and Vrekoussis, M.: Impact of biomass burning and stratospheric intrusions in the remote South Pacific Ocean troposphere, Atmos. Chem. Phys., 22, 4075–4099, https://doi.org/10.5194/acp-22-4075-2022, 2022.

David, R. O., Marcolli, C., Fahrni, J., Qiu, Y., Perez Sirkin, Y. A., Molinero, V., Mahrt, F., Brühwiler, D., Lohmann, U., and Kanji, Z. A.: Pore condensation and freezing is responsible for ice formation below water saturation for porous particles, Proc. Natl. Acad. Sci., 116, 8184–8189, https://doi.org/10.1073/pnas.1813647116, 2019.

Davies, P. L.: Ice-binding proteins: a remarkable diversity of structures for stopping and starting ice growth, Trends Biochem. Sci., 39, 548–555, https://doi.org/https://doi.org/10.1016/j.tibs.2014.09.005, 2014.

Dee, D. P., Uppala, S. M., Simmons, A. J., Berrisford, P., Poli, P., Kobayashi, S., Andrae, U., Balmaseda, M. A., Balsamo, G., Bauer, P., Bechtold, P., Beljaars, A. C. M., van de Berg, L., Bidlot, J., Bormann, N., Delsol, C., Dragani, R., Fuentes, M., Geer, A. J., Haimberger, L., Healy, S. B., Hersbach, H., Hólm, E. V., Isaksen, L., Kållberg, P., Köhler, M., Matricardi, M., Mcnally, A. P., Monge-Sanz, B. M., Morcrette, J. J., Park, B. K., Peubey, C., de Rosnay, P., Tavolato, C., Thépaut, J. N., and Vitart, F.: The ERA-Interim reanalysis: Configuration and performance of the data assimilation system, Q. J. R. Meteorol. Soc., 137, 553–597,

https://doi.org/10.1002/qj.828, 2011.

Demott, P. J., Hill, T. C. J., Mccluskey, C. S., Prather, K. A., Collins, D. B., Sullivan, R. C., Ruppel, M. J., Mason, R. H., Irish, V. E., Lee, T., Yeon, C., Siek, T., Snider, J. R., Mcmeeking, G. R., Dhaniyala, S., Lewis, E. R., and Wentzell, J. J. B.: Sea spray aerosol as a unique source of ice nucleating particles, 113, https://doi.org/10.1073/pnas.1514034112, 2016.

DeMott, P. J., Prenni, A. J., Liu, X., Kreidenweis, S. M., Petters, M. D., Twohy, C. H., Richardson, M. S., Eidhammer, T., and Rogers, D. C.: Predicting global atmospheric ice nuclei distributions and their impacts on climate, Proc. Natl. Acad. Sci. U. S. A., 107, 11217–11222, https://doi.org/10.1073/pnas.0910818107, 2010.

DeMott, P. J., Hill, T. C. J., McCluskey, C. S., Prather, K. A., Collins, D. B., Sullivan, R. C., Ruppel, M. J., Mason, R. H., Irish, V. E., Lee, T., Hwang, C. Y., Rhee, T. S., Snider, J. R., McMeeking, G. R., Dhaniyala, S., Lewis, E. R., Wentzell, J. J. B., Abbatt, J., Lee, C., Sultana, C. M., Ault, A. P., Axson, J. L., Diaz Martinez, M., Venero, I., Santos-Figueroa, G., Stokes, M. D., Deane, G. B., Mayol-Bracero, O. L., Grassian, V. H., Bertram, T. H., Bertram, A. K., Moffett, B. F., and Franc, G. D.: Sea spray aerosol as a unique source of ice nucleating particles, Proc. Natl. Acad. Sci., 113, 201514034, https://doi.org/10.1073/pnas.1514034112, 2015.

Després, V. R., Alex Huffman, J., Burrows, S. M., Hoose, C., Safatov, A. S., Buryak, G., Fröhlich-Nowoisky, J., Elbert, W., Andreae, M. O., Pöschl, U., and Jaenicke, R.: Primary biological aerosol particles in the atmosphere: a review, Tellus B, 64, https://doi.org/10.3402/tellusb.v64i0.15598, 2012.

Diehl, K., Quick, C., Matthias-Maser, S., Mitra, S. K., and Jaenicke, R.: The ice nucleating ability of pollen, Atmos. Res., 58, 75–87, https://doi.org/10.1016/S0169-8095(01)00091-6, 2001.

Döscher, R., Acosta, M., Alessandri, A., Anthoni, P., Arsouze, T., Bergman, T., Bernardello, R., Boussetta, S., Caron, L.-P., Carver, G., Castrillo, M., Catalano, F., Cvijanovic, I., Davini, P., Dekker, E., Doblas-Reyes, F. J., Docquier, D., Echevarria, P., Fladrich, U., Fuentes-Franco, R., Gröger, M., v. Hardenberg, J., Hieronymus, J., Karami, M. P., Keskinen, J.-P., Koenigk, T., Makkonen, R., Massonnet, F., Ménégoz, M., Miller, P. A., Moreno-Chamarro, E., Nieradzik, L., van Noije, T., Nolan, P., O'Donnell, D., Ollinaho, P., van den Oord, G., Ortega, P., Prims, O. T., Ramos, A., Reerink, T., Rousset, C., Ruprich-Robert, Y., Le Sager, P., Schmith, T., Schrödner, R., Serva, F., Sicardi, V., Sloth Madsen, M., Smith, B., Tian, T., Tourigny, E., Uotila, P., Vancoppenolle, M., Wang, S., Wårlind, D., Willén, U., Wyser, K., Yang, S., Yepes-Arbós, X.,

and Zhang, Q.: The EC-Earth3 Earth system model for the Coupled Model Intercomparison Project 6, Geosci. Model Dev., 15, 2973–3020, https://doi.org/10.5194/gmd-15-2973-2022, 2022.

Elbert, W., Taylor, P. E., Andreae, M. O., and Pöschl, U.: Contribution of fungi to primary biogenic aerosols in the atmosphere: wet and dry discharged spores, carbohydrates, and inorganic ions, 7, 4569–4588, https://doi.org/10.5194/acp-7-4569-2007, 2007.

Escudero, M., Querol, X., Pey, J., Alastuey, A., Pérez, N., Ferreira, F., Alonso, S., Rodríguez, S., and Cuevas, E.: A methodology for the quantification of the net African dust load in air quality monitoring networks, Atmos. Environ., 41, 5516–5524, https://doi.org/10.1016/j.atmosenv.2007.04.047, 2007.

Fabbri, D., Torri, C., Simoneit, B. R. T., Marynowski, L., Rushdi, A. I., and Fabiańska, M. J.: Levoglucosan and other cellulose and lignin markers in emissions from burning of Miocene lignites, Atmos. Environ., 43, 2286–2295, https://doi.org/10.1016/j.atmosenv.2009.01.030, 2009.

Facchini, M. C., Decesari, S., Rinaldi, M., Carbone, C., Finessi, E., Mircea, M., Fuzzi, S., Moretti, F., Tagliavini, E., Ceburnis, D., and O'Dowd, C. D.: Important source of marine secondary organic aerosol from biogenic amines., Environ. Sci. Technol., 42, 9116–21, https://doi.org/10.1021/es8018385, 2008.

Fan, J., Leung, L. R., Demott, P. J., Comstock, J. M., Singh, B., Rosenfeld, D., Tomlinson, J. M., White, A., Prather, K. A., Minnis, P., Ayers, J. K., and Min, Q.: Aerosol impacts on California winter clouds and precipitation during calwater 2011: Local pollution versus long-range transported dust, Atmos. Chem. Phys., 14, 81–101, https://doi.org/10.5194/acp-14-81-2014, 2014.

Fanourgakis, G. S., Kanakidou, M., Nenes, A., Bauer, S. E., Bergman, T., Carslaw, K. S., Grini, A., Hamilton, D. S., Johnson, J. S., Karydis, V. A., Kirkevåg, A., Kodros, J. K., Lohmann, U., Luo, G., Makkonen, R., Matsui, H., Neubauer, D., Pierce, J. R., Schmale, J., Stier, P., Tsigaridis, K., van Noije, T., Wang, H., Watson-Parris, D., Westervelt, D. M., Yang, Y., Yoshioka, M., Daskalakis, N., Decesari, S., Gysel Beer, M., Kalivitis, N., Liu, X., Mahowald, N. M., Myriokefalitakis, S., Schrödner, R., Sfakianaki, M., Tsimpidi, A. P., Wu, M., and Yu, F.: Evaluation of global simulations of aerosol particle number and cloud condensation nuclei, and implications for cloud droplet formation, Atmos. Chem. Phys. Discuss., 1–40, https://doi.org/10.5194/acp-2018-1340, 2019.

Field, P. R., Lawson, R. P., Brown, P. R. A., Lloyd, G., Westbrook, C., Moisseev, D., Miltenberger, A., Nenes, A., Blyth, A., Choularton, T., Connolly, P., Buehl, J., Crosier, J., Cui, Z., Dearden, C., DeMott, P., Flossmann, A., Heymsfield, A., Huang, Y., Kalesse, H., Kanji, Z. A., Korolev, A., Kirchgaessner, A., Lasher-Trapp, S., Leisner, T., McFarquhar, G., Phillips, V., Stith, J., and Sullivan, S.: Chapter 7. Secondary Ice Production - current state of the science and recommendations for the future, Meteorol. Monogr., AMSMONOGRAPHS-D-16-0014.1, https://doi.org/10.1175/AMSMONOGRAPHS-D-16-0014.1, 2016.

Forbes, R., Tompkins, A. M., and Untch, A.: 649 A new prognostic bulk microphysics scheme for the IFS, 2012.

France, O. B., France, C. G., Germany, C. H., and Uk, A. J.: Clouds and aerosols, Clim. Chang. 2013 Phys. Sci. Basis Work. Gr. I Contrib. to Fifth Assess. Rep. Intergov. Panel Clim. Chang., 9781107057, 571–658, https://doi.org/10.1017/CBO9781107415324.016, 2013.

Freedman, M. A.: Potential Sites for Ice Nucleation on Aluminosilicate Clay Minerals and Related Materials, J. Phys. Chem. Lett., 6, 3850–3858, https://doi.org/10.1021/acs.jpclett.5b01326, 2015.

Fröhlich-Nowoisky, J., Hill, T. C. J., Pummer, B. G., Yordanova, P., Franc, G. D., and Pöschl, U.: Ice nucleation activity in the widespread soil fungus <i>Mortierella alpina</i>, 12, 1057–1071, https://doi.org/10.5194/bg-12-1057-2015, 2015.

Froyd, K. D., Yu, P., Schill, G. P., Brock, C. A., Kupc, A., Williamson, C. J., Jensen, E. J., Ray, E., Rosenlof, K. H., Bian, H., Darmenov, A. S., Colarco, P. R., Diskin, G. S., Bui, T., and Murphy, D. M.: Dominant role of mineral dust in cirrus cloud formation revealed by global-scale measurements, Nat. Geosci., 15, 177–183, https://doi.org/10.1038/s41561-022-00901-w, 2022.

Gantt, B., Meskhidze, N., and Kamykowski, D.: A new physically-based quantification of marine isoprene and primary organic aerosol emissions, Atmos. Chem. Phys., 9, 4915–4927, https://doi.org/10.5194/acp-9-4915-2009, 2009.

Gantt, B., Meskhidze, N., Facchini, M. C., Rinaldi, M., Ceburnis, D., and O'Dowd, C. D.: Wind speed dependent size-resolved parameterization for the organic mass fraction of sea spray aerosol, Atmos. Chem. Phys., 11, 8777–8790, https://doi.org/10.5194/acp-11-8777-2011, 2011.

Garimella, S., Rothenberg, D. A., Wolf, M. J., David, R. O., Kanji, Z. A., Wang, C., Rösch, M.,

and Cziczo, D. J.: Uncertainty in counting ice nucleating particles with continuous flow diffusion chambers, Atmos. Chem. Phys., 17, 10855–10864, https://doi.org/10.5194/acp-17-10855-2017, 2017.

Georgakaki, P., Sotiropoulou, G., Vignon, É., Billault-Roux, A.-C., Berne, A., and Nenes, A.: Secondary ice production processes in wintertime alpine mixed-phase clouds, Atmos. Chem. Phys., 22, 1965–1988, https://doi.org/10.5194/acp-22-1965-2022, 2022.

Ginoux, P., Prospero, J. M., Torres, O., and Chin, M.: Long-term simulation of global dust distribution with the GOCART model: Correlation with North Atlantic Oscillation, Environ. Model. Softw., 19, 113–128, https://doi.org/10.1016/S1364-8152(03)00114-2, 2004.

Ginoux, P., Prospero, J. M., Gill, T. E., Hsu, N. C., and Zhao, M.: Global-scale attribution of anthropogenic and natural dust sources and their emission rates based on MODIS Deep Blue aerosol products, Rev. Geophys., 50, https://doi.org/10.1029/2012RG000388, 2012.

Gonçalves Ageitos, M., Obiso, V., Miller, R. L., Jorba, O., Klose, M., Dawson, M., Balkanski, Y., Perlwitz, J., Basart, S., Di Tomaso, E., Escribano, J., Macchia, F., Montané, G., Mahowald, N., Green, R. O., Thompson, D. R., and Pérez Garc\'\ia-Pando, C.: Modeling dust mineralogical composition: sensitivity to soil mineralogy atlases and their expected climate impacts, 2023, 1–51, https://doi.org/10.5194/egusphere-2022-1414, 2023.

Gong, S. L.: A parameterization of sea-salt aerosol source function for sub- and super-micron particles, Global Biogeochem. Cycles, https://doi.org/10.1029/2003GB002079, 2003.

Granados-Muñoz, M. J., Sicard, M., Román, R., Benavent-Oltra, J. A., Barragán, R., Brogniez, G., Denjean, C., Mallet, M., Formenti, P., Torres, B., and Alados-Arboledas, L.: Impact of mineral dust on shortwave and longwave radiation: evaluation of different vertically resolved parameterizations in 1-D radiative transfer computations, Atmos. Chem. Phys., 19, 523–542, https://doi.org/10.5194/acp-19-523-2019, 2019.

Granier, C., Guenther, A., and Middleton, P.: POET, a database of surface emissions of ozone precursors, https://doi.org/http://www.aero.jussieu.fr/projet/ACCENT/POET.php., 2005.

Hande, L. B. and Hoose, C.: Partitioning the primary ice formation modes in large eddy simulations of mixed-phase clouds, Atmos. Chem. Phys., 17, 14105–14118, https://doi.org/10.5194/acp-17-14105-2017, 2017.

Harrison, A. D., Whale, T. F., Carpenter, M. A., Holden, M. A., Neve, L., O'Sullivan, D., Vergara Temprado, J., and Murray, B. J.: Not all feldspars are equal: A survey of ice nucleating

properties across the feldspar group of minerals, Atmos. Chem. Phys., 16, 10927–10940, https://doi.org/10.5194/acp-16-10927-2016, 2016.

Harrison, A. D., Lever, K., Sanchez-Marroquin, A., Holden, M. A., Whale, T. F., Tarn, M. D., McQuaid, J. B., and Murray, B. J.: The ice-nucleating ability of quartz immersed in water and its atmospheric importance compared to K-feldspar, Atmos. Chem. Phys. Discuss., 1–23, https://doi.org/10.5194/acp-2019-288, 2019.

Heald, C. L. and Spracklen, D. V: Atmospheric budget of primary biological aerosol particles from fungal spores, Geophys. Res. Lett., 36, L09806, https://doi.org/10.1029/2009GL037493, 2009.

Hill, T. C. J., Demott, P. J., Tobo, Y., Fröhlich-Nowoisky, J., Moffett, B. F., Franc, G. D., and Kreidenweis, S. M.: Sources of organic ice nucleating particles in soils, Atmos. Chem. Phys., 16, 7195–7211, https://doi.org/10.5194/acp-16-7195-2016, 2016.

Hoose, C. and Möhler, O.: Heterogeneous ice nucleation on atmospheric aerosols: A review of results from laboratory experiments, 9817–9854 pp., https://doi.org/10.5194/acp-12-9817-2012, 2012.

Hoose, C., Kristjánsson, J. E., and Burrows, S. M.: How important is biological ice nucleation in clouds on a global scale?, Environ. Res. Lett., 5, 024009, https://doi.org/10.1088/1748-9326/5/2/024009, 2010.

Huang, S., Hu, W., Chen, J., Wu, Z., Zhang, D., and Fu, P.: Overview of biological ice nucleating particles in the atmosphere, Environ. Int., 146, 106197, https://doi.org/10.1016/j.envint.2020.106197, 2021.

Huang, W. T. K., Ickes, L., Tegen, I., Rinaldi, M., Ceburnis, D., and Lohmann, U.: Global relevance of marine organic aerosol as ice nucleating particles, Atmos. Chem. Phys., 18, 11423–11445, https://doi.org/10.5194/acp-18-11423-2018, 2018.

Huang, Y., Kok, J. F., Kandler, K., Lindqvist, H., Nousiainen, T., Sakai, T., Adebiyi, A., and Jokinen, O.: Climate Models and Remote Sensing Retrievals Neglect Substantial Desert Dust Asphericity, Geophys. Res. Lett., 47, 1–11, https://doi.org/10.1029/2019GL086592, 2020.

Huffman, J. A., Sinha, B., Garland, R. M., Snee-Pollmann, A., Gunthe, S. S., Artaxo, P., Martin, S. T., Andreae, M. O., and Pöschl, U.: Size distributions and temporal variations of biological aerosol particles in the Amazon rainforest characterized by microscopy and real-time UV-APS fluorescence techniques during AMAZE-08, 12, 11997–12019,

https://doi.org/10.5194/acp-12-11997-2012, 2012.

Huffman, J. A., Prenni, A. J., DeMott, P. J., Pöhlker, C., Mason, R. H., Robinson, N. H., Fröhlich-Nowoisky, J., Tobo, Y., Després, V. R., Garcia, E., Gochis, D. J., Harris, E., Müller-Germann, I., Ruzene, C., Schmer, B., Sinha, B., Day, D. A., Andreae, M. O., Jimenez, J. L., Gallagher, M., Kreidenweis, S. M., Bertram, A. K., and Pöschl, U.: High concentrations of biological aerosol particles and ice nuclei during and after rain, 13, 6151–6164, https://doi.org/10.5194/acp-13-6151-2013, 2013.

Hulswar, S., Simó, R., Gal\'\i, M., Bell, T. G., Lana, A., Inamdar, S., Halloran, P. R., Manville, G., and Mahajan, A. S.: Third revision of the global surface seawater dimethyl sulfide climatology (DMS-Rev3), Earth Syst. Sci. Data, 14, 2963–2987, https://doi.org/10.5194/essd-14-2963-2022, 2022.

Hummel, M., Hoose, C., Gallagher, M., Healy, D. a., Huffman, J. A., O'Connor, D., Pöschl, U., Pöhlker, C., Robinson, N. H., Schnaiter, M., Sodeau, J. R., Stengel, M., Toprak, E., and Vogel, H.: Regional-scale simulations of fungal spore aerosols using an emission parameterization adapted to local measurements of fluorescent biological aerosol particles, Atmos. Chem. Phys., 15, 6127–6146, https://doi.org/10.5194/acp-15-6127-2015, 2015.

van den Hurk, B. J. J., Dutra, E., Smith, B., Haarsma, R., Hazeleger, W., Balsamo, G., and vd Molen: The EC-Earth modelling challenges, https://www.ecmwf.int/node/15307, 2009.

Ilić, L., Jovanović, A., Kuzmanoski, M., Lazić, L., Madonna, F., Rosoldi, M., Mytilinaios, M., Marinou, E., and Ničković, S.: Mineralogy Sensitive Immersion Freezing Parameterization in DREAM, J. Geophys. Res. Atmos., 127, 1–22, https://doi.org/10.1029/2021JD035093, 2022.

IPCC: IPCC, 2021: Climate Change 2021. The Physical Science Basis. Summary for Policymakers., edited by: Masson-Delmotte, V., P. Zhai, A. Pirani, S. L. Connors, C. Péan, S. Berger, N. Caud, Y. Chen, L. Goldfarb, M. I. Gomis, M. Huang, K. Leitzell, E. Lonnoy, J. B. R. Matthews, T. K. Maycock, T. Waterfield, O. Yelekçi, R. Yu and B. Zhou , Masson-Delmotte, V., R. Y. and B. Z., Cambridge University Press, Cambridge, United Kingdom and New York, NY, USA, 2021.

Ivlev, L. S.: Atmospheric Aerosols, in: Aerosols - Science and Technology, Springer Netherlands, Dordrecht, Heidelberg, New York, London, 343–378, https://doi.org/10.1002/9783527630134.ch12, 2010.

Iwata, A. and Matsuki, A.: Characterization of individual ice residual particles by the single

droplet freezing method: A case study in the Asian dust outflow region, Atmos. Chem. Phys., 18, 1785–1804, https://doi.org/10.5194/acp-18-1785-2018, 2018.

Jacobson, M. Z. and Streets, D. G.: Influence of future anthropogenic emissions on climate, natural emissions, and air quality, J. Geophys. Res., 114, D08118, https://doi.org/10.1029/2008JD011476, 2009.

Jahl, L. G., Brubaker, T. A., Polen, M. J., Jahn, L. G., Cain, K. P., Bowers, B. B., Fahy, W. D., Graves, S., and Sullivan, R. C.: Atmospheric aging enhances the ice nucleation ability of biomass-burning aerosol, Sci. Adv., 7, 1–10, https://doi.org/10.1126/sciadv.abd3440, 2021.

Janssen, R. H. H., Heald, C. L., Steiner, A. L., Perring, A. E., Huffman, J. A., Robinson, E. S., Twohy, C. H., and Ziemba, L. D.: Drivers of the fungal spore bioaerosol budget: observational analysis and global modeling, Atmos. Chem. Phys., 21, 4381–4401, https://doi.org/10.5194/acp-21-4381-2021, 2021.

Jeuken, M., Van Wijk, R., Peleman, J., and Lindhout, P.: An integrated interspecific AFLP map of lettuce (Lactuca) based on two L. sativa × L. saligna F2 populations, Theor. Appl. Genet., 103, 638–647, https://doi.org/10.1007/s001220100657, 2001.

Jimenez, J. L., Canagaratna, M. R., Donahue, N. M., Prevot, A. S. H., Zhang, Q., Kroll, J. H., DeCarlo, P. F., Allan, J. D., Coe, H., Ng, N. L., Aiken, A. C., Docherty, K. S., Ulbrich, I. M., Grieshop, A. P., Robinson, A. L., Duplissy, J., Smith, J. D., Wilson, K. R., Lanz, V. A., Hueglin, C., Sun, Y. L., Tian, J., Laaksonen, A., Raatikainen, T., Rautiainen, J., Vaattovaara, P., Ehn, M., Kulmala, M., Tomlinson, J. M., Collins, D. R., Cubison, M. J., Dunlea, J., Huffman, J. A., Onasch, T. B., Alfarra, M. R., Williams, P. I., Bower, K., Kondo, Y., Schneider, J., Drewnick, F., Borrmann, S., Weimer, S., Demerjian, K., Salcedo, D., Cottrell, L., Griffin, R., Takami, A., Miyoshi, T., Hatakeyama, S., Shimono, A., Sun, J. Y., Zhang, Y. M., Dzepina, K., Kimmel, J. R., Sueper, D., Jayne, J. T., Herndon, S. C., Trimborn, A. M., Williams, L. R., Wood, E. C., Middlebrook, A. M., Kolb, C. E., Baltensperger, U., and Worsnop, D. R.: Evolution of Organic Aerosols in the Atmosphere, Science (80-.)., 326, 1525–1529, https://doi.org/10.1126/science.1180353, 2009.

Journet, E., Balkanski, Y., and Harrison, S. P.: A new data set of soil mineralogy for dust-cycle modeling, Atmos. Chem. Phys., 14, 3801–3816, https://doi.org/10.5194/acp-14-3801-2014, 2014.

Kalivitis, N., Gerasopoulos, E., Vrekoussis, M., Kouvarakis, G., Kubilay, N., Hatzianastassiou, N., Vardavas, I., and Mihalopoulos, N.: Dust transport over the eastern mediterranean

derived from total ozone mapping spectrometer, aerosol robotic network, and surface measurements, J. Geophys. Res. Atmos., 112, https://doi.org/10.1029/2006JD007510, 2007.

Kanakidou, M., Myriokefalitakis, S., and Tsagkaraki, M.: Atmospheric inputs of nutrients to the Mediterranean Sea, Deep. Res. Part II Top. Stud. Oceanogr., 171, https://doi.org/10.1016/j.dsr2.2019.06.014, 2020.

Kandler, K., Schütz, L., Deutscher, C., Ebert, M., Hofmann, H., Jäckel, S., Jaenicke, R., Knippertz, P., Lieke, K., Massling, A., Petzold, A., Schladitz, A., Weinzierl, B., Wiedensohler, A., Zorn, S., and Weinbruch, S.: Size distribution, mass concentration, chemical and mineralogical composition and derived optical parameters of the boundary layer aerosol at Tinfou, Morocco, during SAMUM 2006, Tellus B, 61, https://doi.org/10.3402/tellusb.v61i1.16798, 2009.

Kanji, Z. A., Florea, O., and Abbatt, J. P. D.: Ice formation via deposition nucleation on mineral dust and organics: dependence of onset relative humidity on total particulate surface area, Environ. Res. Lett., 3, 025004, https://doi.org/10.1088/1748-9326/3/2/025004, 2008.

Kanji, Z. A., Ladino, L. A., Wex, H., Boose, Y., Burkert-Kohn, M., Cziczo, D. J., and Krämer, M.: Overview of Ice Nucleating Particles, Meteorol. Monogr., 58, 1.1-1.33, https://doi.org/10.1175/AMSMONOGRAPHS-D-16-0006.1, 2017.

Kanji, Z. A., Sullivan, R. C., Niemand, M., DeMott, P. J., Prenni, A. J., Chou, C., Saathoff, H., and Möhler, O.: Heterogeneous ice nucleation properties of natural desert dust particles coated with a surrogate of secondary organic aerosol, Atmos. Chem. Phys., 19, 5091–5110, https://doi.org/10.5194/acp-19-5091-2019, 2019.

Kärcher, B. and Voigt, C.: Formation of nitric acid/water ice particles in cirrus clouds, Geophys. Res. Lett., 33, L08806, https://doi.org/10.1029/2006GL025927, 2006.

Kay, J. E., Wall, C., Yettella, V., Medeiros, B., Hannay, C., Caldwell, P., and Bitz, C.: Global Climate Impacts of Fixing the Southern Ocean Shortwave Radiation Bias in the Community Earth System Model (CESM), J. Clim., 29, 4617–4636, https://doi.org/10.1175/JCLI-D-15-0358.1, 2016.

Kim, K.-H., Kabir, E., and Kabir, S.: A review on the human health impact of airborne particulate matter., Environ. Int., 74, 136–143, https://doi.org/10.1016/j.envint.2014.10.005, 2015.

Kiselev, A., Bachmann, F., Pedevilla, P., Cox, S. J., Michaelides, A., Gerthsen, D., and Leisner, T.: Active sites in heterogeneous ice nucleation-the example of K-rich feldspars, Science (80-.)., 355, 367–371, https://doi.org/10.1126/science.aai8034, 2017.

Kleanthous, S., Vrekoussis, M., Mihalopoulos, N., Kalabokas, P., and Lelieveld, J.: On the temporal and spatial variation of ozone in Cyprus, Sci. Total Environ., 476–477, 677–687, https://doi.org/10.1016/j.scitotenv.2013.12.101, 2014.

Kohn, M., Lohmann, U., Welti, A., and Kanji, Z. A.: Immersion mode ice nucleation measurements with the new Portable Immersion Mode Cooling chAmber (PIMCA), J. Geophys. Res. Atmos., 121, 4713–4733, https://doi.org/https://doi.org/10.1002/2016JD024761, 2016.

Kok, J. F.: A scaling theory for the size distribution of emitted dust aerosols suggests climate models underestimate the size of the global dust cycle, Proc. Natl. Acad. Sci. U. S. A., 108, 1016–1021, https://doi.org/10.1073/pnas.1014798108, 2011.

Kok, J. F., Ridley, D. A., Zhou, Q., Miller, R. L., Zhao, C., Heald, C. L., Ward, D. S., Albani, S., and Haustein, K.: Smaller desert dust cooling effect estimated from analysis of dust size and abundance, Nat. Geosci., 10, 274–278, https://doi.org/10.1038/ngeo2912, 2017.

Kok, J. F., Adebiyi, A. A., Albani, S., Balkanski, Y., Checa-Garcia, R., Chin, M., Colarco, P. R., Hamilton, D. S., Huang, Y., Ito, A., Klose, M., Leung, D. M., Li, L., Mahowald, N. M., Miller, R. L., Obiso, V., Pérez Garc\'\ia-Pando, C., Rocha-Lima, A., Wan, J. S., and Whicker, C. A.: Improved representation of the global dust cycle using observational constraints on dust properties and abundance, Atmos. Chem. Phys., 21, 8127–8167, https://doi.org/10.5194/acp-21-8127-2021, 2021a.

Kok, J. F., Adebiyi, A. A., Albani, S., Balkanski, Y., Checa-Garcia, R., Chin, M., Colarco, P. R., Hamilton, D. S., Huang, Y., Ito, A., Klose, M., Leung, D. M., Li, L., Mahowald, N. M., Miller, R. L., Obiso, V., Pérez García-Pando, C., Rocha-Lima, A., Wan, J. S., and Whicker, C. A.: Improved representation of the global dust cycle using observational constraints on dust properties and abundance, Atmos. Chem. Phys., 21, 8127–8167, https://doi.org/10.5194/acp-21-8127-2021, 2021b.

Kok, J. F., Storelvmo, T., Karydis, V. A., Adebiyi, A. A., Mahowald, N. M., Evan, A. T., He, C., and Leung, D. M.: Mineral dust aerosol impacts on global climate and climate change, Nat. Rev. Earth Environ., 4, 71–86, https://doi.org/10.1038/s43017-022-00379-5, 2023.

Komurcu, M., Storelvmo, T., Tan, I., Lohmann, U., Yun, Y., Penner, J. E., Wang, Y., Liu, X., and Takemura, T.: Intercomparison of the cloud water phase among global climate models, J. Geophys. Res. Atmos., 119, 3372–3400, https://doi.org/https://doi.org/10.1002/2013JD021119, 2014.

Kumar, P., Sokolik, I. N., and Nenes, A.: Parameterization of cloud droplet formation for global and regional models: Including adsorption activation from insoluble CCN, Atmos. Chem. Phys., 9, 2517–2532, https://doi.org/10.5194/acp-9-2517-2009, 2009.

Kumar, P., Sokolik, I. N., and Nenes, A.: Cloud condensation nuclei activity and droplet activation kinetics of wet processed regional dust samples and minerals, Atmos. Chem. Phys., 11, 8661–8676, https://doi.org/10.5194/acp-11-8661-2011, 2011.

Lacher, L., Lohmann, U., Boose, Y., Zipori, A., Herrmann, E., Bukowiecki, N., Steinbacher, M., and Kanji, Z. A.: The Horizontal Ice Nucleation Chamber HINC: INP measurements at Conditions Relevant for Mixed-Phase Clouds at the High Altitude Research Station Jungfraujoch, Atmos. Chem. Phys. Discuss., 1–49, https://doi.org/10.5194/acp-2017-474, 2017.

Lacher, L., DeMott, P. J., Levin, E. J. T., Suski, K. J., Boose, Y., Zipori, A., Herrmann, E., Bukowiecki, N., Steinbacher, M., Gute, E., Abbatt, J. P. D., Lohmann, U., and Kanji, Z. A.: Background Free-Tropospheric Ice Nucleating Particle Concentrations at Mixed-Phase Cloud Conditions, J. Geophys. Res. Atmos., 123, 10,506-10,525, https://doi.org/10.1029/2018JD028338, 2018.

Lacher, L., Clemen, H. C., Shen, X., Mertes, S., Gysel-Beer, M., Moallemi, A., Steinbacher, M., Henne, S., Saathoff, H., Mohler, O., Hohler, K., Schiebel, T., Weber, D., Schrod, J., Schneider, J., and Kanji, Z. A.: Sources and nature of ice-nucleating particles in the free troposphere at Jungfraujoch in winter 2017, Atmos. Chem. Phys., 21, 16925–16953, https://doi.org/10.5194/acp-21-16925-2021, 2021.

Lana, A., Bell, T. G., Simó, R., Vallina, S. M., Ballabrera-Poy, J., Kettle, A. J., Dachs, J., Bopp, L., Saltzman, E. S., Stefels, J., Johnson, J. E., and Liss, P. S.: An updated climatology of surface dimethlysulfide concentrations and emission fluxes in the global ocean, Global Biogeochem. Cycles, 25, n/a-n/a, https://doi.org/10.1029/2010GB003850, 2011.

Lebel, T., Parker, D. J., Flamant, C., Bourlès, B., Marticorena, B., Mougin, E., Peugeot, C., Diedhiou, A., Haywood, J. M., Ngamini, J. B., Polcher, J., Redelsperger, J. L., and Thorncroft, C. D.: The AMMA field campaigns: Multiscale and multidisciplinary observations in the West

African region, Q. J. R. Meteorol. Soc., 136, 8–33, https://doi.org/10.1002/qj.486, 2010.

Lupi, L., Hudait, A., and Molinero, V.: Heterogeneous Nucleation of Ice on Carbon Surfaces, J. Am. Chem. Soc., 136, 3156–3164, https://doi.org/10.1021/ja411507a, 2014.

Mahowald, N., Jickells, T. D., Baker, A. R., Artaxo, P., Benitez-Nelson, C. R., Bergametti, G., Bond, T. C., Chen, Y., Cohen, D. D., Herut, B., Kubilay, N., Losno, R., Luo, C., Maenhaut, W., McGee, K. A., Okin, G. S., Siefert, R. L., and Tsukuda, S.: Global distribution of atmospheric phosphorus sources, concentrations and deposition rates, and anthropogenic impacts, Global Biogeochem. Cycles, 22, 1–19, https://doi.org/10.1029/2008GB003240, 2008a.

Mahowald, N., Jickells, T. D., Baker, A. R., Artaxo, P., Benitez-Nelson, C. R., Bergametti, G., Bond, T. C., Chen, Y., Cohen, D. D., Herut, B., Kubilay, N., Losno, R., Luo, C., Maenhaut, W., McGee, K. A., Okin, G. S., Siefert, R. L., and Tsukuda, S.: Global distribution of atmospheric phosphorus sources, concentrations and deposition rates, and anthropogenic impacts, Global Biogeochem. Cycles, 22, https://doi.org/https://doi.org/10.1029/2008GB003240, 2008b.

Marcolli, C.: Deposition nucleation viewed as homogeneous or immersion freezing in pores and cavities, Atmos. Chem. Phys., 14, 2071–2104, https://doi.org/10.5194/acp-14-2071-2014, 2014.

Marcolli, C.: Technical note: Fundamental aspects of ice nucleation via pore condensation and freezing including Laplace pressure and growth into macroscopic ice, Atmos. Chem. Phys., 20, 3209–3230, https://doi.org/10.5194/acp-20-3209-2020, 2020.

Marinou, E., Tesche, M., Nenes, A., Ansmann, A., Schrod, J., Mamali, D., Tsekeri, A., Pikridas, M., Baars, H., Engelmann, R., Voudouri, K. A., Solomos, S., Sciare, J., Groß, S., Ewald, F., and Amiridis, V.: Retrieval of ice-nucleating particle concentrations from lidar observations and comparison with UAV in situ measurements, Atmos. Chem. Phys., 19, 11315–11342, https://doi.org/10.5194/acp-19-11315-2019, 2019.

Marticorena, B., Chatenet, B., Rajot, J. L., Traoré, S., Coulibaly, M., Diallo, A., Koné, I., Maman, A., Ndiaye, T., and Zakou, A.: Temporal variability of mineral dust concentrations over West Africa: Analyses of a pluriannual monitoring from the AMMA Sahelian Dust Transect, Atmos. Chem. Phys., 10, 8899–8915, https://doi.org/10.5194/acp-10-8899-2010, 2010.

Mason, R. H., Si, M., Li, J., Chou, C., Dickie, R., Toom-Sauntry, D., Pöhlker, C., Yakobi-Hancock,

J. D., Ladino, L. A., Jones, K., Leaitch, W. R., Schiller, C. L., Abbatt, J. P. D., Huffman, J. A., and Bertram, A. K.: Ice nucleating particles at a coastal marine boundary layer site: Correlations with aerosol type and meteorological conditions, Atmos. Chem. Phys., 15, 12547–12566, https://doi.org/10.5194/acp-15-12547-2015, 2015.

Maters, E. C., Dingwell, D. B., Cimarelli, C., Müller, D., Whale, T. F., and Murray, B. J.: The importance of crystalline phases in ice nucleation by volcanic ash, Atmos. Chem. Phys., 19, 5451–5465, https://doi.org/10.5194/acp-19-5451-2019, 2019.

McCluskey, C. S., DeMott, P. J., Prenni, A. J., Levin, E. J. T., McMeeking, G. R., Sullivan, A. P., Hill, T. C. J., Nakao, S., Carrico, C. M., and Kreidenweis, S. M.: Characteristics of atmospheric ice nucleating particles associated with biomass burning in the US: Prescribed burns and wildfires, J. Geophys. Res. Atmos., 119, 10458–10470, https://doi.org/https://doi.org/10.1002/2014JD021980, 2014.

McCluskey, C. S., Ovadnevaite, J., Rinaldi, M., Atkinson, J., Belosi, F., Ceburnis, D., Marullo, S., Hill, T. C. J., Lohmann, U., Kanji, Z. A., O'Dowd, C., Kreidenweis, S. M., and DeMott, P. J.: Marine and Terrestrial Organic Ice-Nucleating Particles in Pristine Marine to Continentally Influenced Northeast Atlantic Air Masses, J. Geophys. Res. Atmos., 123, 6196–6212, https://doi.org/10.1029/2017JD028033, 2018.

McCluskey, C. S., DeMott, P. J., Ma, P. -L., and Burrows, S. M.: Numerical Representations of Marine Ice-Nucleating Particles in Remote Marine Environments Evaluated Against Observations, Geophys. Res. Lett., 46, 7838–7847, https://doi.org/10.1029/2018GL081861, 2019.

Menezes, H. C., Amorim, L. C. A., and Cardeal, Z. L.: Sampling and Analytical Methods for Determining VOC in Air by Biomonitoring Human Exposure, Crit. Rev. Environ. Sci. Technol., 43, 1–39, https://doi.org/10.1080/10643389.2011.604239, 2013.

Mertes, S., Verheggen, B., Walter, S., Connolly, P., Ebert, M., Schneider, J., Bower, K. N., Cozic, J., Weinbruch, S., Baltensperger, U., and Weingartner, E.: Counterflow Virtual Impactor Based Collection of Small Ice Particles in Mixed-Phase Clouds for the Physico-Chemical Characterization of Tropospheric Ice Nuclei: Sampler Description and First Case Study, Aerosol Sci. Technol., 41, 848–864, https://doi.org/10.1080/02786820701501881, 2007.

Meyers, Michael P., Paul DeMott, and W. C.: New Primary Ice-Nucleation Parameterizations in an Explicit Cloud Model, J. Appl. Meteorol. Climatol., 1992.

Mihalopoulos, N., Stephanou, E., Kanakidou, M., Pilitsidis, S., and Bousquet, P.: Tropospheric aerosol ionic composition in the Eastern Mediterranean region, Tellus, Ser. B Chem. Phys. Meteorol., 49B, 314–326, https://doi.org/10.3402/tellusb.v49i3.15970, 1997.

Mitts, B. A., Wang, X., Lucero, D. D., Beall, C. M., Deane, G. B., DeMott, P. J., and Prather, K. A.: Importance of Supermicron Ice Nucleating Particles in Nascent Sea Spray, Geophys. Res. Lett., 48, e2020GL089633, https://doi.org/https://doi.org/10.1029/2020GL089633, 2021.

Möhler, O., DeMott, P. J., Vali, G., and Levin, Z.: Microbiology and atmospheric processes: the role of biological particles in cloud physics, 4, 1059–1071, https://doi.org/10.5194/bg-4-1059-2007, 2007.

Murray, B. J., O'Sullivan, D., Atkinson, J. D., and Webb, M. E.: Ice nucleation by particles immersed in supercooled cloud droplets, Chem. Soc. Rev., 41, 6519, https://doi.org/10.1039/c2cs35200a, 2012.

Murray, B. J., Carslaw, K. S., and Field, P. R.: Opinion: Cloud-phase climate feedback and the importance of ice-nucleating particles, Atmos. Chem. Phys., 21, 665–679, https://doi.org/10.5194/acp-21-665-2021, 2021.

Myriokefalitakis, S., Vignati, E., Tsigaridis, K., Papadimas, C., Sciare, J., Mihalopoulos, N., Facchini, M. C., Rinaldi, M., Dentener, F. J., Ceburnis, D., Hatzianastasiou, N., O'Dowd, C. D., van Weele, M., and Kanakidou, M.: Global Modeling of the Oceanic Source of Organic Aerosols, Adv. Meteorol., 2010, 1–16, https://doi.org/10.1155/2010/939171, 2010.

Myriokefalitakis, S., Daskalakis, N., Mihalopoulos, N., Baker, A. R., Nenes, A., and Kanakidou, M.: Changes in dissolved iron deposition to the oceans driven by human activity: a 3-D global modelling study, 12, 3973–3992, https://doi.org/10.5194/bg-12-3973-2015, 2015.

Myriokefalitakis, S., Nenes, A., Baker, A. R., Mihalopoulos, N., and Kanakidou, M.: Bioavailable atmospheric phosphorous supply to the global ocean: a 3-D global modelling study, Biogeosciences Discuss., 0, 1–28, https://doi.org/10.5194/bg-2016-215, 2016.

Myriokefalitakis, S., Fanourgakis, G., and Kanakidou, M.: The Contribution of Bioaerosols to the Organic Carbon Budget of the Atmosphere, in: Perspectives on Atmospheric Sciences, edited by: Karacostas, T., Bais, A., and Nastos, P. T., Springer International Publishing, Cham, 845–851, https://doi.org/10.1007/978-3-319-35095-0_121, 2017.

Myriokefalitakis, S., Daskalakis, N., Kalivitis, N., Chatziparaschos, M., Myriokefalitakis, S., Daskalakis, N., Myriokefalitakis, S., Fanourgakis, G., Origin, M., and Presentation, P.: Arios

hatziparaschos, 23–24, 2021.

Myriokefalitakis, S., Bergas-massó, E., Gonçalves-ageitos, M., and García-pando, C. P.: Multiphase processes in the EC-Earth model and their relevance to the atmospheric oxalate , sulfate , and iron cycles, 3079–3120, 2022.

Nagare, B., Marcolli, C., Welti, A., Stetzer, O., and Lohmann, U.: Comparing contact and immersion freezing from continuous flow diffusion chambers, Atmos. Chem. Phys., 16, 8899–8914, https://doi.org/10.5194/acp-16-8899-2016, 2016.

Nani Guarieiro, L. L. and Nani Guarieiro, A. L.: Vehicle Emissions: What Will Change with Use of Biofuel?, in: Biofuels - Economy, Environment and Sustainability, edited by: Fang, Z., InTech, Rijeka, https://doi.org/10.5772/52513, 2013.

Nazaroff, W. W.: Indoor particle dynamics, Indoor Air, 14, 175–183, https://doi.org/10.1111/j.1600-0668.2004.00286.x, 2004.

Negron, A., DeLeon-Rodriguez, N., Waters, S. M., Ziemba, L. D., Anderson, B., Bergin, M., Konstantinidis, K. T., and Nenes, A.: Using flow cytometry and light-induced fluorescence to characterize the variability and characteristics of bioaerosols in springtime in Metro Atlanta, Georgia, Atmos. Chem. Phys., 20, 1817–1838, https://doi.org/10.5194/acp-20-1817-2020, 2020.

Nickovic, S., Vukovic, A., Vujadinovic, M., Djurdjevic, V., and Pejanovic, G.: Technical Note: High-resolution mineralogical database of dust-productive soils for atmospheric dust modeling, Atmos. Chem. Phys., 12, 845–855, https://doi.org/10.5194/acp-12-845-2012, 2012.

Niehaus, J. and Cantrell, W.: Contact Freezing of Water by Salts, J. Phys. Chem. Lett., 6, 3490–3495, https://doi.org/10.1021/acs.jpclett.5b01531, 2015.

Niehaus, J., Bunker, K. W., China, S., Kostinski, A., Mazzoleni, C., and Cantrell, W.: A Technique to Measure Ice Nuclei in the Contact Mode, J. Atmos. Ocean. Technol., 31, 913–922, https://doi.org/10.1175/JTECH-D-13-00156.1, 2014.

Niemand, M., Möhler, O., Vogel, B., Vogel, H., Hoose, C., Connolly, P., Klein, H., Bingemer, H., Demott, P., Skrotzki, J., and Leisner, T.: A particle-surface-area-based parameterization of immersion freezing on desert dust particles, J. Atmos. Sci., 69, 3077–3092, https://doi.org/10.1175/JAS-D-11-0249.1, 2012.

Van Noije, T. P. C., Le Sager, P., Segers, A. J., Van Velthoven, P. F. J., Krol, M. C., Hazeleger,

W., Williams, A. G., and Chambers, S. D.: Simulation of tropospheric chemistry and aerosols with the climate model EC-Earth, Geosci. Model Dev., 7, 2435–2475, https://doi.org/10.5194/gmd-7-2435-2014, 2014.

van Noije, T., Bergman, T., Le Sager, P., O'Donnell, D., Makkonen, R., Gonçalves-Ageitos, M., Döscher, R., Fladrich, U., Hardenberg, V., J., K., J.-P., Korhonen, H., Laakso, A., Myriokefalitakis, S., Ollinaho, P., Pérez García-Pando, C., Reerink, T., Schrödner, R., Wyser, K., and Yang, S.: EC-Earth3-AerChem, a global climate model with interactive aerosols and atmospheric chemistry participating in CMIP6, Geosci. Model Dev., in review, https://doi.org/10.5194/gmd-2020-413, 2020.

van Noije, T., Bergman, T., Le Sager, P., O'Donnell, D., Makkonen, R., Gonçalves-Ageitos, M., Döscher, R., Fladrich, U., von Hardenberg, J., Keskinen, J.-P., Korhonen, H., Laakso, A., Myriokefalitakis, S., Ollinaho, P., Pérez Garc\'\ia-Pando, C., Reerink, T., Schrödner, R., Wyser, K., and Yang, S.: EC-Earth3-AerChem: a global climate model with interactive aerosols and atmospheric chemistry participating in CMIP6, Geosci. Model Dev., 14, 5637–5668, https://doi.org/10.5194/gmd-14-5637-2021, 2021.

O'Dowd, C. D., Langmann, B., Varghese, S., Scannell, C., Ceburnis, D., and Facchini, M. C.: A combined organic-inorganic sea-spray source function, Geophys. Res. Lett., 35, L01801, https://doi.org/10.1029/2007GL030331, 2008.

O'Sullivan, D., Murray, B. J., Malkin, T. L., Whale, T. F., Umo, N. S., Atkinson, J. D., Price, H. C., Baustian, K. J., Browse, J., and Webb, M. E.: Ice nucleation by fertile soil dusts: Relative importance of mineral and biogenic components, Atmos. Chem. Phys., 14, 1853–1867, https://doi.org/10.5194/acp-14-1853-2014, 2014.

O'Sullivan, D., Murray, B. J., Ross, J. F., Whale, T. F., Price, H. C., Atkinson, J. D., Umo, N. S., and Webb, M. E.: The relevance of nanoscale biological fragments for ice nucleation in clouds, Sci. Rep., 5, 1–7, https://doi.org/10.1038/srep08082, 2015.

O'Sullivan, D., Murray, B. J., Ross, J. F., and Webb, M. E.: The adsorption of fungal ice-nucleating proteins on mineral dusts: a terrestrial reservoir of atmospheric ice-nucleating particles, Atmos. Chem. Phys., 16, 7879–7887, https://doi.org/10.5194/acp-16-7879-2016, 2016.

O'Sullivan, D., Adams, M. P., Tarn, M. D., Harrison, A. D., Vergara-Temprado, J., Porter, G. C. E., Holden, M. A., Sanchez-Marroquin, A., Carotenuto, F., Whale, T. F., McQuaid, J. B., Walshaw, R., Hedges, D. H. P., Burke, I. T., Cui, Z., and Murray, B. J.: Contributions of biogenic

material to the atmospheric ice-nucleating particle population in North Western Europe, Sci. Rep., 8, 1–9, https://doi.org/10.1038/s41598-018-31981-7, 2018.

Park, C. H., Sohn, Y. H., Lee, W. S., Joo, Y. E., Choi, S. K., Rew, J. S., and Kim, S. J.: The usefulness of endoscopic hemoclipping for bleeding Dieulafoy lesions., Endoscopy, 35, 388–392, https://doi.org/10.1055/s-2003-38780, 2003.

Paukert, M. and Hoose, C.: Modeling immersion freezing with aerosol-dependent prognostic ice nuclei in Arctic mixed-phase clouds, J. Geophys. Res., 119, 9073–9092, https://doi.org/10.1002/2014JD021917, 2014.

Pérez García-Pando, C., Miller, R. L., Perlwitz, J. P., Rodríguez, S., and Prospero, J. M.: Predicting the mineral composition of dust aerosols: Insights from elemental composition measured at the Izaña Observatory, Geophys. Res. Lett., 43, 10,520-10,529, https://doi.org/10.1002/2016GL069873, 2016.

Perlwitz, J. P., Pérez García-Pando, C., and Miller, R. L.: Predicting the mineral composition of dust aerosols – Part 1: Representing key processes, Atmos. Chem. Phys., 15, 11593–11627, https://doi.org/10.5194/acp-15-11593-2015, 2015.

Philip, S., Martin, R. V., Van Donkelaar, A., Lo, J. W. H., Wang, Y., Chen, D., Zhang, L., Kasibhatla, P. S., Wang, S., Zhang, Q., Lu, Z., Streets, D. G., Bittman, S., and Macdonald, D. J.: Global chemical composition of ambient fine particulate matter for exposure assessment, Environ. Sci. Technol., 48, 13060–13068, https://doi.org/10.1021/es502965b, 2014.

Phillips, V. T. J., Andronache, C., Christner, B., Morris, C. E., Sands, D. C., Bansemer, A., Lauer, A., McNaughton, C., and Seman, C.: Potential impacts from biological aerosols on ensembles of continental clouds simulated numerically, 6, 987–1014, https://doi.org/10.5194/bg-6-987-2009, 2009.

Pikridas, M., Vrekoussis, M., Sciare, J., Kleanthous, S., Vasiliadou, E., Kizas, C., Savvides, C., and Mihalopoulos, N.: Spatial and temporal (short and long-term) variability of submicron, fine and sub-10 Mm particulate matter (PM1, PM2.5, PM10) in Cyprus, Atmos. Environ., 191, 79–93, https://doi.org/10.1016/j.atmosenv.2018.07.048, 2018.

Pope, C. A.: Epidemiology of fine particulate air pollution and human health: biologic mechanisms and who's at risk?, Environ. Health Perspect., 108, 713–723, https://doi.org/10.1289/ehp.108-1637679, 2000.

Pöschl, U., Martin, S. T., Sinha, B., Chen, Q., Gunthe, S. S., Huffman, J. A., Borrmann, S.,

Farmer, D. K., Garland, R. M., Helas, G., Jimenez, J. L., King, S. M., Manzi, A., Mikhailov, E., Pauliquevis, T., Petters, M. D., Prenni, A. J., Roldin, P., Rose, D., Schneider, J., Su, H., Zorn, S. R., Artaxo, P., and Andreae, M. O.: Rainforest Aerosols as Biogenic Nuclei of Clouds and Precipitation in the Amazon, Science (80-.)., 329, 1513–1516, https://doi.org/10.1126/science.1191056, 2010.

Pratt, K. a., DeMott, P. J., French, J. R., Wang, Z., Westphal, D. L., Heymsfield, A. J., Twohy, C. H., Prenni, A. J., and Prather, K. a.: In situ detection of biological particles in cloud ice-crystals, Nat. Geosci., 2, 398–401, https://doi.org/10.1038/ngeo521, 2009.

Prenni, A. J., Petters, M. D., Kreidenweis, S. M., Heald, C. L., Martin, S. T., Artaxo, P., Garland, R. M., Wollny, A. G., and Pöschl, U.: Relative roles of biogenic emissions and Saharan dust as ice nuclei in the Amazon basin, Nat. Geosci., 2, 402–405, https://doi.org/10.1038/ngeo517, 2009.

Prospero, J. M.: Long-term measurements of the transport of African mineral dust to the southeastern United States: Implications for regional air quality, J. Geophys. Res. Atmos., 104, 15917–15927, https://doi.org/10.1029/1999JD900072, 1999.

Prospero, J. M., Barkley, A. E., Gaston, C. J., Gatineau, A., Campos y Sansano, A., and Panechou, K.: Characterizing and Quantifying African Dust Transport and Deposition to South America: Implications for the Phosphorus Budget in the Amazon Basin, Global Biogeochem. Cycles, 34, 1–24, https://doi.org/10.1029/2020GB006536, 2020.

Pruppacher, H. R., Klett, J. D., and Wang, P. K.: Microphysics of Clouds and Precipitation, Aerosol Sci. Technol., 28, 381–382, https://doi.org/10.1080/02786829808965531, 1998a.

Pruppacher, H. R., Klett, J. D., and Wang, P. K.: Microphysics of Clouds and Precipitation, Aerosol Sci. Technol., 28, 381–382, https://doi.org/10.1080/02786829808965531, 1998b.

Pummer, B. G., Budke, C., Augustin-Bauditz, S., Niedermeier, D., Felgitsch, L., Kampf, C. J., Huber, R. G., Liedl, K. R., Loerting, T., Moschen, T., Schauperl, M., Tollinger, M., Morris, C. E., Wex, H., Grothe, H., Pöschl, U., Koop, T., and Fröhlich-Nowoisky, J.: Ice nucleation by water-soluble macromolecules, Atmos. Chem. Phys., 15, 4077–4091, https://doi.org/10.5194/acp-15-4077-2015, 2015.

Pye, H. O. T., Nenes, A., Alexander, B., Ault, A. P., Barth, M. C., Clegg, S. L., Collett, J. L., Fahey, K. M., Hennigan, C. J., Herrmann, H., Kanakidou, M., Kelly, J. T., Ku, I. T., Faye McNeill, V., Riemer, N., Schaefer, T., Shi, G., Tilgner, A., Walker, J. T., Wang, T., Weber, R., Xing, J.,

Zaveri, R. A., and Zuend, A.: The acidity of atmospheric particles and clouds, 4809–4888 pp., https://doi.org/10.5194/acp-20-4809-2020, 2020.

Qiu, C., Khalizov, A. F., and Zhang, R.: Soot aging from OH-initiated oxidation of toluene., Environ. Sci. Technol., 46, 9464–9472, https://doi.org/10.1021/es301883y, 2012.

Rau, J. A.: Composition and Size Distribution of Residential Wood Smoke Particles, Aerosol Sci. Technol., 10, 181–192, https://doi.org/10.1080/02786828908959233, 1989.

Reid, J. S., Eck, T. F., Christopher, S. A., Koppman, R., Dubovik, O., Eleuterio, D. P., Holben, B. N., Reid, E. A., and Zhang, J.: A review of biomass burning emissions part III: Intensive optical properties of biomass burning particles, Atmos. Chem. Phys., 5, 827–849, https://doi.org/10.5194/acp-5-827-2005, 2005.

Rinaldi, M., Fuzzi, S., Decesari, S., Marullo, S., Santoleri, R., Provenzale, A., von Hardenberg, J., Ceburnis, D., Vaishya, A., O'Dowd, C. D., and Facchini, M. C.: Is chlorophyll-a the best surrogate for organic matter enrichment in submicron primary marine aerosol?, J. Geophys. Res. Atmos., 118, 4964–4973, https://doi.org/https://doi.org/10.1002/jgrd.50417, 2013.

Rinaldi, M., Belosi, F., Nicosia, A., Santachiara, G., Decesari, S., and Cristina, M.: Ice Nucleating Particles at Mace Head during the 2015 BACCHUS campaign through off-line measurements, 18, 15063, 2016.

Rinaldi, M., Santachiara, G., Nicosia, A., Piazza, M., Decesari, S., Gilardoni, S., Paglione, M., Cristofanelli, P., Marinoni, A., Bonasoni, P., and Belosi, F.: Atmospheric Ice Nucleating Particle measurements at the high mountain observatory Mt. Cimone (2165 m a.s.l., Italy), Atmos. Environ., 171, 173–180, https://doi.org/10.1016/j.atmosenv.2017.10.027, 2017.

Rood, M. J. and Currie, R. M.: Absorption of NH3 and SO2 during activation of atmospheric cloud condensation nuclei, Atmos. Environ., 23, 2847–2854, https://doi.org/https://doi.org/10.1016/0004-6981(89)90565-9, 1989.

Schill, G. P., DeMott, P. J., Emerson, E. W., Rauker, A. M. C., Kodros, J. K., Suski, K. J., Hill, T. C. J., Levin, E. J. T., Pierce, J. R., Farmer, D. K., and Kreidenweis, S. M.: The contribution of black carbon to global ice nucleating particle concentrations relevant to mixed-phase clouds, Proc. Natl. Acad. Sci., 117, 22705–22711, https://doi.org/10.1073/pnas.2001674117, 2020.

Schneider, J., Höhler, K., Heikkilä, P., Keskinen, J., Bertozzi, B., Bogert, P., Schorr, T., Umo, N. S., Vogel, F., Brasseur, Z., Wu, Y., Hakala, S., Duplissy, J., Moisseev, D., Kulmala, M., Adams, M. P., Murray, B. J., Korhonen, K., Hao, L., Thomson, E. S., Castarède, D., Leisner, T., Petäjä,

T., and Möhler, O.: The seasonal cycle of ice-nucleating particles linked to the abundance of biogenic aerosol in boreal forests, Atmos. Chem. Phys., 21, 3899–3918, https://doi.org/10.5194/acp-21-3899-2021, 2021.

Schrod, J., Weber, D., Drücke, J., Keleshis, C., Pikridas, M., Ebert, M., Cvetković, B., Nickovic, S., Marinou, E., Baars, H., Ansmann, A., Vrekoussis, M., Mihalopoulos, N., Sciare, J., Curtius, J., and Bingemer, H. G.: Ice nucleating particles over the Eastern Mediterranean measured by unmanned aircraft systems, Atmos. Chem. Phys., 17, 4817–4835, https://doi.org/10.5194/acp-17-4817-2017, 2017.

Schrod, J., Thomson, E. S., Weber, D., Kossmann, J., Pöhlker, C., Saturno, J., Ditas, F., Artaxo, P., Clouard, V., Saurel, J. M., Ebert, M., Curtius, J., and Bingemer, H. G.: Long-term deposition and condensation ice-nucleating particle measurements from four stations across the globe, Atmos. Chem. Phys., 20, 15983–16006, https://doi.org/10.5194/acp-20-15983-2020, 2020.

Schwarz, J. P., Spackman, J. R., Fahey, D. W., Gao, R. S., Lohmann, U., Stier, P., Watts, L. A., Thomson, D. S., Lack, D. A., Pfister, L., Mahoney, M. J., Baumgardner, D., Wilson, J. C., and Reeves, J. M.: Coatings and their enhancement of black carbon light absorption in the tropical atmosphere, J. Geophys. Res. Atmos., 113, https://doi.org/https://doi.org/10.1029/2007JD009042, 2008.

Seifert, P., Ansmann, A., Groß, S., Freudenthaler, V., Heinold, B., Hiebsch, A., Mattis, I., Schmidt, J., Schnell, F., Tesche, M., Wandinger, U., and Wiegner, M.: Ice formation in ash-influenced clouds after the eruption of the Eyjafjallajökull volcano in April 2010, J. Geophys. Res., 116, D00U04, https://doi.org/10.1029/2011JD015702, 2011.

Seinfeld, J. H., Bretherton, C., Carslaw, K. S., Coe, H., DeMott, P. J., Dunlea, E. J., Feingold, G., Ghan, S., Guenther, A. B., Kahn, R., Kraucunas, I., Kreidenweis, S. M., Molina, M. J., Nenes, A., Penner, J. E., Prather, K. A., Ramanathan, V., Ramaswamy, V., Rasch, P. J., Ravishankara, A. R., Rosenfeld, D., Stephens, G., and Wood, R.: Improving our fundamental understanding of the role of aerosol-cloud interactions in the climate system, Proc. Natl. Acad. Sci. U. S. A., 113, 5781–5790, https://doi.org/10.1073/pnas.1514043113, 2016.

Si, M., Evoy, E., Yun, J., Xi, Y., Hanna, S. J., Chivulescu, A., Rawlings, K., Veber, D., Platt, A., Kunkel, D., Hoor, P., Sharma, S., Richard Leaitch, W., and Bertram, A. K.: Concentrations, composition, and sources of ice-nucleating particles in the Canadian High Arctic during spring 2016, Atmos. Chem. Phys., 19, 3007–3024, https://doi.org/10.5194/acp-19-3007-2019, 2019.

Simó, R. and Pedrós-Alió, C.: Short-term variability in the open ocean cycle of dimethylsulfide, Global Biogeochem. Cycles, 13, 1173–1181, https://doi.org/https://doi.org/10.1029/1999GB900081, 1999.

Sindelarova, K., Granier, C., Bouarar, I., Guenther, A., Tilmes, S., Stavrakou, T., Müller, J.-F., Kuhn, U., Stefani, P., and Knorr, W.: Global data set of biogenic VOC emissions calculated by the MEGAN model over the last 30 years, Atmos. Chem. Phys., 14, 9317–9341, https://doi.org/10.5194/acp-14-9317-2014, 2014.

Sofiev, M., Berger, U., Prank, M., Vira, J., Arteta, J., Belmonte, J., Bergmann, K.-C., Chéroux, F., Elbern, H., Friese, E., Galan, C., Gehrig, R., Khvorostyanov, D., Kranenburg, R., Kumar, U., Marécal, V., Meleux, F., Menut, L., Pessi, A.-M., Robertson, L., Ritenberga, O., Rodinkova, V., Saarto, A., Segers, A., Severova, E., Sauliene, I., Siljamo, P., Steensen, B. M., Teinemaa, E., Thibaudon, M., and Peuch, V.-H.: MACC regional multi-model ensemble simulations of birch pollen dispersion in Europe, Atmos. Chem. Phys., 15, 8115–8130, https://doi.org/10.5194/acp-15-8115-2015, 2015.

Solomon, A., De Boer, G., Creamean, J. M., McComiskey, A., Shupe, M. D., Maahn, M., and Cox, C.: The relative impact of cloud condensation nuclei and ice nucleating particle concentrations on phase partitioning in Arctic mixed-phase stratocumulus clouds, Atmos. Chem. Phys., 18, 17047–17059, https://doi.org/10.5194/acp-18-17047-2018, 2018.

Sotiropoulou, G., Sullivan, S., Savre, J., Lloyd, G., Lachlan-Cope, T., Ekman, A. M. L., and Nenes, A.: The impact of secondary ice production on Arctic stratocumulus, Atmos. Chem. Phys., 20, 1301–1316, https://doi.org/10.5194/acp-20-1301-2020, 2020.

Spracklen, D. V. and Heald, C. L.: The contribution of fungal spores and bacteria to regional and global aerosol number and ice nucleation immersion freezing rates, Atmos. Chem. Phys., 14, 9051–9059, https://doi.org/10.5194/acp-14-9051-2014, 2014.

Steinke, I., Hiranuma, N., Funk, R., Höhler, K., Tüllmann, N., Umo, N. S., Weidler, P., Möhler, O., and Leisner, T.: Complex plant-derived organic aerosol as ice-nucleating particles – more than a sum of their parts?, Atmos. Chem. Phys. Discuss., 1–17, https://doi.org/10.5194/acp-2019-869, 2019.

Stevens, R. and Dastoor, A.: A Review of the Representation of Aerosol Mixing State in Atmospheric Models, Atmosphere (Basel)., 10, https://doi.org/10.3390/atmos10040168, 2019.

Sullivan, R. C., Petters, M. D., DeMott, P. J., Kreidenweis, S. M., Wex, H., Niedermeier, D., Hartmann, S., Clauss, T., Stratmann, F., Reitz, P., Schneider, J., and Sierau, B.: Irreversible loss of ice nucleation active sites in mineral dust particles caused by sulphuric acid condensation, Atmos. Chem. Phys., 10, 11471–11487, https://doi.org/10.5194/acp-10-11471-2010, 2010.

Suski, K. J., Hill, T. C. J., Levin, E. J. T., Miller, A., DeMott, P. J., and Kreidenweis, S. M.: Agricultural harvesting emissions of ice-nucleating particles, Atmos. Chem. Phys., 18, 13755–13771, https://doi.org/10.5194/acp-18-13755-2018, 2018.

Tang, M., Huang, X., Lu, K., Ge, M., Li, Y., Cheng, P., Zhu, T., Ding, A., Zhang, Y., Gligorovski, S., Song, W., Ding, X., Bi, X., and Wang, X.: Heterogeneous reactions of mineral dust aerosol: implications for tropospheric oxidation capacity, Atmos. Chem. Phys., 17, 11727–11777, https://doi.org/10.5194/acp-17-11727-2017, 2017.

Tegen, I., Harrison, S. P., Kohfeld, K., Prentice, I. C., Coe, M., and Heimann, M.: Impact of vegetation and preferential source areas on global dust aerosol: Results from a model study, J. Geophys. Res. Atmos., 107, https://doi.org/10.1029/2001JD000963, 2002.

Tobo, Y., Prenni, A. J., Demott, P. J., Huffman, J. A., McCluskey, C. S., Tian, G., Pöhlker, C., Pöschl, U., and Kreidenweis, S. M.: Biological aerosol particles as a key determinant of ice nuclei populations in a forest ecosystem, J. Geophys. Res. Atmos., 118, 10,100-10,110, https://doi.org/10.1002/jgrd.50801, 2013.

Tobo, Y., Demott, P. J., Hill, T. C. J., Prenni, A. J., and Franc, G. D.: Organic matter matters for ice nuclei of agricultural soil origin, 8521–8531, https://doi.org/10.5194/acp-14-8521-2014, 2014.

Tsigaridis, K. and Kanakidou, M.: Global modelling of secondary organic aerosol in the troposphere: a sensitivity analysis, Atmos. Chem. Phys., 3, 1849–1869, https://doi.org/10.5194/acp-3-1849-2003, 2003.

Tsiodra, I., Grivas, G., Tavernaraki, K., Bougiatioti, A., Apostolaki, M., Paraskevopoulou, D., Gogou, A., Parinos, C., Oikonomou, K., Tsagkaraki, M., Zarmpas, P., Nenes, A., and Mihalopoulos, N.: Annual exposure to polycyclic aromatic hydrocarbons in urban environments linked to wintertime wood-burning episodes, Atmos. Chem. Phys., 21, 17865–17883, https://doi.org/10.5194/acp-21-17865-2021, 2021.

Twohy, C. H., McMeeking, G. R., DeMott, P. J., McCluskey, C. S., Hill, T. C. J., Burrows, S. M., Kulkarni, G. R., Tanarhte, M., Kafle, D. N., and Toohey, D. W.: Abundance of fluorescent

biological aerosol particles at temperatures conducive to the formation of mixed-phase and cirrus clouds, 1–34, https://doi.org/10.5194/acp-2016-112, 2016.

Twohy, C. H., DeMott, P. J., Russell, L. M., Toohey, D. W., Rainwater, B., Geiss, R., Sanchez, K. J., Lewis, S., Roberts, G. C., Humphries, R. S., McCluskey, C. S., Moore, K. A., Selleck, P. W., Keywood, M. D., Ward, J. P., and McRobert, I. M.: Cloud-Nucleating Particles Over the Southern Ocean in a Changing Climate, Earth's Futur., 9, e2020EF001673, https://doi.org/https://doi.org/10.1029/2020EF001673, 2021.

Ullrich, R., Hoose, C., Möhler, O., Niemand, M., Wagner, R., Höhler, K., Hiranuma, N., Saathoff, H., and Leisner, T.: A new ice nucleation active site parameterization for desert dust and soot, J. Atmos. Sci., 74, 699–717, https://doi.org/10.1175/JAS-D-16-0074.1, 2017.

Usher, C. R., Michel, A. E., and Grassian, V. H.: Reactions on Mineral Dust, Chem. Rev., 103, 4883–4940, https://doi.org/10.1021/cr020657y, 2003.

Vali, G., DeMott, P. J., Möhler, O., and Whale, T. F.: Technical Note: A proposal for ice nucleation terminology, Atmos. Chem. Phys., 15, 10263–10270, https://doi.org/10.5194/acp-15-10263-2015, 2015.

Vergara-temprado, J., Holden, M. A., Orton, T. R., Sullivan, D. O., Umo, N. S., Browse, J., Reddington, C., Baeza-romero, M. T., Jones, J. M., Lea-langton, A., Williams, A., and Carslaw, K. S.: Is Black Carbon an Unimportant Ice-Nucleating Particle in Mixed-Phase Clouds ?, 4273–4283, 2018.

Vergara-Temprado, J., Murray, B. J., Wilson, T. W., O'Sullivan, D., Browse, J., Pringle, K. J., Ardon-Dryer, K., Bertram, A. K., Burrows, S. M., Ceburnis, D., Demott, P. J., Mason, R. H., O'Dowd, C. D., Rinaldi, M., and Carslaw, K. S.: Contribution of feldspar and marine organic aerosols to global ice nucleating particle concentrations, Atmos. Chem. Phys., 17, 3637–3658, https://doi.org/10.5194/acp-17-3637-2017, 2017.

Vergara-Temprado, J., Miltenberger, A. K., Furtado, K., Grosvenor, D. P., Shipway, B. J., Hill, A. A., Wilkinson, J. M., Field, P. R., Murray, B. J., and Carslaw, K. S.: Strong control of Southern Ocean cloud reflectivity by ice-nucleating particles, Proc. Natl. Acad. Sci. U. S. A., 115, 2687–2692, https://doi.org/10.1073/pnas.1721627115, 2018.

Vignati, E., Facchini, M. C., Rinaldi, M., Scannell, C., Ceburnis, D., Sciare, J., Kanakidou, M., Myriokefalitakis, S., Dentener, F., and O'Dowd, C. D.: Global scale emission and distribution of sea-spray aerosol: Sea-salt and organic enrichment, Atmos. Environ., 44, 670–677,

https://doi.org/10.1016/j.atmosenv.2009.11.013, 2010.

Violaki, K., Nenes, A., Tsagkaraki, M., Paglione, M., Jacquet, S., Sempéré, R., and Panagiotopoulos, C.: Bioaerosols and dust are the dominant sources of organic P in atmospheric particles, npj Clim. Atmos. Sci., 4, https://doi.org/10.1038/s41612-021-00215-5, 2021.

Vogel, F., Lacher, L., Nadolny, J., Saathoff, H., Leisner, T., and Möhler, O.: Development and validation of a new cloud simulation experiment for lab-based aerosol-cloud studies, Rev. Sci. Instrum., 93, https://doi.org/10.1063/5.0098777, 2022.

Vonnegut, B.: The Nucleation of Ice Formation by Silver Iodide, J. Appl. Phys., 18, 593–595, https://doi.org/10.1063/1.1697813, 1947.

Wagner, R., Kiselev, A., Möhler, O., Saathoff, H., and Steinke, I.: Pre-activation of ice-nucleating particles by the pore condensation and freezing mechanism, Atmos. Chem. Phys., 16, 2025–2042, https://doi.org/10.5194/acp-16-2025-2016, 2016.

Wang, B., Laskin, A., Roedel, T., Gilles, M. K., Moffet, R. C., Tivanski, A. V., and Knopf, D. A.: Heterogeneous ice nucleation and water uptake by field-collected atmospheric particles below 273 K, J. Geophys. Res. Atmos., 117, 1–15, https://doi.org/10.1029/2012JD017446, 2012.

Wang, M., Chen, Y., Fu, H., Qu, X., Li, B., Tao, S., and Zhu, D.: An investigation on hygroscopic properties of 15 black carbon (BC)-containing particles from different carbon sources: roles of organic and inorganic components, Atmos. Chem. Phys., 20, 7941–7954, https://doi.org/10.5194/acp-20-7941-2020, 2020a.

Wang, N., Zhao, X., Wang, J., Yin, B., Geng, C., Niu, D., Yang, W., Yu, H., and Li, W.: Chemical Composition of PM2.5 and Its Impact on Inhalation Health Risk Evaluation in a City with Light Industry in Central China, Atmosphere (Basel)., 11, https://doi.org/10.3390/atmos11040340, 2020b.

Welti, A., Müller, K., Fleming, Z. L., and Stratmann, F.: Concentration and variability of ice nuclei in the subtropical maritime boundary layer, 5307–5320, 2018.

Welti, A., Bigg, E. K., Demott, P. J., Gong, X., Hartmann, M., Harvey, M., Henning, S., Herenz, P., Hill, T. C. J., Hornblow, B., Leck, C., Löffler, M., Mccluskey, C. S., Rauker, A. M., Schmale, J., Tatzelt, C., and Pinxteren, M. Van: Ship-based measurements of ice nuclei concentrations over the Arctic , Atlantic , Pacific and Southern oceans, 15191–15206, 2020.

Weng, H., Lin, J., Martin, R., Millet, D. B., Jaeglé, L., Ridley, D., Keller, C., Li, C., Du, M., and Meng, J.: Global high-resolution emissions of soil NOx, sea salt aerosols, and biogenic volatile organic compounds., Sci. data, 7, 148, https://doi.org/10.1038/s41597-020-0488-5, 2020.

Werner, M., Tegen, I., Harrison, S. P., Kohfeld, K. E., Prentice, I. C., Balkanski, Y., Rodhe, H., and Roelandt, C.: Seasonal and interannual variability of the mineral dust cycle under present and glacial climate conditions, J. Geophys. Res. Atmos., 107, AAC 2-1-AAC 2-19, https://doi.org/https://doi.org/10.1029/2002JD002365, 2002.

Westbrook, C. D. and Illingworth, A. J.: The formation of ice in a long-lived supercooled layer cloud, Q. J. R. Meteorol. Soc., 139, 2209–2221, https://doi.org/10.1002/qj.2096, 2013.

Wex, H., Huang, L., Zhang, W., Hung, H., Traversi, R., Becagli, S., Sheesley, R. J., Moffett, C. E., Barrett, T. E., Bossi, R., Skov, H., Hünerbein, A., Lubitz, J., Löffler, M., Linke, O., Hartmann, M., Herenz, P., and Stratmann, F.: Annual variability of ice-nucleating particle concentrations at different Arctic locations, Atmos. Chem. Phys., 19, 5293–5311, https://doi.org/10.5194/acp-19-5293-2019, 2019.

Wexler, A. S.: Atmospheric aerosol models for systems including the ions H + , NH 4 + , Na + , SO 4 2− , NO 3 − , Cl − , Br − , and H 2 O, J. Geophys. Res., 107, 4207, https://doi.org/10.1029/2001JD000451, 2002.

Wilson, T. W., Ladino, L. A., Alpert, P. A., Breckels, M. N., Brooks, I. M., Browse, J., Burrows, S. M., Carslaw, K. S., Huffman, J. A., Judd, C., Kilthau, W. P., Mason, R. H., McFiggans, G., Miller, L. A., Nájera, J. J., Polishchuk, E., Rae, S., Schiller, C. L., Si, M., Temprado, J. V., Whale, T. F., Wong, J. P. S., Wurl, O., Yakobi-Hancock, J. D., Abbatt, J. P. D., Aller, J. Y., Bertram, A. K., Knopf, D. A., and Murray, B. J.: A marine biogenic source of atmospheric ice-nucleating particles, Nature, 525, 234–238, https://doi.org/10.1038/nature14986, 2015.

Xu, F., Shi, X., Qiu, X., Jiang, X., Fang, Y., Wang, J., Hu, D., and Zhu, T.: Investigation of the chemical components of ambient fine particulate matter (PM2.5) associated with in vitro cellular responses to oxidative stress and inflammation, Environ. Int., 136, 105475, https://doi.org/https://doi.org/10.1016/j.envint.2020.105475, 2020.

Yin, J., Wang, D., and Guoqing, Z.: An Evaluation of Ice Nuclei Characteristics from the Long-term Measurement Data over North China An Evaluation of Ice Nuclei Characteristics from the Long-term Measurement Data over North China, https://doi.org/10.1007/s13143-012-0020-8, 2012.

Yun, Y. and Penner, J. E.: An evaluation of the potential radiative forcing and climatic impact of marine organic aerosols as heterogeneous ice nuclei, Geophys. Res. Lett., 40, 4121–4126, https://doi.org/https://doi.org/10.1002/grl.50794, 2013.

Zhang, X., Mao, M., Chen, H., Yin, Y., and Tang, S.: Lensing Effect of Black Carbon With Brown Coatings: Dominant Microphysics and Parameterization, J. Geophys. Res. Atmos., 126, 1–10, https://doi.org/10.1029/2020JD033549, 2021.

Zuidema, P., Alvarez, C., Kramer, S. J., Custals, L., Izaguirre, M., Sealy, P., Prospero, J. M., and Blades, E.: Is summer African dust arriving earlier to Barbados?, Bull. Am. Meteorol. Soc., 100, 1981–1986, https://doi.org/10.1175/BAMS-D-18-0083.1, 2019.